DSE - Advanced Regional Aircraft

Design of a regional aircraft implementing the latest technologies

M. Blom	4166809	F.S. Heeres	4230779
M.P. Bobeldijk	4224205	K.J.M. Mattheus	4197585
A.M.R.M. Bruggeman	4223977	U. Mehmood	4229630
D.J.H. Cederløf	4132955	P.C.L. Mestrom	1328972
M. Haddaoui	4205596	M. Miedema	4162862

Final Report

Design Synthesis Excercise

ARA-15

TUDelft — Delft University of Technology

Aerospace Engineering

June 30, 2015

Preface

This report is the last in a series of reports that elaborate on the design of an advanced regional aircraft. Readers will find a detailed description of the design of the aircraft. This includes the choice of configuration, the preliminary design and the detailed designs of several subsystems. Furthermore, the logistics required to commercially fly an aircraft and the way the aircraft will be produced as well as maintained have been investigated. This all resulted in the ARA - Advanced Regional Aircraft.

Our team would like to thank some people whom without this report would not have been of the current quality. First of all, we would like to thank Jos Sinke, Marianella Hernandez and Richard Curran for their guidance and helpful feedback as coaches of our project. Furthermore, we would like to thank the people whom we could talk to and ask questions regarding the challenges we were encountering during the design of our aircraft. These people include Joris Melkert, Roelof Vos, Leo Veldhuis, Durk Steenhuizen, Mostafa Abdalla, Calvin Rans, Nando Timmer, Mohamed El Abbassi and Ali Elham.

Delft, June 2015

M. Blom	4166809
M.P. Bobeldijk	4224205
A.M.R.M. Bruggeman	4223977
D.J.H. Cederløf	4132955
M. Haddaoui	4205596
F.S. Heeres	4230779
K.J.M. Mattheus	4197585
U. Mehmood	4229630
P.C.L. Mestrom	1328972
M. Miedema	4162862

Summary

This report is the final report in a series of four reports that deals with the design of an advanced regional aircraft. The first step in the design is to determine the overall configuration of the ARA. By identifying the feasible configurations based on a literature study and performing a trade-off, the conventional low wing with GTF engines underneath the wings configuration is found to be the optimal configuration for the ARA. After selecting the aircraft configuration, the preliminary subsystem design is initiated. Class I and II weight estimations are performed and a MTOW of 34500kg is determined. The selected wing planform is a two-piece complex sweptback planform with a wing area of $105m^2$ and a wing span of 30.7m. The thrust will be provided by two PW1217G GTFs with a maximum thrust of 76kN each. For the fuselage design, several configuration options are analysed taking into account structural and aerodynamic considerations. A trade-off is performed and the 4 abreast configuration with cargo in the tail is found to be the best choice. The tricycle configuration is chosen for the landing gear. The main gear is positioned 17.1m from the nose, while the nose gear is positioned 3.6m from the nose. The control surfaces comprising ailerons, spoilerons, elevators and rudder, are sized for extreme load cases. For roll control at low speeds outboard ailerons are used and spoilerons are used for roll control at high speeds. The elevators are sized to meet take-off and trim requirements. The rudder is sized to counteract the yawing moment with one-engine inoperative. Furthermore, the high-lift devices are sized. It is found that in order to fulfill landing and take-off requirements double-slotted Fowler flaps are required.

A more detailed design has been performed for the winglets, morphing control surfaces and the structural design of the fuselage cargo bay. For the winglet, an aerodynamic and structural analysis is performed to determine the optimal design. A winglet is designed which is not yet on the market and is called the FLOTIN winglet. The final design choice consists of both an upper and a downward winglet, both featuring raked tips. This winglet improves the fuel efficiency by 6.1%. For the morphing control surfaces, several concepts are analysed. A trade-off is performed and the fishbone concept is selected. The required dimensions are calculated by using requirements such as maximum deflection and failure types such as column buckling. Furthermore, a more detailed structural analysis and design of the cargo section of the ARA is performed. The purpose of the analysis and design is to determine the material type and topology of the fuselage section and predict the corresponding weight and cost reductions. The stresses are analysed for a metal fuselage and composite fuselage and subsequently the layout is optimised with respect to stringer and skin thickness. The optimised HSCF-APC2 cross-section is found to be 21.9% lighter than the optimised Al-7175 T61511 cross-section.

The first steps in planning the infrastructure concerning the manufacturing and logistics are presented in the production plan. Considering the large capital investment involved, the need for outsourcing is a necessity. A communication framework is set-up which uses primary and secondary communication. Primary communication consists of direct communication between the involved parties and the secondary communication consists of a digital environment where a centralised network allows for rapid adaption to process changes.

Concluding, all of the requirements are met, except for the requirement to produce 25 aircraft per month. It is decided to deviate from this value, since 100 aircraft per year fits the reflected order amount better. The ARA should obtain a leading market share due to technical advantages over the competition. The individual aircraft price is 42 million dollars (FY:2015), which accounts for a 27% profit. The total profit for 'The Company' selling 1100 aircraft will be approximately 8.1 billion dollars.

Contents

List of Figures

List of Tables

List of Symbols

Symbol	Variable	Unit
a	3D Lift Slope Coefficient	$[-]$
A	Aspect Ratio	$[-]$
b	Wing Span	$[m]$
c	Chord Length	$[m]$
c_r	Root Chord Length	$[m]$
C_D	Drag Coefficient	$[-]$
C_l	Lift Coefficient (2D)	$[-]$
C_L	Lift Coefficient (3D)	$[-]$
C_m	Moment Coefficient	$[-]$
C_p	Pressure Coefficient	$[-]$
d	Diameter	$[m]$
D	Drag	$[N]$
E	Elasticity Modulus	$[GPa]$
F	Force	$[N]$
g	Gravitational Acceleration	$[\frac{m}{s^2}]$
G	Shear Modulus	$[GPa]$
h	Height	$[m]$
H	Height	$[m]$
i	Incidence Angle	$[°]$
I	Moment of Inertia	$[kgm^2]$
l	Length	$[m]$
K_c	Buckling Coefficient	$[-]$
K	Stiffness	$[\frac{N}{m}]$
K_g	Gust Alleviation Coefficient	$[-]$
K_r	Aircraft Response Factor	$[-]$
L	Lift	$[N]$
M	Mach Number	$[-]$
M	Moment	$[Nm]$
M_{max}	Maximum Mach Number	$[-]$
M_{MO}	Mach Maximum Operating	$[-]$
n	Load Factor	$[-]$
P	Pressure	$[\frac{N}{m^2}]$
P	Roll Rate	$[N]$
q	Dynamic Pressure	$[\frac{N}{m^2}]$
q	Distributed Load	$[\frac{N}{m}]$
q	Shear Flow	$[\frac{N}{m}]$
S	Surface Area	$[m^2]$
S	Shear Force	$[N]$
t	Thickness	$[m]$
T	Thrust	$[N]$
U	Gust Speed	$[\frac{m}{s}]$
V	Speed	$[\frac{m}{s}]$
V_A	Design Manoeuvring Speed	$[\frac{m}{s}]$
V_B	Bad Weather Speed	$[\frac{m}{s}]$
V_C	Design Cruise Speed	$[\frac{m}{s}]$
V_D	Design Dive Speed	$[\frac{m}{s}]$
V_S	Stall speed	$[\frac{m}{s}]$
W	Weight	$[N]$
x_{LEMAC}	Distance from nose to Leading edge MAC	$[m]$
y	Location of Aileron	$[m]$
α	Angle of Attack	$[°]$
β	Side Slip Angle	$[°]$
δ	Deflection Angle	$[°]$

Symbol	Variable	Unit
ϵ	Strain	$[-]$
η	Efficiency	$[-]$
κ	Curvature	$[m^{-1}]$
λ	Taper Ratio	$[-]$
λ	Fineness Ratio	$[-]$
Λ	Sweep Angle	$[°]$
ρ	Density	$[\frac{kg}{m^3}]$
σ	Stress	$[MPa]$
τ	Effectiveness Parameter	$[-]$
τ	Shear Stress	$[MPa]$
Φ	Roll Angle	$[°]$

List of Abbreviations

Abbreviation	Full description
ARA	Advanced Regional Aircraft
ATC	Air Traffic Control
ATM	Air Traffic Management
BEP	Break-Even Point
c.g.	Centre of gravity
CBS	Cost Breakdown Structure
CC	Combined Cargo
CCA	Composite Cylinder Assemblage
CF	Carbon Fibre
CFD	Computational Fluid Dynamics
CLC	Combined Load Case
CT	Cargo Tail
CU	Cargo Under
DATCOM	Data Compendium
DOC	Direct Operational Cost
DSE	Design Synthesis Exercise
EAS	Equivalent Air Speed
EGTS	Electrical Green Taxiing System
ERAA	European Regions Airline Association
FAA	Federal Aviation Administration
FOD	Foreign Object Damage
GAO	Government Accountability Office
GD	General Dynamics
GTF	Geared TurboFan
HPC	High Pressure Compressor
HSCF	High-Strength Carbon Fibre
ICAO	International Civil Aviation Organisation
IFCS	Intelligent Flight Control System
IOC	Indirect Operational Cost
ISA	International Standard Atmosphere
LE	Leading Edge
LNG	Liquefied Natural Gas
MAC	Mean Aerodynamic Chord
MRJ	Mitsubishi Regional Jet
MTOW	Maximum Take-Off Weight
OEM	Original Equipment Manufacturer
OEW	Operational Empty Weight
ORE	Open Rotor Engine
PD & DL	Project Design and Development Logic
PEEK	PolyEther Ether Ketone
RAMS	Reliability, Availability, Maintainability and Safety
RMA	Risk Map Approach
RPM	Revolutions Per Minute
R&D	Research & Development
SMA	Shape-Memory Alloy
TAS	True Air Speed
TE	Trailing Edge
TOP	Take-Off Parameter
ULC	Unit Load Case
ULD	Unit Loading Device
UD	Uni-Directional
VLM	Vortex Lattice Method
V&V	Verification & Validation

1 | Introduction

Regional aircraft are used on short routes to transport passengers between smaller airfields as well as hub airports. Currently, a lot of technological developments emerge in different domains concerning aerospace engineering such as propulsion, materials, structures and aerodynamics. As a Design Synthesis Exercise (DSE) at the TU Delft, the team has been assigned to design an advanced regional aircraft according to the latest technologies with a capacity of 75-90 passengers. The latest technologies should be ready for the market within 5 to 10 years. In addition, a specified aircraft manufacturing rate should be achieved.

This report finalises the 10 week design process was performed. The report will give an overview of the steps that were taken to get to the final design of the Advanced Regional Aircraft, or ARA. It will give a review of the possible concepts and the trade-off that determined the aircraft's configuration. A detailed description will be given of the preliminary design of the overall aircraft and detailed design of certain subsystems. The manufacturing of the aircraft and the logistics both on the ground as well as in the air are further investigated in this report.

This report consists of six parts. The first part describes the set requirements, market need, design philosophy and project planning for ARA. This can be found in chapters 2, 3, 4 and 5, respectively. Part two of this report consists of the preliminary subsystem sizing. Which includes the design configuration choice, the iteration process, the class I and II weight estimation and sizing of several subsystems, shown in chapters 6 to 15. The third part consists of the detailed design of the winglets, the structural design of the cargo bay and the control surfaces. This detailed design will be elaborated on in chapters 16, 17 and 18. Part four gives a discription of the aircraft's performance including a sensitivity analysis in chapters 19, 20 and 21. The fifth part will give an insight in the production, the operational life and the required investment of the ARA. This can be found in chapters 22 to 26. Finally, the sixth part of this report consists of a post-project planning for the ARA given in chapter 27 and the conclusion and recommendations for the current design given in chapter 28. This report will not feature a communication flow, an electrical block, a data handling block, hardware- and software block diagram as stated in the project reader, as it is found to be not relevant at this stage of the ARA design.

Part I

Project Management

2 | Requirements

In order to design an advanced regional aircraft which implements advanced technology, is realisable within 5-10 years and is competitive with today's existing regional jets a clear set of requirements have to be determined. This set of requirements is obtained from the key requirements set by the assignment and additional requirements from future stakeholders. The requirements are stipulated in section 2.1. Next to the set of requirements it is important to determine the mission profile of the ARA, which is further elaborated on in section 2.2

2.1 Requirements

The following list of requirements are derived from the key requirements set by the assignment and additional requirements from future stakeholders. Stakeholders include airports, governmental bodies and operators. Five main categories of requirements have been determined: production, operations, dimensional, performance and regulations.

Production

- **Pr-req1**: The ARA shall be market ready in 2025.
- **Pr-req2**: The production process shall be able to produce 25 aircraft per month, with an option to increase to 40 per month.

Operations

- **O-req1** The ARA shall be able to accommodate 75 to 90 passengers.
- **O-req2** The ARA shall be able to accommodate a total of 100kg payload per person.
- **O-req2-1** The ARA shall be able to accommodate 15kg cargo per person to be stored in the cargo bay.
- **O-req2-2** The ARA shall be able to accommodate 85kg per person including hand baggage to be stored in the cabin.
- **O-req3** The ARA shall be able to take-off with 100% MTOW at a 1500m runway.
- **O-req4** The ARA shall be able to land with 90% MTOW at a 1500m runway
- **O-req5** The ARA shall be able to be handled by the ground crew on code C airports as classified under the ICAO Aerodrome Reference Code Annex 14 Volume 1. [1]

Dimensional

- **D-req1** The aircraft shall have a wing span of maximum 36m to comply with airports defined in O-req5.
- **D-req2** The aircraft engines shall have a 5° clearance angle with respect to the main gear tire, plus an additional 15cm with respect to the ground to comply with CS-25. [2]

Performance

- **Pe-req1**: The minimum range of the aircraft shall be 1500km.
- **Pe-req2**: The aircraft shall have at least a 10% lower fuel burn on a 1000km trip when compared to the Embraer 175s.

Regulations

- **R-req1** The aircraft shall comply with the safety requirements as stipulated in CS-25 book 2. [2]
- **R-req2** The aircraft shall comply with the noise emission regulations under CS-36. [3]
- **R-req3** The aircraft shall comply with exhaust emission regulations under CS-34. [4]
- **R-req4** The aircraft shall comply with CS-25 performance requirements as stipulated in book 1 of CS-25. [2]
- **R-req5** The aircraft shall comply with CS-25 requirements for loiter. [2]
- **R-req6** The aircraft shall comply with CS-25 requirements for the maximum load factor. [2]

2.2 Mission Profile

The ARA is a commercial aircraft designed to carry a moderate amount of passengers over short distances. The mission of such an aircraft is visualised in figure 2.1. The main mission phases are take-off, cruise and landing. Because the designed aircraft is flying short distances, take-off and landing are relatively larger mission phases compared to longer range aircraft. An additional loiter phase can be seen which has been taken into account for safety reasons, according to R-req5.
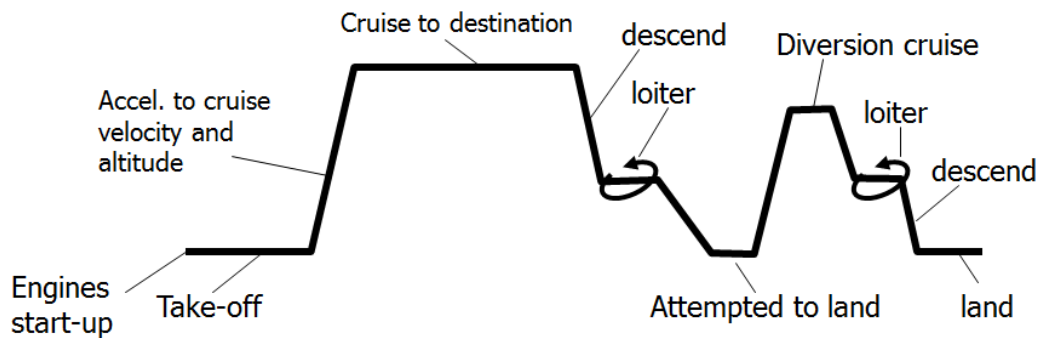
Figure 2.1: Mission profile [5]

3 | Market Analysis and Return on Investment

In this chapter main topics from the market analysis are discussed. In sections 3.1, 3.2 and 3.3 the market is analysed. This analysis is used to estimate how the financial status of 'The Company' will develop in the years to come, as can be seen in section 3.4. Finally, in section 3.5, recommendations are given.

3.1 Market Volume

Aircraft manufacturers perform annual global forecasts of the aviation market for the upcoming 20 years. These global market forecasts indicate the expected number of aircraft to be newly produced for the upcoming years and their distribution over the world regions. Data from Embraer [6], Bombardier [7], Boeing [8] and Airbus [9] is consulted. The considered aircraft manufacturers do not use the same regions and the same aircraft categories, but a global indication is derived from the predicted numbers. In this report single aisle aircraft are referred to as narrow-body aircraft, they are divided into regional and non-regional narrow-body aircraft. Regional aircraft predominantly transport 60-110 passengers over 500-2500km and its non-regional counterparts typically transport 150-250 passengers over 3000-6000km.

The main regions for the predicted need of regional aircraft are Asia Pacific (including China and India), North-America and Europe. Even though the predictions vary between manufacturers, they forecast a positive future for the regional aircraft market, with a need of about 2500 new regional aircraft till 2034.

The promising forecast for the regional aircraft market is supported by a study conducted by the European Regions Airline Association (ERAA). [10] The main findings of the study are that, while the amount of operations of regional aircraft is smaller than for non-regional aircraft, the scale of regional aircraft operations is substantial. Furthermore, regional aircraft provide the right capacity for many routes that do not justify the use of non-regional aircraft. Also, regional aircraft can compete favourably with the operating costs of non-regional aircraft; particularly for short distances. Finally, over 50% of the passengers in aviation travel distances under 900km which is in the regional aircraft segment.

The largest predicted market is for narrow-body aircraft. The following list shows the most important differences between the two with respect to their applications and feasibility. [10]

- Regional aircraft are not as restricted by airport and runway limitations due to a lower MTOW and aircraft size.
- Regional aircraft are financially more attractive for short range flights, because they are designed for flights over shorter ranges.
- While the market for regional aircraft is increasing, the market for the narrow-body aircraft is doing so more rapidly.

The difference in aircraft used with respect to the range is shown in figure 3.1. Market analysis showed another trend, non-regional aircraft are being replaced by regional aircraft on short haul flights. This has a positive effect on the market share for the ARA. [10]

In figure 3.1 a noteworthy deviation from the trend line at 1501-2000km is seen for regional jets, which indicates a niche that the ARA could fill. For this reason, the range requirement of 2000km is set.

3.2 Purchase Price & Achievable Market Share

There are many competitors in the regional jet market. However, only several new aircraft can be compared to the ARA due to the incorporated state-of-the-art technology, these are listed in table 3.1. [1]

Table 3.1 contains seven alphabetically listed turbojet aircraft. [11] [12] All of these aircraft are relatively new, so they will be flying for the next couple of decades. In order to be able to compete with these aircraft, the ARA should be a market leader in terms of performance and operating cost. One of the newest and most alike reference aircraft is the MRJ, which is still under development and expected to start delivering aircraft in 2017. This aircraft is highly advanced, but since it has not been taken into service yet, there is limited

---

[1]url: http://planes.axlegeeks.com [CITED: 23 April 15]
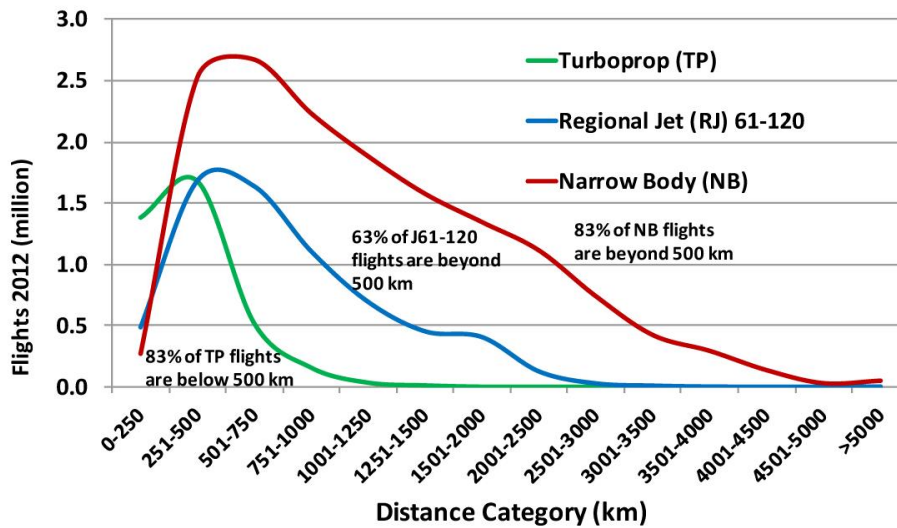
Figure 3.1: Flight distribution compared to the range [10]

Table 3.1: Overview of reference aircraft

Aircraft	Seats [-]	Distance [km]	Price [$ million]	Orders (delivered)	First Flight
Bombardier CRJ 700	66-78	2022	40.69	349(333)	May 1999
Bombardier CRJ 900	79-90	1982	44.7	306(268)	February 2001
Bombardier CS-100	108-133	2778	67.75	63(0)	September 2013
Comac ARJ-21	78-105	2222	n/a	252(0)	November 2008
Embraer E175	78-88	3241	n/a	315(175)	June 2003
MRJ (Mitsubishi Regional Jet)	78-92	1670	45.8	165(0)	2015(expected)
Sukhoi Superjet 100	68-108	1800	n/a	202(22)	May 2008

information available. Due to its similarity in specifications and being the newest reference aircraft to go into production, it is an interesting design and can be used as a reference aircraft for some of the aircraft parameters such as MTOW, OEW and purchase price.

Based on the values given in table 3.1 and the further analysis on the ARA, the purchase price is set at 42 million dollars. This is a 5% increase on the initial estimate, to cover increased costs in the R&D and production regions, due to a significant use of composites as well as other new technologies. The increased purchase price remains competitive for the market, as operational costs are projected to decrease by 10%. [13]

Table 3.1 shows the number of ordered and delivered aircraft by type. By designing the ARA as a technologically advanced aircraft with a design range of 2000km as well as a capacity of 90 passengers, to better cater wishes by the market, the ARA is expected to take a market share of 45%, becoming the leading aircraft in the regional aircraft market. This is comparable to the sales figures of the Embraer E-series. [12]

3.3 Life Cycle Costs

The life cycle cost is divided between purchase price and ownership cost. In section 3.2 the purchase price of the ARA is determined. Based on the purchase price and figure 3.2, the other life cycle costs are estimated.
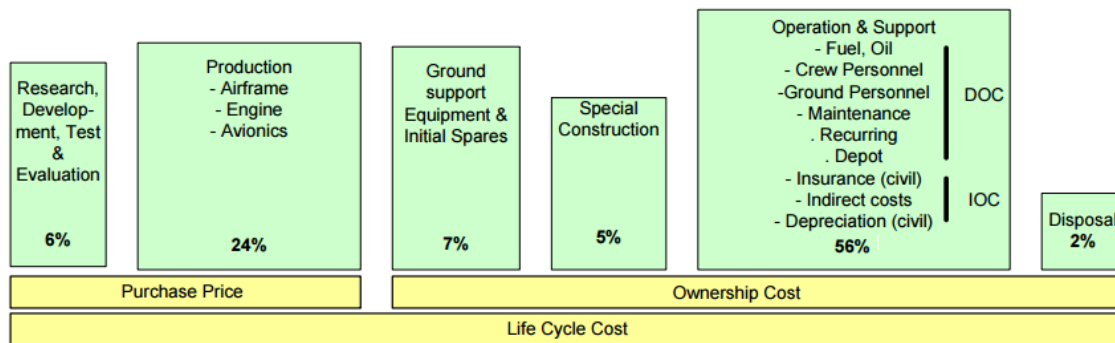
Figure 3.2: Cost distribution per life cycle phase for aircraft in general [14]

.

Purchase Price
The purchase price is divided in two components. The R&D costs form 20% and the production costs the other 80%. These are the cost 'The Company' deals with and total to 33 million dollars per aircraft. The costs for a customer are 27% higher, due to the profit margin 'The Company' envisions, this totals the civil purchase price to 42 million dollars per aircraft.

Ownership Costs
Ownership costs make up 70% of the life cycle costs. 80% of these costs are due to the Direct and Indirect Operational Costs (DOC & IOC). Note that these percentage are based on aircraft which are mostly made out of metals and less technologically advanced than the ARA. Therefore the R&D and Production costs are assumed to be 10% higher for the ARA, even though assembly costs are lowered due to the use of large composite parts, consequentially lowering the percentage of the ownership costs. The 5% for special construction is assumed to not be applicable for the ARA as there are no non-standard needs, such as liquid hydrogen storage as a fuel, as is later discussed in section 10.1.

In order to design a successful advanced aircraft, there are certain performance parameters that have to be evaluated. 'The Company' aims to have low operational costs, which primarily depend on costs due to crew of four, fuel and maintenance, as can be seen in figure 3.3.
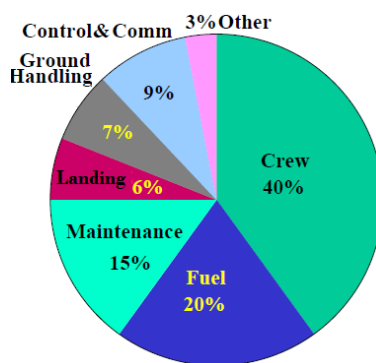
Figure 3.3: DOC per flight for aircraft in general [15]

The costs induced by fuel and maintenance can be influenced by the design of the aircraft, as such care is given to reduce these as much as possible, while maintaining a high reliability. Low operational costs result in a higher demand for the ARA. Since approximately 70% of the total costs are operational costs, reducing these costs is important. Having set the purchase price of one aircraft at 42 million dollars, which amounts to 33% of the costs for the aircraft operator (increased by 10%), the operational costs amount to 84 million dollars per aircraft per life cycle, without inflation. While the operational costs are not directly visible for potential buyers, parameters like fuel burn and maintenance give an indication of the aircraft expenditure. Therefore lowering these costs makes the aircraft more interesting for potential buyers.

3.4 Financial Forecast

In order for the newly designed aircraft to be successful, it does not only need to perform well, it also needs to be profitable for 'The Company'. The costs, revenues and profit over time are further evaluated as shown

in figure 3.4.

A full scale development phase of 7 years is planned for the ARA, running until 2022. The last year is the most costly as 3 to 4 full-scale aircraft will be tested. Up until this point 4.2 billion dollars is required. In 2021 the production of aircraft is expected to start at an initial rate of 1 aircraft per month. In the next year this will be ramped up to 4 per month and the following years to 7 per month. After the Break Even Point (BEP) is reached in 2027, the production will be further scaled up to its maximum of 100 aircraft per year, reaching the expected market share in 2034. In 2022 'The Company' will experience its largest debt of 4.1 billion dollars and in 2034, after saturating the market, 'The Company' will have established a maximum profit of 8.1 billion dollars. From 2022 until reaching the BEP in 2027 the budget for R&D is reduced to an annual 75 million. From 2027 onwards the R&D budget is increased to 125 million annually in anticipation of designing modified versions of the ARA. For this estimation it is assumed that aircraft are produced while they are already ordered as is common in aerospace industry in order to avoid the need of storage.
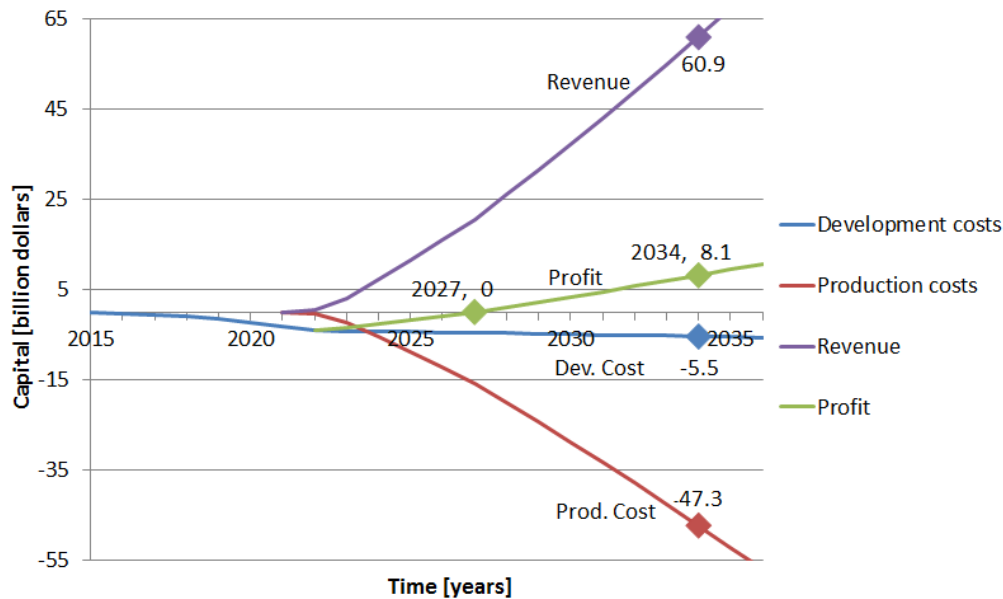
Figure 3.4: Capital flows during the project

3.5   Recommendations

It is concluded that the production rate requirement, which stipulates a production rate of 25 aircraft per month, is not necessary for the ARA. It would saturate the market within 4 years. Having a higher than necessary production rate would be detrimental for the profit of 'The Company' as more costs would be involved for such production facilities. As such a different rate is recommended, as can be seen in 3.4. At this rate the market will saturate in 2034 which is the end of the forecast and is projected in section 3.1. Another recommendation is to keep investing money in R&D to facilitate updates in the original design as well as new models which will allow 'The Company' to stay the leading player in the market, even after 2034. This enables 'The Company' to remain a positive stimulus for the contemporary and future economic climate, as is its policy.

4 | Design Philosophy

Aircraft design depends on many factors such as customer demand, safety protocols and economic constraints. In the design of an aircraft a clear design philosophy is required. This philosophy is necessary to produce an aircraft which will surpass the competitors in sustainability, maintainability, and ease of manufacturing and operating the aircraft. These points of attention will be improved by implementing the latest technologies and considering them throughout the whole design process. This chapter will elaborate on these considerations.

Cabin Comfort Passenger comfort is a important design consideration during the design of the ARA. The cabin should not only be attractive and innovative, it should also be quiet and comfortable to provide the most enjoyable flights for the passengers. The modern standard for cabin comfort should be met by having the cabin dimensions such that it caters for a large percentile of European men. Important cabin dimensions are seat width and seat pitch. The seat width is an important criterion for cabin comfort which is often overlooked by aircraft manufacturers. Offering seats with a greater width than the competitors can be a major advantage regarding the cabin comfort. Furthermore, attention should be paid to the quality of cabin air. It should be less pollutant than on current regional aircraft.

Sustainability As the aviation industry continues to grow, it brings with it an increasing responsibility to ensure that the impact on the environment is minimised. Therefore, sustainability is a major part of the design philosophy. Aircraft manufacturers are developing innovative engine technologies aiming at improving propulsion efficiency and thus reducing fuel burn and simultaneously reducing noise levels. The greatest gains in fuel burn reduction have come from improved engines. Featuring a state-of-the-art engine can significantly cut the fuel consumption. Attention should also be paid to the engine noise, since a quiet engine is pleasant for both the passengers and airport environment. Awareness of the human impact on the environment continues to grow, with one of the biggest contributors to climate change being CO_2. By featuring an advanced engine, the ARA will cut the emissions of greenhouse gases and contribute to a cleaner environment. Besides the engines, other technologies which will reduce the noise should be investigated. A reduction in weight also contributes to a more sustainable aircraft. The weight can significantly be reduced by using lightweight materials. However, notice should be given to make sure that the material, as well as its production technique, are sustainable (non-toxic). Finally, aerodynamic efficiency is an aspect which is of great importance. Companies are developing new technologies which can improve the aerodynamic efficiency significantly. Examples of these technologies are jet actuators, vortex generators and state-of-the-art winglets.

Operational Efficiency The final consideration which is part of the design philosophy is the operational efficiency. An aircraft with an improved operational efficiency will be more attractive for the market. The operational efficiency can be improved by minimising the turn-around times. Attention should be paid to an efficient cargo handling. Likewise, efficient taxiing is an important point, especially in the case of regional aircraft. Maintenance should as well be taken into account during the design.

5 | Project Process

In order to design the ARA first the functions of the aircraft have to be identified. This is achieved through a functional flow diagram in section 5.1 and a functional breakdown structure in section5.2 .

5.1 Functional flow diagram

The functional flow diagram can be seen in figure 5.1. The main function of the functional flow diagram is to discover the functions of the aircraft with respect to its environment. The flight of the ARA is divided in seven stages. Every stage is subdivided in different functions. The diagram shows the chronological order of the functions the aircraft must perform. During the design these functions have to be taken into account, to ensure that the aircraft is capable of performing the required functions.

5.2 Functional breakdown structure

In figure 5.2 the functional breakdown structure is shown. The main goal of the functional breakdown structure is to discover the functions of the different subsytems. These functions have to be taken into account to ensure that a feasible design is obtained.

1.0 Start-up aircraft — **2.0** Taxi — **3.0** Take-off — **4.0** Cruise — **5.0** Land — **6.0** Taxi — **7.0** Shut-down

Start → ... → Stop

1.0
- **1.1a** Tank fuel
- **1.1b** Load the payload
- **1.1c** Load the catering

1.2 Start engine — **1.3** Initialize subsystems — **1.4** Perform pre-flight check ...

2.0
- **2.1** Perform a push-back using the electrical motors
- **2.2** Taxi to runway
- **2.3** Brake before runway
- **2.4** Deploy high lift devices ...

3.0
- **3.1** Get clearance from ATM
- **3.2** Perform pre-take-off check
- **3.3** Taxi to the start of the runway
- **3.4** Perform last checks
- **3.5** Provide thrust
- **3.6** Deflect elevator for pitch-up
- **3.7** Lift-off
- **3.8** Retract landing gear
- **3.9** Check landing gear retraction (+ / -)
- **3.10** Retract high lift devices
- **3.11** Climb to cruise altitude
- **3.12** Check altitude (+ / -) ...

4.0
- **4.1a** Check cruise speed (+ / -)
- **4.1b** Decrease / Increase speed
- **4.2** Switch on auto-pilot
- **4.3** Apply heading
- **4.4** Check for heading at waypoints (-)
- **4.5** Check for last waypoint (+)
- **4.6** Switch off auto-pilot (optional) ...

5.0
- **5.1** Loiter (if needed)
- **5.2** Divert to another airport (if needed)
- **5.3** Start landing
- **5.4** Reduce thrust
- **5.5** Deploy high lift devices
- **5.6** Deploy landing gear
- **5.7** Deflect elevator for required pitch-up
- **5.8** Touch-down
- **5.9** Everything oke? (- / +)
- **5.10a** Provide thrust
- **5.10b** Brake
- **5.11** Deflect elevator for pitch-up
- **5.12** Lift-off
- **5.13** Retract landing gear
- **5.14** Make a go around

6.0
- **6.1** Retract high lift devices
- **6.2** Taxi to the right gate
- **6.3** Stop at the gate ...

7.0
- **7.1** Perform post flight check
- **7.2** Shut-down
- **7.3** Unload the payload ...

Figure 5.1: The functional flow diagram of the ARA
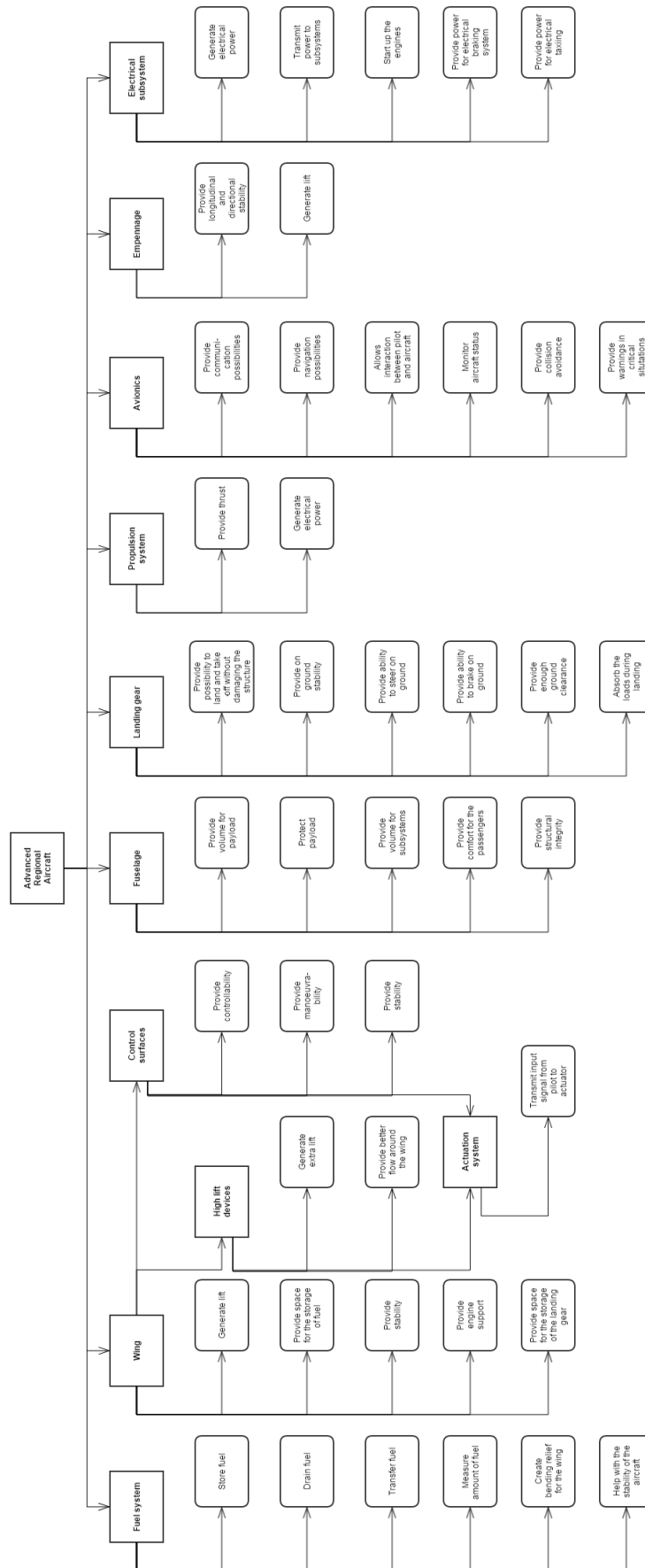
Figure 5.2: The functional breakdown diagram of the ARA

Part II

Preliminary Subsystem Sizing

6 | Configuration Design

The configuration of the ARA entails the engine type, engine location, wing position and aircraft configuration. In section 6.1 the trade-off is described. Section 6.2 discusses the feasible configuration options. In section 6.3 the selected configuration is given. The detailed trade-off to determine the configuration is given in [13].

6.1 Configuration Trade-off

The configuration for the ARA is determined by identifying the feasible configurations based on a literature study and then performing a trade-off for all of these configurations. The trade-off consists of six trade-off criteria. The trade-off criteria are based on the requirements discussed in chapter 2 and the competition discussed in chapter 3. The trade-off criteria are then given qualitative scores with respect to a conventional low-wing with GTF engines underneath the wings configuration. The trade-off criteria and the weights are the following:

- Structural weight
- Aerodynamic efficiency
- Fuel efficiency
- Noise
- Development risk
- Maintenance cost

- 1: extremely poor
- 3: poor
- 5: average
- 7: good
- 10: excellent

6.2 Design Configuration Considerations

Section 6.2.1 and 6.2.2 discuss the engine type and their location, respectively. Section 6.2.3 discusses the aircraft configuration and section 6.2.4 discusses the chosen wing position.

6.2.1 Engine type

From a literature study it is found that only the Geared TurboFan (GTF) is a feasible options for the ARA design. Two other initial promising engines are the Open Rotor Engine (ORE) and turboprop, but are discarded after further considerations. The option of Open Rotor Engines (ORE) is discarded, because the ORE is not feasible within 5-10 years which violates the requirements (see chapter 2). The option of the turboprops is discarded, because there has been limited development in the segment of the turboprops in the past decade and it is expected that there will be no significant improvements for turboprop for the next 10 years. [16]

6.2.2 Engine location

Four engine locations are considered. First of all, the engines can be mounted underneath the wing. Secondly, the engines can be mounted at the fuselage. Thirdly, the engines can be mounted on top of the tail. Finally, the engines can be mounted on top of the wing. The option of mounting engines on top of the tail is discarded, because the added weight and stability implications of this location outweigh the advantages. The option of mounting the engines on top of the wing is discarded, because it results in a heavier structure than for engine mounted underneath the wing due to an increased instability of the engine mounting. The length of the landing gear could decrease, since less clearance for engines is required. However, engine clearance is not a critical requirement to determine the landing gear length [2]. Therefore, it is concluded that engines mounted underneath the wing or mounted at the fuselage are the only feasible options for the ARA.

6.2.3 Aircraft configuration

Three aircraft configurations are considered for the ARA design: 3-surface configuration, canard configuration and conventional configuration. The 3-surface configuration requires much more development as a 3-surface design tends to add more weight than reduce weight. [17] Therefore, the 3-surface configuration has been discarded as it is deemed to add too much development risk and unrealisable in the allocated time span

---

[2] url: `http://adg.stanford.edu/aa241/propulsion/engineplacement.html` [CITED: 23 June 2015]

of 5-10 years. The canard configuration has been discarded due to the difficulty to achieve stall at the canard prior to the wing. Furthermore, the canard configuration provides less favourable stability characteristics for the ARA compared to other configurations. [18] Therefore, only the conventional configuration remains feasible for the ARA design.

6.2.4 Wing position

Three wing positions are considered for the ARA design: high-wing, mid-wing and low-wing. The mid-wing option is discarded due to it's inconvenience for passenger transport aircraft as the wing box may not progress through the middle of the fuselage and a solution for this problem leads to weight increase. The high-wing configuration is discarded because it is less stable than the low-wing configuration. Therefore, only the low-wing remains as a feasible option for the ARA.

6.3 ARA Configuration

Using the method discussed in section 6.1 and the feasible design configuration from the discussion in section 6.2 the conventional low-wing with GTF engines underneath the wings configuration is found to be the optimal configuration for the ARA. In figure 6.1 the configuration is shown.
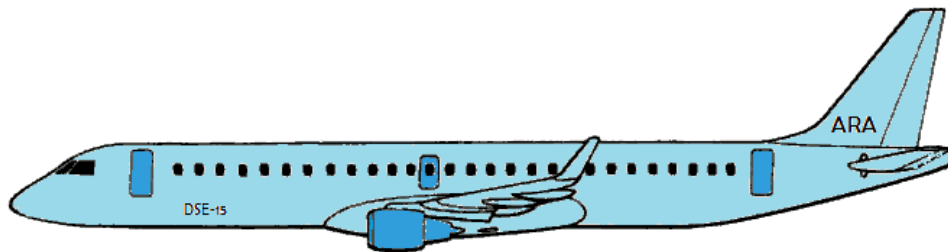
Figure 6.1: Selected configuration for the ARA

7 | Iteration Process

In this chapter the iteration method to estimate the weight of the ARA and the ARA's subsystems and the preliminary sizing of the wing, fuselage, landing gear, high lift devices, empennage and ailerons is described. Section 7.1 discusses the iteration method and section 7.2 presents the iteration results.

7.1 Iteration Method

The explanation of the iteration method below is based on figure 7.1.
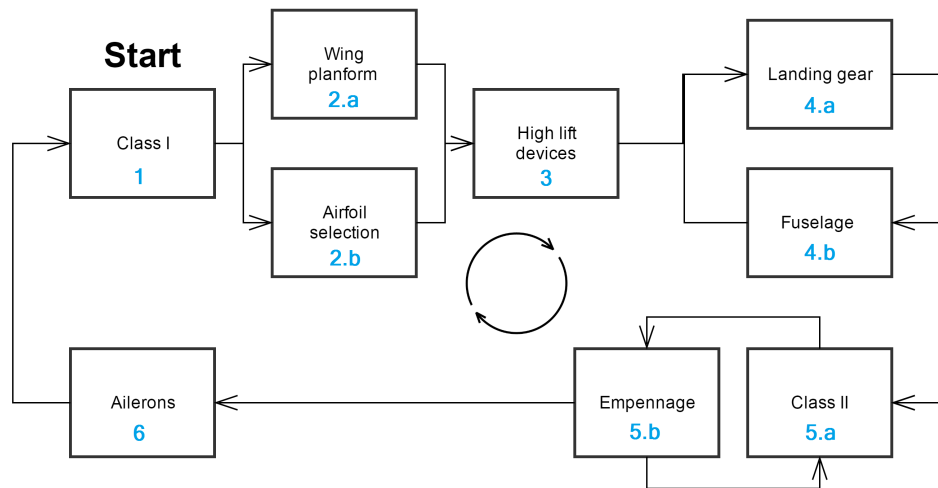
Figure 7.1: Iteration process

Step 1: A class I weight estimation is performed by using the method from [19]. The class I weight estimation uses as input the MTOW and OEW from reference aircraft (the data of the reference aircraft is plotted in figure 8.1), the effective aspect ratio, payload, design range and loiter time of the aircraft to determine the required fuel weight. From the class I estimation a first estimate of the OEW, MTOW and fuel weight and payload range diagram is obtained. Additionally, a wing loading versus thrust loading diagram is obtained, in order to determine the design point for the thrust and surface area. Inputs to generate the wing loading versus thrust loading diagram diagram are obtained from CS-25 [2]. A more detailed discussion of the method and the results of the class I weight estimation can be found in chapter 8.

Step 2: After the class I estimation, the wing surface area is updated so that it satisfies the wing loading design point obtained from the class I estimation. Using this wing surface area other wing plan form dimensions are determined such as the wingspan and root and tip cord. A more detailed discussion on the method and the results of the wing sizing can be found in chapter 9. The airfoil of the wing is selected simultaneously with the wing plan form sizing. The airfoil selection process is discussed in chapter 9.

Step 3: The next step is to size the high lift devices by using the parameters of the wing plan form and airfoil as input. The sizing and results of the high lift devices can be found in chapter 12.

Step 4: Using the MTOW obtained from the class I estimation, the wing planform dimensions and the position of the high lift devices, the landing gear is sized and positioned. It is checked that the landing gear can partially be stored in the wing, otherwise a redesign of the fuselage is required to satisfy the tip over requirement (the wheel track must be sufficient). To position the landing gear, also the clearance angle at take-off should be high enough, this requirement is satisfied by either increasing the landing gear height or to increase the kink at the end of the fuselage. The fuselage preliminary sizing can be found in chapter 11 and the landing gear sizing can be found in chapter 13.

Step 5: Next, the class II weight estimation is performed using the parameters obtained from the previous steps. From the class II estimation a weight estimation for the various subsystems is obtained. Furthermore, during the class II estimation the centre of gravity location for the aircraft and the subsystems of the aircraft are determined. Using the locations of the centre of gravity the empennage is sized so that it satisfies controllability and stability requirements, while remaining as small as possible. A change in the

empennage results in a change in weight and centre of gravity location. Therefore, an iteration is performed for the empennage sizing and class II weight estimation. The final results of the class II weight estimation can be found in chapter 8. More details on the empennage sizing can be found in chapter 14.

Step 6: The final step is the sizing of the ailerons. The inputs are obtained from the previous steps. More information about the sizing of the ailerons can be found in chapter 15.

The iteration loop is terminated if the difference of the parameters from the current loop and the previous loop are less than 1%, which is sufficiently accurate.

7.2 Results

Some intermediate values of the most influencing parameters which were obtained during the iterations are summarised in table 7.1. It is concluded that after one iteration the OEW difference between class I and II was less then 1%, however one additional iteration is required to also reduce the difference of other parameters beneath 1%. This leads to a OEW difference of 0.08%.

It is concluded that after two iterations the estimated OEW converged to 19945kg which is rounded to 20000kg. The MTOW converged to 34465kg which is rounded to 34500kg.

Table 7.1: Intermediate values obtained during iteration class I and II

Iteration	S [m^2]	T [kN]	c_r [m]	MAC length [m]	MTOW [kg]	OEW classI [kg]	OEW classII [kg]	Δ OEW [%]
0	107.81	118.25	5.92	3.89	35454	20776	20087	3.31
1	105.32	115.52	5.77	3.82	34634	20087	19961	0.63
2	104.86	115.02	5.77	3.82	34484	19961	19945	0.08
Final result	104.81	115.02	5.77	3.82	34465	19945	-	-

8 | Class I & Class II Weight Estimations

In this chapter the method and the results of the class I and class II weight estimation are explained. First of all, the methods of the class I and class II weight estimations are discussed in section 8.1. In sections 8.2 and 8.3 the results of the class I and class II weight estimations are presented.

8.1 Class I & Class II Methods

A class I weight estimation is performed according to the method from [19]. The first time the class I estimation is used, the OEW is determined from reference aircraft weights given in table B.1 in appendix B. The class I outputs are an estimated maximum take-off weight and fuel weight. During the iteration the OEW is obtained from the class II estimation as discussed in chapter 7. After the preliminary weight estimations a T/W-W/S diagram is constructed. From this diagram the required thrust and wing area is obtained. The thrust loading and wing loading have to meet the requirements for the different phases and conditions in flight. There are requirements for the stall speed, take-off, landing, cruise, climb and manoeuvring. The method used to calculate these requirements can be found in [20] and [21].

A class II weight estimation is performed according to the General Dynamics (GD) method described in [22]. The class II weight estimation calculates subsystem weights based on statistical data of reference aircraft. The required inputs for the class II weight estimation are obtained from the class I estimation, initial subsystem sizing (chapter 6 till 15) and reference aircraft data found in table B.1 in appendix B. The subsystem components which are calculated with the GD method are listed in table 8.3 in section 8.3. The GD method is based on metallic reference aircraft. Therefore, it is necessary to compensate for the use of composite materials which leads to a lower aircraft weight, if correctly designed. Three subsystems are mostly affected by the use of composites: the fuselage, wing and empennage. Therefore, the weights obtained from the class II estimation for these three subsystems are reduced. The weight of the fuselage is reduced with 15%[23][24], the wing weight is reduced with 10% [23][24] and the empennage weight is reduced with 20%. [24][25]

Furthermore, the centre of gravity locations of the subsystem components from the class II weight estimation are estimated. In order to estimate the aircraft's centre of gravity it is required to first identify the locations of the several subsystems with respect to a common reference frame. The aircraft's nose is chosen as the origin with the reference frame defined positive towards the tail. All the lengths in this section are defined from the nose of the aircraft. It is convenient for the empennage sizing (see chapter 14) to divide the subsystems in a fuselage group and a wing group. The centre of gravity of the components of the wing group are not only expressed relative to the nose, but also relative to the leading edge of the Mean Aerodynamic Chord (MAC) to evaluate the stability and controllability of the ARA (see section 9.3). The fuselage group consists of: auxiliary gear (aircraft emergency equipment), baggage cargo handling equipment, crew, electrical system, furnishing, fuselage, horizontal tail, instruments, avionics and cockpit electronics, oxygen system, paint and vertical tail. The centre of gravity locations are estimated from aircraft geometry from [26] and aircraft subsystem lay-outs from [22]. Additionally, the centre of gravity of the crew is estimated to be located in the middle of the passenger cabin as in the worst case the flight deck crew is located in the front of the aircraft and the cabin crew in the aft-galley. The centres of gravity of the fuselage group with respect to the nose are shown in table 8.3. The wing group consists of: air conditioning, pressurisation and de-icing systems, engines, engine controls, engine starting systems and nacelles, flight control system, fuel system, hydraulic and pneumatic systems, landing gear and the wing. The centre of gravity locations are estimated from aircraft geometry from [26] and aircraft subsystem lay-outs from [22]. Additionally, it is assumed that the centres of gravity of the air-induction system, engines, engine controls, engine starting systems and nacelles coincide and that the fuel system centre of gravity coincides with the wing's centre of gravity. The centres of gravity of the wing group are shown in table 8.3 as a function of the leading edge MAC distance of the wing from the nose (x_{LEMAC}).

8.2 Class I Results

The estimated weights of the ARA based on the design mission range of 2000km, wing area S and required thrust T are given in table 8.1. The mass of the fuel weight for the various aircraft mission stages is given

in table 8.2. Furthermore, figure 8.1 shows the regression line used to obtain the initial OEW for the class I weight estimation. The payload-range diagram for the ARA is shown in figure 8.2.

Table 8.1: Estimated weights and parameters of the ARA for a 2000km range after the final iteration

Parameter	Symbol	Value	Unit
Empty weight	W_e	19859	$[kg]$
Trapped fuel and oil weight	W_{tf}	86	$[kg]$
Operational empty weight	OEW	19945	$[kg]$
Fuel weight	W_f	5520	$[kg]$
Payload weight	W_{pl}	9000	$[kg]$
Maximum take-off weight	$MTOW$	34465	$[kg]$
Required thrust	T	115	$[kN]$
Wing area	S	105	$[m^2]$

Table 8.2: Fuel weight fractions the ARA

Flight phase	Fuel weight [kg]
Engine start and warm-up	345
Taxi	345
Take-off	172
Climb and accelerate to cruise	689
Cruise	2499
Descent 1	345
Loiter	709
Loiter climb and descent	517
Landing, taxi and shutdown	276
Total	**5520**

Payload-Range Diagram
In figure 8.2 the payload-versus range diagram of the ARA can be found. Point A indicates the harmonic range of the aircraft of 1500km, point B indicates the design mission range of the ARA of 2000km, point C indicates the maximum range of 2250km that can be obtained when the ARA takes off at MTOW with full fuel tanks and reduced payload and point D indicates the ferry range of 4136km.
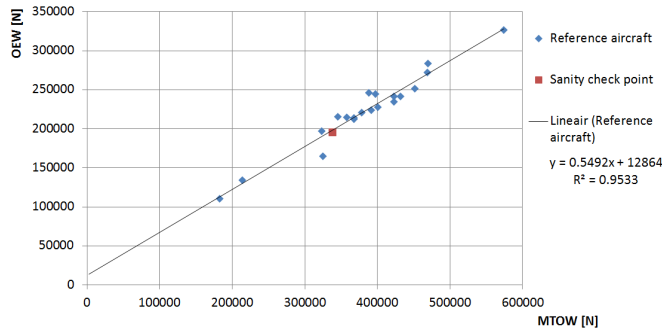
Figure 8.1: Graph MTOW versus OEW from reference aircraft including regression line and sanity check point
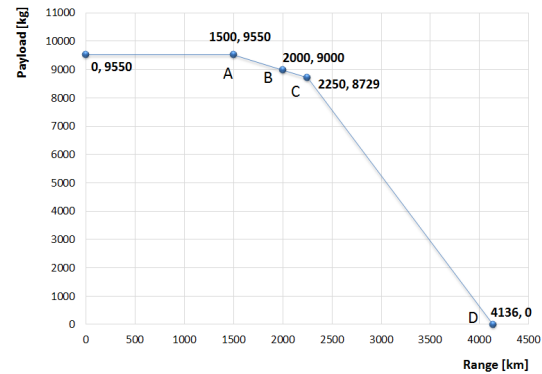
Figure 8.2: Payload versus range diagram

Wing-Loading versus Thrust-Loading Diagram
The class I estimation method also outputs the allowable wing loading (W/S) and the allowable thrust loading (T/W) as discussed in chapter 7. The resulting thrust and wing loading diagram can be seen in figure 8.3. For the design of an aircraft it is beneficial to have the highest wing loading and the lowest thrust loading, so in the diagram a design point as far to the bottom right as possible should be chosen. At that point both the thrust and wing area are the smallest, and thus are the engine and wings the lightest. The requirements limit the possible design space. For the ARA the design space is the marked area. The two optimal points are indicated with circles A and B. At circle B the lowest thrust is obtained and at circle A the lowest wing area is obtained. Design point A is chosen as the design point for the ARA, so that the wing area and thus the span is the smallest. Hence, the ARA is able to operate at smaller airports.

8.3 Class II Results

After the final iteration the estimated OEW of the aircraft converged to 19945kg, which results in a MTOW of 34465kg, which is rounded to 34500kg. The final weights of the different components obtained from the class II weight estimation can be found in table 8.3.
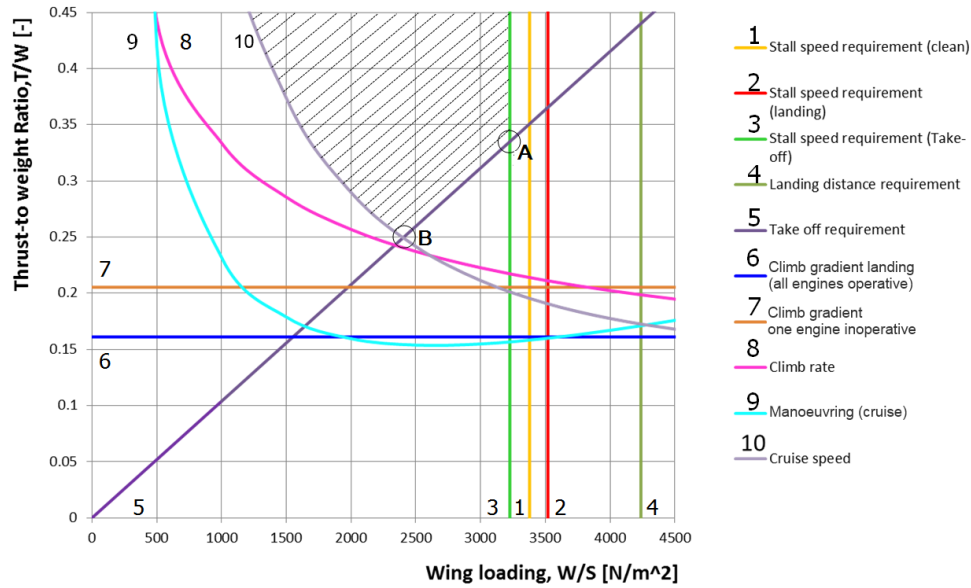
Figure 8.3: The thrust and wing loading diagram

Table 8.3: Subsystem weights and centre of gravity locations obtained from the class II weight estimation after two iterations.

Component	Weight [kg]	Centre of gravity [m]
Air-conditioning, pressurisation de-icing systems	1053	$x_{LEMAC} + 0.35$
Auxiliary power unit	452	35
Auxiliary gear	199	15.1
Caggage and cargo handling aft cargo bay	249	27.7
Crew	400	15.1
Electrical system	673	6
Engines	4900	$x_{LEMAC} - 2$
Engine control	62	$x_{LEMAC} - 2$
Engine starting systems	157	$x_{LEMAC} - 2$
Flight control systems	543	$x_{LEMAC} + 4$
Fuel system	290	$x_{LEMAC} + 1.3$
Furnishing	1698	15.1
Fuselage	3818	15.7
Horizontal tail plane	228	34.6
Hydraulic and pneumatic systems	208	$x_{LEMAC} + 5.4$
Instrumentation avionics and cockpit electronics	443	2
Landing gear	1079	$x_{LEMAC} - 0.3$
Oxygen system	77	15.1
Paint	139	17.88
Vertical tail plane	171	33.3
Wing	3105	$x_{LEMAC} + 1.3$
OEW	**19945**	15.7
Payload	9000	
Fuel	5520	
MTOW	**34465**	

9 | Initial Wing Sizing

In this chapter the sizing of the wing is discussed. Wing parameters such as the wing surface area, wing span and wing sweep are determined. Section 9.1 discusses the wing plan form selection. Furthermore, the airfoil is selected in section 9.2. Lastly, section 9.3 presents the overall dimensions of the wing.

9.1 Promising Wing Planform

Out of three different wing plan forms, presented in figure 9.1, 9.2 and 9.3, the best wing plan form is selected. The most promising wing plan form is determined to be the two-piece complex sweptback plan form as shown in figure 9.3. A more detailed version of the wing plan form can be found in appendix A. More information about the selection process of the wing plan forms can be found in de midterm report. [13]
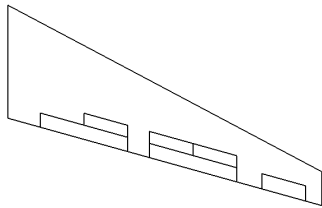
Figure 9.1: Simple sweptback wing plan form
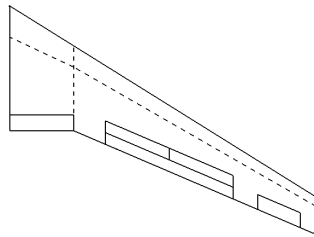
Figure 9.2: Two-piece simple sweptback wing plan form
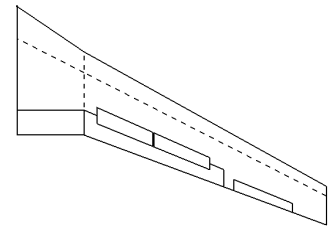
Figure 9.3: The selected wing plan form: two-piece complex sweptback planform

Several advantages of the selected wing plan form (figure 9.3) are listed below:

- It contains a zero sweep trailing edge near the fuselage. Therefore the flaps do not interfere with the fuselage and can be placed next to the fuselage.

- There is more usable space to store the flaps (the flaps can be placed next to the fuselage). This extra space is required to provide sufficient area for high-lift devices to obtain the required $C_{L_{max}}$ of 2.4.

- More lift is generated at the root because of the larger area which reduces the moment at the root caused by the lift (smaller arm). Additionally, more fuel can be stored at the root which relieves the moment due to lift. This all leads to a lighter wing structure

- More usable space will be available near the root to store the landing gear system.

- The plan form has a kink in the leading edge which creates a vortex that reduces the spanwise flow component. This results in the tip providing less lift which leads to a lower angle of attack at the wing tip and therefore tip stall is delayed.

9.2 Airfoil

For the airfoil selection a comparison between 71 airfoils is performed. These airfoils are selected based on airfoil data availability sampling an as large as possible broad spectrum of airfoil designs. The airfoil characteristics are analysed using an aerodynamics analysis tool (XFLR5) at a Reynolds number of $20 \cdot 10^6$. The characteristics that are used in the trade-off are t/c, $C_L/C_{D_{max}}$, $C_{l_{max}}$, C_{l_0}, M_{crit} and C_{m_0}.

Sizing parameters
The sizing parameters for the airfoil are the design lift coefficient at zero angle of attack $C_{l_{des}}$ and the critical Mach number M_{crit}. These parameters are calculated using the method provided in [27]. The incidence angle of the wing should have a maximum value of $\pm 3°$ due to structural constraints. Therefore, the C_{l_0} of the airfoil should be within this range of $C_{l_{des}}$ in order to be feasible. The critical Mach number is the free stream Mach number at which the flow over the airfoil reaches a speed of Mach 1. This Mach number has to be avoided as it increases the drag significantly. The aircraft will fly at Mach 0.8 [13], therefore the M_{crit} of an airfoil should be lower than this Mach number compensated with the wing sweep to be feasible.

Trade-off
The weights given to the different criteria are presented in table 9.1. They are set by their overall importance in the further sizing of the aircraft. $C_{l_{max}}$ is, for example, important for the high-lift devices. The drag in cruise (important for the aerodynamic efficiency) depends on t/c, $C_L/C_{D_{max}}$ and C_{l_0}. Furthermore, the aircraft should be able to fly at a cruise Mach number of 0.8, therefore M_{crit} has a high weight factor. C_{m_0} has only a small contribution to the aircraft performance and is therefore assigned a low weight. The sum of the weights is 100.

Table 9.1: Airfoil selection criteria and their corresponding weights

Criteria	t/c	$C_L/C_{D_{max}}$	$C_{l_{max}}$	C_{l_0}	M_{crit}	C_{m_0}	Total grade
Weight factor	15	15	20	23	22	5	100

The airfoils are analysed for their compliance with the requirements and their resulting grades based on their characteristics using a MATLAB program. The program performs this analysis for a range of 20° to 35° of sweep because at different sweep angles different airfoils are feasible or preferable to others. The Mach number is restricting and results in only 2 to 5 feasible airfoils at respectively, 20° and 35° sweep. The NACA-1408 airfoil is the most optimal airfoil at the lowest favourable sweep angle (27°) and will thus be used on the ARA. A lower sweep angle results in a lighter and more efficient wing. The airfoil characteristics can be found in table 9.2. The Mach Drag Divergence number (M_{DD}) is calculated using equation 9.1. [27]

$$M_{DD} = M_{cr} \cdot (1.02 + 0.08 \cdot (1 - cos(\Lambda_{0.25C}))) = 0.83 \tag{9.1}$$

Table 9.2: NACA-1408 characteristics at Re $= 20 \cdot 10^6$

Characteristic	$(t/c)_{max}$	$C_L/C_{D_{max}}$	$C_{l_{max}}$	C_{l_0}	M_{cr}	C_{m_0}	$C_{l_\alpha}[1/deg]$
	0.08	147	1.97	0.12	0.757	-0.026	0.110

9.3   Overall Wing Dimensions

This section presents the overall wing dimensions. The wing dimensions are subjected to iterations with respect to the wing surface area, root chord and wing span. However, this section only presents the final values. A detailed drawing of the wing plan form with dimensions can be found in figure A.1 in appendix A.

Wing Surface Area, S
In chapter 8 the wing loading is determined to be $3226N/m^2$ with an estimated MTOW of 34500kg. This leads to a total wing surface area, S of $105m^2$.

Aspect ratio, A
The geometrical aspect ratio of the wing plan form is determined to be 9, which is based on reference aircraft. The aerodynamic aspect ratio due to influence of the winglet extension increases with 20% to 10.8 (used in aerodynamic calculations). More information about the winglet design can be found in chapter 16.

Wing Span, b
Equation 9.3 is used to determine the wing span b. Note that the geometrical aspect ratio should be used, which leads to a total wing span of 30.7m.

Sweep Angle, Λ
As discussed in section 9.2 the chosen airfoil is feasible at a sweep angle higher than 27°. Due to structural considerations the sweep angle is determined to be 27°.

Incidence Angle, i
The incidence angle is determined using equation 9.2. Substituting the values for the NACA-1408 gives an incidence angle of 1.84°.

Taper, λ
Taper is the ratio between the root and the tip chord. The taper of the wing is calculated using equation 9.4. The tip and root chord are determined to be 1.73m and 5.77m, respectively. Therefore, the taper of the wing is 0.3.

$$i = \frac{(C_{l_{des}} - C_{l_0})}{C_{l_\alpha}} \tag{9.2}$$

$$b = \sqrt{A \cdot S} \qquad (9.3)$$

Dihedral Angle, Γ

The dihedral angle of the wing depends on i.a. the position of the engines, the length of the landing gear and stability requirements. In chapter 13 the dihedral angle is determined to be 3°.

Mid-chord

The chosen wing plan form consist of two parts, the connection between those parts, is called the mid-chord and is placed at a distance of 3m next to the root of the wing. The length of the mid-chord is determined to be 3.73m. This value is used in calculations like for example the fuel volume sizing.

Mean Aerodynamic Chord

The Mean Aerodynamic Chord (MAC) length, is determined by drawing an equivalent trapezoidal wing plan form that has the same wing area and tip chord as the original plan form. The equivalent root cord of the trapezoidal plan from is measured to be 5.30m. This leads to an equivalent taper ratio λ of 3.33. The length of the MAC is calculated to be 3.82m by using equation 9.5. The position on the wing is determined to be 2.87m from the root by measurement. [27]

$$\lambda = \frac{c_t}{c_r} \qquad (9.4)$$

$$MAC = \frac{2C_r}{3} \frac{1 + \lambda + \lambda^2}{1 + \lambda} \qquad (9.5)$$

Table 9.3: Parameters of wing lay-out

Characteristic	Value
Wing area	104.81m^2
Aspect ratio, geometric	9.0
Aspect ratio, aerodynamic (with winglets)	10.8
Wing span	30.71m
Root chord	5.77m
Tip chord	1.73m
Sweep	27.0°
Taper tip-root	0.3
Incidence angle	1.84 °
Dihedral angle	3.00 °
Mid chord length	3.73m
Distance mid chord <> root chord	3.00m
MAC length	3.82m
Distance MAC<> root chord	2.87m

10 | Propulsion Systems

In this chapter the propulsion system is discussed. In section 10.1 the engine specifications are given and the fuel type is discussed. In section 10.2 the fuel tank sizing is discussed. Finally, in section 10.3, it is checked if the requirement of fuel burn is fulfilled.

10.1 Engine and Fuel

The ARA will feature innovative GTF engines with state-of-the-art aerodynamic design and noise reduction technologies, which will significantly cut the fuel consumption, noise and operating costs. The architecture of a GTF provides unique advantages. The gearbox in a GTF allows the engine turbine to rotate at its most efficient speed, while the fan rotates slower at its optimum RPM. This leads to a reduction in fuel consumption of 16% compared to a current Turbofan. [28] The fan rotates at a lower speed, avoiding supersonic fan tip speeds which reduces the noise. Since the low pressure compressor of the engine is able to 'supercharge' the air before it enters the high pressure compressor (HPC), fewer HPC stages are required to accomplish the same work[3]. This allows for better maintainability of the engines for the aircraft operators. The specifications of the chosen engine, the PW1217G, are given in table 10.1[3].

Table 10.1: Engine parameters - PW1217G

Parameter	Value	Unit
Number of engines	2	—
Engine Weight	2450	kg
Engine thrust	76000	N
Bypass ratio	9:1	—
Specific fuel consumption	0.014	$\frac{g}{Ns}$
Fan diameter	1.4	m
Engine diameter (incl. nacelle)	1.6	m

The engine nacelles will have rear-edge chevrons. These sawtooth patterns are used for noise reduction. The edges smooth the mixing of the bypass air exiting the engine with the outside air, reducing turbulence which creates noise. The noise can be reduced up to $2dB$ by using chevron nacelles. [29] In the midterm report [13] a trade-off was performed to select the fuel type. The numerous challenges associated with fuel types such as LNG and LH_2 mean that they can only be viewed as a long term possibility. Therefore, jet fuel will be used on the aircraft.

10.2 Fuel Tank Sizing

After the fuel type is selected, the fuel tank can be sized. The required fuel at maximum range (including all the necessary reserves) is $5791kg$. At maximum range the most fuel is required, thus the $5791kg$ is equal to the maximum required fuel capacity. Using the density of jet fuel ($0.81\frac{kg}{dm^3}$) the required volume for the fuel tank is determined. When sizing the fuel tank it must be considered that 5% of the fuel tank must be left empty to account for the expansion of the fuel. Furthermore an extra 4% must be left empty to take into account the space taken by structures and systems like ribs and pumps. [27] Using these values a required fuel tank volume of $7.84m^3$ is obtained.

The fuel will be stored in the wing between the front and the rear spar. This is the most preferable place for the tank, because it is close to the engines and it will cause a bending relief for the wing. This will result in a lighter wing structure. The wingbox will have the function of tank to store the fuel. So the fuel will be stored between the spars and skins of the wing. These parts will be covered in a coating to make them resistant to the fuel.

The wingbox will act as the main fuel tank, leaving space for other subsystems such as the high lift devices. The flaps used on the ARA, double slotted Fowler flaps (see chapter 12), will take up 35% of the wing chord. Another 5% of the wing chord is reserved for control systems required for the flaps. [27] Therefore the rear spar will be placed at 60% of the wing chord measured from the leading edge. The front spar is typically located at 15% from the leading edge. [27]

---

[3]url:https://www.pw.utc.com/Content/PurePowerPW1000G_Engine/pdf/B-1-1_PurePowerEngineFamily_SpecsChart.pdf
[CITED: 21 May 2015]

Furthermore, the fuel tank will not span the entire length of the wing. The reason for this is that the tip has a higher risk of being hit by lightening strikes. [27] Therefore the fuel tank will only extend until 85% of the wing span for safety. At the root there has to be some space left for the landing gear. The landing gear is sized and positioned in chapter 13. From this sizing and positioning it can be concluded that there is still some space between the leading edge and the landing gear to store fuel. The fuel tank will be too large if all of the available space in the wing is used. As it is preferable to have the fuel closer to the tip than to the root (due to bending relief and safety) it is decided to start the fuel tank $0.65m$ away from the fuselage instead of right next to the fuselage. This results in a total fuel tank volume of $8.05m^3$ in the wing, which is sufficient to store all the required fuel. An additional fuel tank in the fuselage is not required. The final fuel tank size and lay-out can be seen in figure 10.1. The striped area indicates the fuel tank.
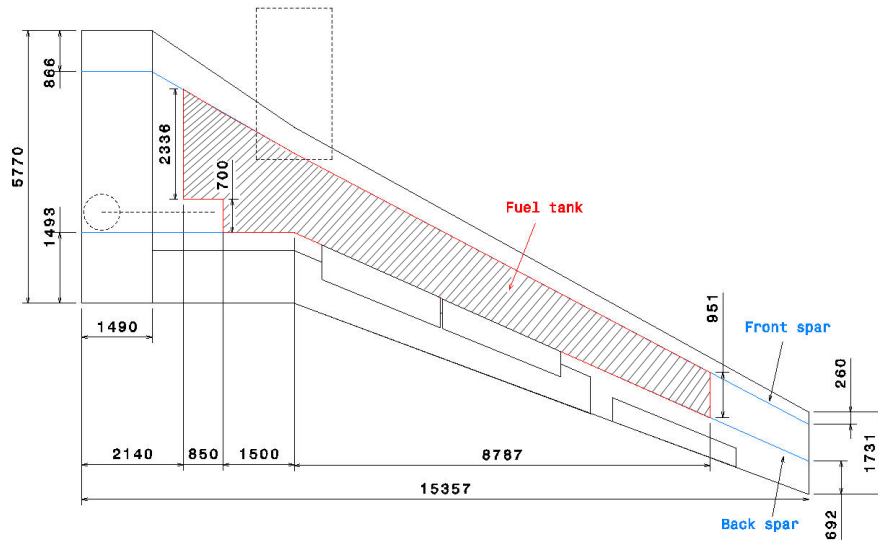
Figure 10.1: Final lay-out and positioning of the fuel tank

10.3   Fuel Burn Requirement

The requirement regarding the fuel burn is the following: The aircraft should have a 10% lower fuel burn on a $1000km$ trip when compared to a direct competitor which is in operation today. In this section it is calculated if the ARA complies with the requirement. The comparison is done with the Embraer E190 which features two turbofans (CF34). The engines on the aircraft are GTFs with a specific fuel consumption of $0.014\frac{g}{N\cdot s}$. The specific fuel consumption of CF34 is found to be $0.019\frac{g}{N\cdot s}$ [4]. The comparison is performed using the thrust at cruise and cruise speed. The cruise thrust of the ARA is calculated with equation 10.1 [5]. In this equation F_T is the thrust at cruise altitude, $F_{T_{sl}}$ the thrust at sea level, P_c the pressure at cruise altitude, P_{sl} the pressure at sea level, T_c the temperature at cruise altitude and T_{sl} the temperature at sea level.

$$F_T = F_{T_{sl}} \cdot \frac{P_c}{P_{sl}} \cdot \sqrt{\frac{T_{sl}}{T_c}} \tag{10.1}$$

From equation 10.1 a thrust of $29.6kN$ is obtained. The cruise speed of the ARA is $236\frac{m}{s}$, therefore the ARA travels a $1000km$ in $4236s$ (or $1.18hrs$). Using these values, the fuel burn is calculated to be $1744kg$. The fuel consumption of the Embraer E190 is found to be $1850\frac{kg}{hr}$ [6]. Since the Embraer 190 has the same cruise speed as the ARA, it takes the Embraer $4236s$ to travel a distance of $1000km$ [7]. This leads to a fuel burn of $2177kg$. Comparing the fuel burn values, it is calculated that the reduction in fuel burn is 20% in comparison to the Embraer 190. This implies that the requirement is fulfilled. In this calculation, the effect of winglets and weight reduction due to composites is not taken into account. This means that the calculation is rather conservative and the fuel burn will be reduced even more.

---

[4] url: `http://www.aircraftenginedesign.com/TableB3.html` [CITED: 18 June 2015]
[5] url: `https://www.grc.nasa.gov/www/k-12/Missions/Jim/Project1ans.htm` [CITED: 18 June 2015]
[6] url: `http://www.finnairgroup.com/group/group_9_11.html` [CITED: 18 June 2015]
[7] url: `http://www.embraercommercialaviation.com/AircraftPDF/E190_Performance.pdf` [CITED: 18 June 2015]

11 | Fuselage

In this chapter a preliminary sizing of the fuselage and fuselage lay-out is presented. Section 11.1 discusses the design philosophy used for the fuselage design and the possible configurations for the fuselage. Section 11.2 presents preliminary calculations on the fuselage design concepts and the design choice based on the preliminary calculations. Lastly, section 11.3 briefly summarises the chosen fuselage design concept and discusses further recommendations for the fuselage design.

11.1 Fuselage Configuration Options

In this section the different design options are discussed and non-feasible options are discarded. The fuselage is designed from the inside out, therefore the payload is the driving factor. Passengers and their luggage (cargo) are part of the payload. Several design options for both cargo and seating layouts are discussed. The fineness ratio of the fuselage is used as a low fidelity method to determine the aerodynamic efficiency of a cylindrical fuselage. It is defined as the length of the fuselage divided by its diameter. Optimal fineness ratios are in the range of 8-10. [26]

11.1.1 Aisles

A double or more aisle configuration for 90 passengers will result in an aerodynamically inefficient fineness ratio compared to the single aisle configuration. Therefore, a single aisle configuration will be used for the ARA.

11.1.2 Abreast Seating

For a single aisle layout two abreast seating options have been identified: four or five abreast in a 2-2 or 2-3 configuration, respectively. A three abreast (1-2) configuration would result in a low aisle height, less storage room below deck and a non-feasible fuselage length of more than 40 meters. Six abreast seating (3-3) would result in a wide fuselage diameter and due to the low passenger number an aerodynamically inefficient fineness ratio. [30] A 2-3 or 2-2 layout offers a fineness ratio which is both aerodynamically and structurally more efficient than the previously mentioned configurations, providing enough headroom in the cabin and sufficient storage possibilities beneath the deck or behind the passenger section. Therefore, only a 2-2 or 2-3 layout is viable for the application of the ARA.

11.1.3 Cargo Placement

Cargo may be placed in holds beneath the floorboards of the cabin (Cargo Under (CU)) or in the rear of the fuselage behind the cabin in a separate cargo segment (Cargo Tail or CT). Accessibility, both to and within, the cargo holds are key factors in choosing the layout. Combined CU and CT configurations (Combined Cargo or CC) must also be considered. Storing cargo only in the tail when using the 2-3 seating configuration is not an efficient solution, as a lot of space in the bottom of the fuselage will go unused. This design option is therefore eliminated.

11.1.4 Cargo Type

Cargo can be transported in standardised containers (Unit Loading Devices (ULD) and pallets) or as loose cargo in the cargo hold.

The benefits of using a standardised system is the short ramp loading times and better manifest overview. The smallest available container is the LD3-45, which is made specifically for the A320 series aircraft. Implementing this container in the ARA would result in either an inefficient fineness ratio or insufficient aisle headroom. Pallets have the same width as containers and therefore will have either an inefficient fineness ratio or have suboptimal volume usage when compared to loose cargo. Custom sized pallets are cheap to manufacture, but require a straight cargo bay cross section (i.e. no taper) and ground handling equipment at all operated airports. Since the ARA is a regional aircraft it may often be operated at smaller airports with fewer facilities. Therefore, pallets will not be used in the ARA. Custom containers are a possibility if they are used in a straight section of the fuselage. Loose cargo is a more time consuming loading option, but offers a more efficient usage of the cargo hold volume when compared to containers. This cargo type does not require any additional investments by the airport in terms of cargo handling equipment.

11.1.5 Classes, Galleys and Lavatories

In the interior design of the ARA the option of two classes is provided. This allows airliners to choose between a single economy-class layout or a combined business- and economy-class. The ARA has a total of two lavatories and two galleys (one of each at the front and rear of the cabin), which opens the possibility to cater for a two class configuration.

11.1.6 Cross-sectional Shape

A variety of cross-sectional shapes are considered for the fuselage such as the circular, oval and double bubble shapes. From an analysis of the cross-sectional shapes it is found that the circular cross-sectional shape is the best shape for the ARA design. [13] The circular shape has a better aerodynamic and structural efficiency and is easier to manufacture.[30][26][31] The disadvantage of a circular fuselage is the sub-optimal usage of the internal volume. Especially in smaller diameter aircraft the seats may not be placed flush to the inner wall. However, during the analysis of the cross-sectional shapes it was found that the sub-optimal usage of internal volume is not a driving consideration and that the aerodynamic, structural and manufacturing advantages of the circular shape are more driving. Therefore, it is decided to use a circular cross-sectional shape for the ARA fuselage.

11.2 Preliminary Fuselage Concepts

For the fuselage design the inside out philosophy is used. Based on the design options discussed in section 11.1, there are five remaining feasible concepts and by using a trade-off one final concept is selected. There are two possible configurations of abreast seating: four or five abreast. For the four abreast seating, cargo may be stored either in an extra tail section (2-2 CT), under the floorboards (2-2 CU) or in a combined configuration (2-2 CC). The five abreast seating configuration also has two options for cargo storage; under the floorboards (2-3 CU) or in a combined configuration (2-3 CC).

In appendix B the relevant ratios and dimensions of reference fuselages are presented, these are obtained from statistical and empirical sources. In subsection 11.2.2 the mid section cross-section is sized. Next an optional cargo hold is sized in the rear, between the passenger and tail section. In subsection 11.2.3, the cockpit and tail sections of the two fuselages are sized.

11.2.1 Fuselage Design Parameters

To guide the reader through the sizing process the naming convention used for the various parameters is presented in figure E.2 in appendix E. In tables B.3 and B.4 in appendix B parameters and dimensions are given for reference aircraft. Additional parameter descriptions are found in the list of symbols.

11.2.2 Cabin Sizing

The cabin is defined as the seating area in the fuselage (excluding the galleys and lavatories). It is sized using seat dimensions and pitch obtained from reference data presented in table B.2 in appendix B. The cabin dimensions are sized such that it caters for the 95th percentile of European men. The seat pitch is determined from the reference aircraft in table B.3 in appenix B and is chosen to be 762mm, providing adequate comfort to the passengers during the short flight duration. [13] The total interior width follows from the seat width and spacing between them. The length of the mid section fuselage depends on the abreast seating configuration, the seat pitch and the required number of rows.

The cabin dimensions are sized and are shown in table 11.1. The outer diameter for a configuration is obtained by adding twice the wall thickness of the fuselage to the inner diameter. An estimation of the wall thickness is obtained from [32].

11.2.3 Cockpit and Tail Sizing

The lengths of the forward and aft fuselage sections ($l_{cockpit}$ and l_{tail}) are initially sized using respective fineness ratios. Reference data presented in appendix B, table B.3 is used to determine the tail fineness ratio. A relation between the Mach Drag Divergence number (calculated in section 9.2) and the cockpit

Table 11.1: Preliminary sized cabin dimensions in [mm]

	4-Abreast (2-2)	5-Abreast (2-3)
Aisle width	500	500
Cabin height	2000	2000
Cabin interior width (inner diameter)	2780	3270
Total furnishing thickness	120	130
Fuselage exterior diameter	2980	3530
Gap between wall and seat	25.4	12.7
Seat pitch	762	762
Seat width	470	470
Elbowroom	51	51

fineness ratio is used to determine the cockpit length[8]. In table 11.2 the lengths for each configuration are presented.

The initial value for the tail angle is determined to be 12 degrees if a 2-3 configuration is chosen and 14 degrees if a 2-2 configuration is chosen. [26] This distinction is made, because the 2-3 configuration has a smaller fuselage length behind the main landing gear than a 2-2 configuration. This increases the chance of a tail-strike for the 2-2 configuration and therefore a larger initial value for the tail angle is chosen for the 2-2 configuration.

11.2.4 Fuselage Subcomponent Sizing

In the following section the performance of the four remaining concepts is evaluated with respect to cargo capacity, available subsystem volume and relative mass. The relevant equations and assumptions are stated, in table 11.2 the dimensions are presented for the remaining configurations.

Cargo Hold Length
The required cargo volume is necessary to determine the cargo hold lengths. The required cargo volume is calculated with a luggage density of $200\frac{kg}{m^3}$ and 25% of unused space. [26] The maximum cargo mass is already determined in section 8.2 and is $1900kg$. This requires a cargo volume of $12.7m^3$. Dividing the required volume with the cross sectional area of the cargo hold results in the length of the cargo hold (l_{cargo}).

CU Cargo Hold Cross-Sectional Area
In case of a cargo hold under the floor the cross-sectional area of the space under the cabin floor is calculated and then multiplied by a factor of 0.85 to take into account non-usable space beneath the cabin floor such as the space required for subsystems.

CT Cargo Hold Cross-Sectional Area
For tail section cargo it is assumed that the cabin floor is extended into the cargo hold. Therefore the available area is equal to the cabin area. If cargo is to be stored in the tapered tail section of the tail a reduced area is available.

Subsystem Volume
The subsystem volume is the total volume underneath the cabin floor of the non-tapered fuselage minus the available cargo hold volume underneath the cabin floor.

Total Fuselage Length
The total fuselage length can be calculated with equation 11.1, where $l_{g,l}$ is the additional length due to the presence of galleys and lavatories. For all the configurations it is assumed that $4m$ of fuselage length is required to accommodate the galleys and lavatories. Finally, in case of an additional tail cargo hold, the required cargo hold length is added to the total length. Note that the calculated length is conservative as it is assumed that the different sections do not overlap.

$$l_{fus} = l_{cockpit} + l_{cabin} + l_{g,l} + l_{cargo} + l_{tail} \tag{11.1}$$

Fuselage Mass
A sensitivity analysis is performed to determine the change in mass due to an increase in fuselage diameter. Mass is directly proportional to the volume of the fuselage structure, assuming a material of constant

---
[8]url: http://adg.stanford.edu/aa241/AircraftDesign.html [CITED: 4 June 2015]

density is used. Therefore, the volume increase of the structure of the 2-3 configuration relative to the 2-2 configuration is calculated.

The volume is calculated by multiplying the surface area of the two fuselages with the skin thickness. The mid section is modelled as a cylinder, the cockpit and tail section are modelled as cones. It is assumed that due to pressurisation stresses a 1% increase in fuselage diameter increases the required skin thickness by 1%. The 2-3 configuration has a 17% larger diameter compared to the 2-2 configuration which will act as the reference. In table 11.2 the increase in fuselage mass is presented for the 2-3 CU and 2-2 CT with respect to the 2-2 CC which is the lightest option.

Concept Parameter Calculations

The values calculated in this section are summarised in table 11.2.

Table 11.2: Concept Parameter Calculations

Parameter	Unit	2-2 CT	2-2 CC	2-3 CU
Inner diameter	m	2.78	2.78	3.27
Outer diameter	m	2.98	2.98	3.53
Area above floor	m^2	4.97	4.97	5.74
Area under floor	m^2	1.10	1.10	2.66
Tail cargo section length	m	3.30	2.00	-
Belly cargo section length	m	-	5.90	8.20
Mid section subsystem volume	m^3	22.90	16.90	30.80
Cockpit fineness ratio	m^3	1.60	1.60	1.60
Cockpit section length	m	4.80	4.80	5.50
Tail fineness ratio	-	2.70	2.70	2.70
Tail section length	m	8.10	8.10	9.40
Total fuselage length	m	37.60	36.30	32.60
Fineness ratio	-	12.60	12.20	9.40
Tail angle	deg	14	14	12
Increased fuselage mass	%	4.43	0	16.90

2-3 CU This design option is discarded since it is less efficient than either 2-2 configuration, both aerodynamically (larger cross sectional area) and structurally, as displayed in table 11.2.

2-3 CC Since it is possible to store all of the cargo in the belly cargo holds with a 2-3 configuration it is superfluous to design an additional fuselage section to hold extra cargo. The 2-3 configuration with an additional tail cargo section is therefore eliminated from the considered design options.

2-2 CU This design does not have the required cargo volume therefore it is not a feasible design option.

2-2 CC The total fuselage length is 1.3m shorter than for the 2-2 CT configuration which allows for a more aerodynamic design. However, the required cargo hold below the cabin floor is $5.5m$ long and just 0.5m tall which impedes the ground crew accessibility during loading of the cargo. This can be solved with extra cargo doors, which in turn leads to a heavier structure. Additionally there is $6m^3$ less volume available for subsystems in the fuselage. It is decided that a design with cargo under the floorboards with a 2-2 configuration leads to an inefficient cargo hold in terms of weight and ground operations, therefore eliminating it as a feasible design option.

2-2 CT This configuration shows a slightly larger structural mass due to the increased fuselage length. In chapter 14 it is calculated that despite the tail-heavy cargo compartment, stability and controllability requirements are met for this configuration.

11.3   Design Choice

The final design choice is the 2-2 CT configuration with all the cargo stored in an additional cargo section behind the cabin in the tail section. Following the selection of the seat and cargo configuration a detailed study is performed to size and position the galleys, emergency exits, cabin crew seats and lavatories.

11.3.1 Cabin Layout

The interior space of the fuselage is to be optimised. Initially 23 rows of seats were planned which would accommodate two extra passengers. Removing two seats from the last row leaves room for a more compact rear galley and layout. In figure E.2, appendix E the proposed layout of the cabin is presented.

Emergency Exits
Airworthiness regulation CS 25.807 [2] determines the dimensions and number of emergency exits. There must be at least two exits on each side of the aircraft, of which one must be a type I (or larger). For logistical reasons two type I doors and two type A doors have been selected. Where the type A doors provide comfortable embarking for the passengers and the type I doors complete the CS 25.807 safety requirement.

Galleys and Lavatories
Two galleys and two lavatories will be used, one on each end of the cabin due to the design choice of implementing the option to use a 2-class configuration (section 11.1). The dimensions of the lavatories are obtained from [26]. The galley dimensions are based on reference data [26] and standard trolley dimensions are obtained from a manufacturer [9].

Cabin Crew Seats
Cabin crew sits on foldable seats near the galleys in the front and rear of the cabin. The dimensions are roughly estimated since seat sizes are not widely available.

All dimensions of the interior elements are presented in table 11.3. Length is defined in the longitudinal direction of fuselage, width is defined in the transverse direction of fuselage. All other dimensions are discussed in previous sections, see tables 11.2 and 11.1 for more details.

Table 11.3: Dimensions of cabin interior fittings in [mm]

Item	Width	Length
Galley	762	915
Trolley	300	750
Lavatory	915	915
Type 1 Exit		610
Type A Exit		1067
Crew Seat	410	550

Taking the previous dimensions into account, the lengths of the forward and aft utility sections, consisting of the galley, lavatory and exits, can be accurately sized. Two seats are removed from the 23rd row to meet the required number of passengers. The two remaining seats are to be incorporated in the aft galley section of the fuselage. In order to reduce the aft cargo section, part of the tail is utilised as a cargo hold. Using up to 1.8m of the tail cone section to store cargo enables a 1.3m reduction of the aft cargo section. Due to the fact that cargo is stored in the tapered section of the tail it is not feasible to use ULDs, custom cargo containers or pallets. Combined with the optimised galley layout this offers a reduction of 1.6m of the total fuselage length. The results are shown in table 11.4. As the cockpit and tail section sizing is based on reference aircraft these respective lengths may change as more detailed sizing methods are performed.

Table 11.4: Dimensions of forward and aft galley in [mm]

Item	Length
Cockpit	4530
Forward utility area	275
Cabin	16765
Aft utility area	2240
Cargo Section	2000
Tail	8050
Total fuselage	35760

---

[9]url: `http://www.worldtravelcateringexpo.com/__novadocuments/5039` [CITED: 21 May 2015]

12 | High-Lift Devices

In this chapter the preliminary design of the high-lift devices is presented. In section 12.1, the method used to estimate the types and size of the high-lift devices is discussed. In section 12.2 the results from the high-lift device sizing are presented.

12.1 Sizing Method

In this section the general outline of the high-lift device sizing and assumptions are discussed. The high-lift devices are sized by using the method presented in [27] and will not be discussed in detail in this report.

The Data Compendium (DATCOM) method is used to calculate 3D wing properties in clean configuration based on the chosen airfoil and wing planform discussed in chapter 9. The DATCOM method is found to be valid for Mach numbers between 0.2 and 0.6. Therefore, the free stream Mach number is taken to be 0.2, as the take-off and landing speed are close to this value. A change in this value would not have a significant change on the wing properties, as long as this value stays between 0.2 and 0.6 due to compressibility. The landing and take-off speeds have been calculated from the specified runway length and the method stipulated by [19]. The Reynolds number is evaluated for this speed and is different from the Reynolds number found in chapter 9. The required 3D wing parameters in clean configuration for the high-lift device sizing are the $C_L - \alpha$ slope $C_{L\alpha_{clean}}$, the maximum lift coefficient $C_{L_{max,clean}}$, the stall angle $\alpha_{s,clean}$ and zero-lift angle of attack $\alpha_{0L,clean}$. The input parameters for this method are obtained from chapter 9. Furthermore, the DATCOM method requires the airfoil efficiency factor η which is taken to be 0.95 because the lift gradient as function of Mach number obtained from experimental data is not available, thus reference data was used. [27] Lastly, the aerodynamic aspect ratio is increased by 20% during the calculations of the DATCOM method to account for winglets based on [27]. According to [27] this is a good assumption to properly design winglets.

In order to size the high-lift devices the required increase in lift during landing and take-off has to be determined. $C_{L_{max, land}}$ and $C_{L_{max, TO}}$ are obtained from the Class I weight estimation in chapter 8 and are 2.4 and 2.2, respectively. The maximum landing weight is taken to be the maximum take-off weight such that a safety factor is included to account for the most extreme case. The $C_{L_{max, land}}$ and $C_{L_{max, TO}}$ already include the landing and take-off distance requirements. Therefore, the runway length is implicitly included in the high-lift device sizing presented in this chapter. The required $\Delta C_{L_{max, land}}$ for landing is 0.84 and the required $\Delta C_{L_{max, TO}}$ for take-off is 0.63. Note that $\Delta C_{L_{max, land}}$ and $\Delta C_{L_{max, TO}}$ are increased by 5% to account for the negative lift caused by the horizontal tail to trim the aircraft. [27]

The required high-lift device type and it's dimensions are first sized for landing. The method calculates the maximum lift coefficient $C_{L_{max,land}}$, the $C_L - \alpha$ slope $C_{L\alpha_{flapped}}$, the stall angle $\alpha_{s,land}$ and the zero-lift angle of attack $\alpha_{0L,land}$. The input parameters based on the wing plan form are obtained from chapter 9 and input parameters dependent on the type of high-lift devices are obtained from [30]. Leading edge flaps are not taken into consideration as the contribution to the lift characteristics is minimal. Leading edge flaps are mostly used to prevent leading edge stall. If at a later stage in the design it is found that leading edge devices are required it is still possible to implement them. However, this will increase the weight and complexity of the flap system and is therefore not desirable.

When the aircraft is in take-off configuration, the high-lift devices are not fully deployed. To take into account this partial deployment a lower $\Delta C_{L_{max}}$, about 60-80% of those calculated for the landing configuration should be used. [27] As not enough details of the high-lift device systems are known yet at this stage of the design, an average value of 70 % is assumed. The same approach is used as for the landing configuration and the method calculates the maximum lift coefficient $C_{L_{max,TO}}$, the $C_L - \alpha$ slope $C_{L\alpha_{flapped}}$, the stall angle $\alpha_{s,TO}$ and zero-lift angle of attack $\alpha_{0L,TO}$.

Lastly, the tail-strike angle should be evaluated for the angles of attack during landing and take-off. For regional aircraft the angle of attack during take-off and landing is generally in the range of 10-14°. [27] If it is found that the required angle of attack is too large, a larger flap area or more complex high-lift devices are required.

12.2   High-Lift Device Characteristics

From the method discussed in section 12.1 it is found that in order to comply with the required maximum lift coefficients during landing and take-off configuration and tail-strike requirements a double-slotted Fowler flap is required. The results of the high-lift device sizing for a double-slotted Fowler flap are given in table 12.1. In figure 12.1 the C_L-α plots for clean, landing and take-off configuration are shown and the required C_L for clean, landing and take-off configurations are indicated. As can be seen in figure 12.1 the $C_{L_{max}}$ for landing and take-off configuration is much larger than required. However, this is necessary in order to stay in the angle of attack range of 10-14° for the landing and take-off configurations.
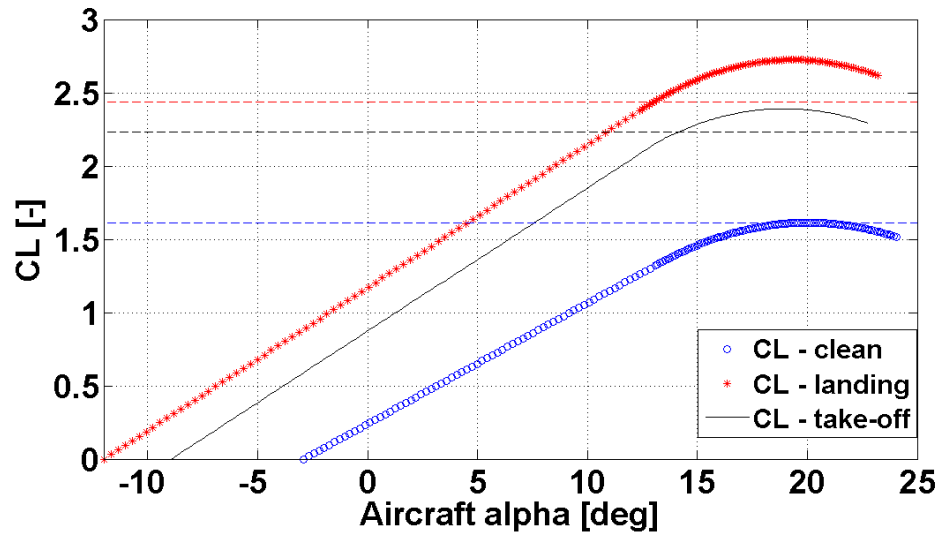
Figure 12.1: C_L-α curve

Table 12.1: High-Lift Device sizing results

Parameter	Value	Units
$C_{L\alpha_{clean}}$	4.7	$\left[\frac{1}{rad}\right]$
$C_{L\alpha_{flapped}}$	5.6	$\left[\frac{1}{rad}\right]$
$C_{L_{max\ clean}}$	1.6	$[-]$
$C_{L_{max\ land}}$	2.7	$[-]$
$C_{L_{max\ TO}}$	2.4	$[-]$
$\alpha_{0L,clean}$	-2.9	$[deg]$
$\alpha_{0L,land}$	-12.0	$[deg]$
$\alpha_{0L,TO}$	-8.9	$[deg]$
$\alpha_{s,\ clean}$	20.0	$[deg]$
$\alpha_{s,\ land}$	19.3	$[deg]$
$\alpha_{s,\ TO}$	18.9	$[deg]$
$\Delta C_{L_{max,\ land}}$	0.84	$[-]$
$\Delta C_{L_{max,\ TO}}$	0.63	$[-]$

13 | Landing Gear

In this chapter the designing, positioning and sizing of the landing gear of the ARA is described. First, the positioning of the landing gear is determined in section 13.1. The sizing of the landing gear is discussed in section 13.2. This includes determining the static and dynamic loads and choosing the tire type and tire dimensions. Thirdly, green taxiing is discussed in section 13.3. Finally, recommendations are given regarding the landing gear design in section 13.4.

13.1 Positioning

In this section the position and the height of the landing gear are determined. The position and height are mainly determined by requirements, which prescribe enough ground clearance for the entire aircraft and prevent tip-over during operation, and the centre of gravity position of the total aircraft. The requirements which the aircraft and landing gear must fulfil are stated below.

- **Overturn angle:** The wheel track has to satisfy two overturn angles. If these angles are not big enough the aircraft will easily roll over during a turn or due to cross wind. The first angle is shown in figure 13.1, the second angle is shown in figure 13.2, in which h_{cg} is the distance between the ground and the cg position. Both these angles have to be larger than 25°. [33]

- **Take-off clearance:** During take-off there has to be enough clearance between the fuselage and the runway. The clearance height H_c as shown in figure 13.3 is typically between 0.2-0.5m. For the ARA this clearance height is set at 0.3m. Furthermore, the clearance angle α_c in this figure is typically 12-16°. [33]

- **Tip-over angle:** When the aircraft is loaded on the ground it may not tip-over to the back. So the centre of gravity position of the aircraft may never lie behind the main gear. [33] The most aft center of gravity location occurs when the cargo is loaded at the back of the aircraft and the passengers all board the aircraft from the back. Typically, the angle shown in figure 13.4 is around 15° when the aircraft is loaded for take-off. [34] Therefore, a requirement for the ARA is imposed that this tip-over angle has to be at least 15° before take-off and the most-aft centre of gravity position may never lie behind the main gear.

- **Engine ground clearance:** When the aircraft is on the ground there has to be enough clearance between the engines and the ground. The clearance angle is set on 5° and an extra of 15cm is added as can be seen in figure 13.6. [35] The 15cm is added to make sure that when the aircraft lands during strong cross-wind and the wings are not level, still a clearance exists between the ground and the engine.

- **Engine spray criteria:** When the aircraft takes off or lands on a wet runway there is a chance that spray from the nose gear will go to the back of the aircraft. The nose gear and engines must be placed such that this water spray will not enter the engines. Too much water in the engine can cause performance degradation or even engine failure. This requirement is checked during testing. As testing is not possible at this stage of the design, reference aircraft are used to determine angle A and B from figure 13.5. It is found that angle A has to be at least 25°, and angle B has to be around 11°. [22]

Using the previous discussed requirements some parameters of the landing gear and aircraft are calculated. From the take-off clearance height, the length of the fuselage, the take-off angle, the length of the tail, several parameters of the fuselage are calculated. These parameters are the minimum height of the fuselage (measured from the ground), the distance between the main landing gear and the upswept point in the fuselage and the upswept point angle. One of the driving requirements of the landing gear is that it has to be folded into the fuselage. From this the wheeltrack is calculated. The wheeltrack has to be larger than the minimum wheeltrack which is calculated from the overturn angles.

As it is beneficial to have the landing gear as far back as possible, the landing gear is placed at the most allowable aft location on the wing, taking into account that some space is reserved for the flaps and the rear spar. With this position the tip-over angle is calculated and checked whether it is large enough. From the ground clearance, the height of the engine, the engine pylon height and the height of the landing gear the required dihedral angle is calculated. After this calculation it is found that dihedral is not required for ground clearance. However, dihedral is positive for rolling stability, but the dihedral cannot be too large. In that case the aircraft will be too difficult to roll and there will be Dutch roll instability. As small dihedral angles have a positive effect, the dihedral is set on 3°. The last requirement, the engine spray criteria,
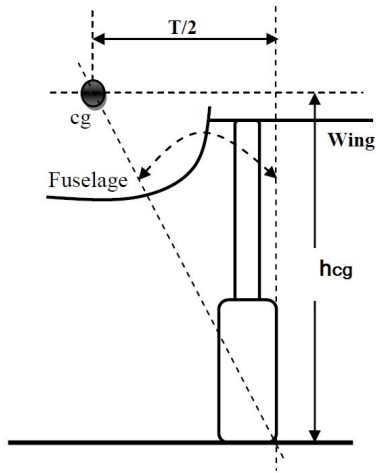
Figure 13.1: Overturn angle 1 [33]
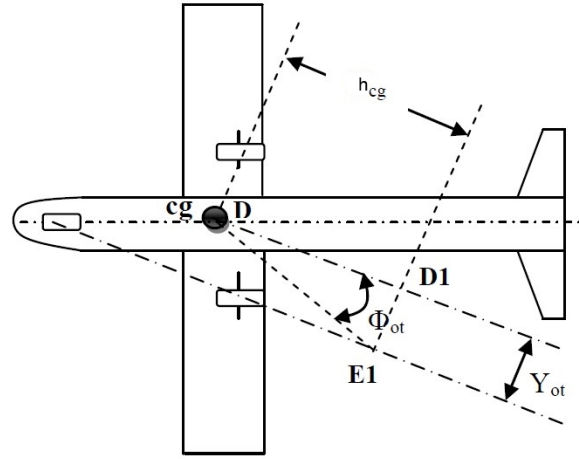
Figure 13.2: Overturn angle 2[33]
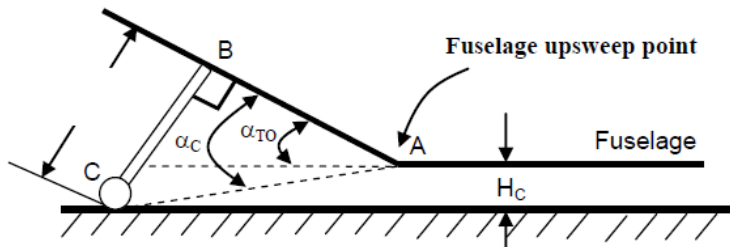
Figure 13.3: Take-off clearance [33]
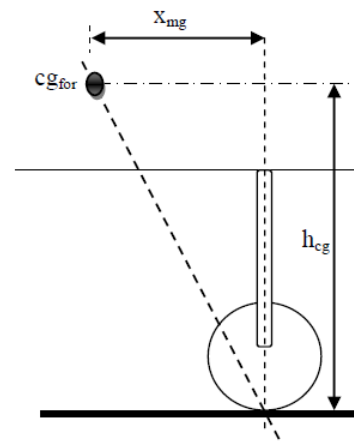
Figure 13.4: Ground stability, tip over [33]
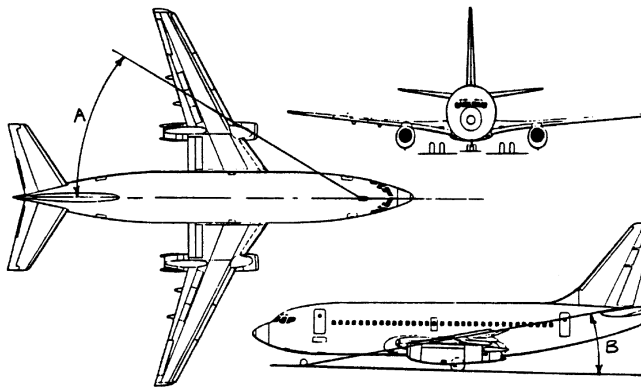
Figure 13.5: Spray requirements engine [22]
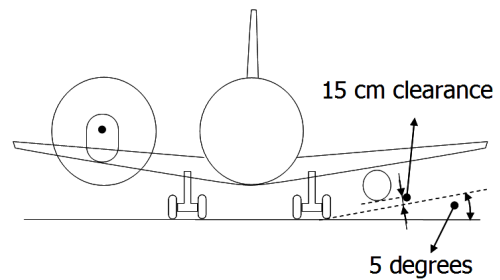
Figure 13.6: Engine clearance [35]

determine the position of the nose wheel. The results of the calculations can be seen in table 13.1. Table 13.2 checks whether all of the requirements are met.

From table 13.2 it can be concluded that all the requirements are met. Some of the angles are even much larger than the required minimum. The cause of this is that other requirements, such as the tail length, are driving in some of the landing gear positioning parameters.

Table 13.1: Landing gear and aircraft parameters

Parameter	Value	Unit
Landing gear height	2.76	m
Fuselage height	2.61	m
Wheeltrack	5.60	m
Wheelbase	13.50	m
Distance from nose to main gear	17.10	m
Distance from nose to nose gear	3.60	m
Dihedral angle	3.00	°
Distance from nose to fuselage upswept point	27.71	m
Fuselage upswept point angle	12.50	°

Table 13.2: Landing gear and aircraft parameters

Requirement	Limit	Angle at ARA	Requirement met?
Overturn angle one figure 13.1	>25°	46.8°	Yes
Overturn angle two figure 13.2	>25°	36.4°	Yes
Take-off clearance	≥ 0.3m	0.3m	Yes
Tip-over angle	>15°	22.9°	Yes
Engine ground clearance	>0.36m	0.95m	Yes
Engine spray angle A	>25 °	25.2°	Yes
Engine spray angle B	Around 11-12°	11.6°	Yes

13.2 Sizing of Landing Gear

This section describes the sizing of the landing gear. The static and dynamic loads acting on the landing gear are discussed in section 13.2.1 and 13.2.2, respectively. In section 13.2.3 a tire is chosen for the nose and main gear.

13.2.1 Static Loads

Using moment equilibrium, it is calculated that the total main gear load is 89.6% of the maximum ramp weight. The nose gear load is then 10.4% of the maximum ramp weight. The maximum ramp weight is taken as 1.01 times the take-off weight. [22] Also, the aircraft needs to be CS 25 certified, therefore the load is multiplied with 1.07. [22] Since the main gear consists of two struts, with two tires each, the static load on the main gear per tire is 76.0kN. The nose gear consists of two tires, which results in a static load on the nose gear per tire of 16.9kN.

13.2.2 Dynamic Loads

The maximum dynamic load per nose gear tire can be determined with equation 13.1. [22]

$$P_{dyn} = W_{TO} \cdot \frac{l_m + (\frac{a_x}{g} \cdot h_{cg})}{n_t \cdot (l_m + l_n)} \tag{13.1}$$

In equation 13.1 W_{TO} is the take-off weight, l_m the distance from the front to the main landing gear, l_n the distance from the front to the nose gear, h_{cg} the height of the centre of gravity, n_t the number of tires and a_x the acceleration and g the gravitational acceleration. The value for $\frac{a_x}{g}$ is 0.45 for dry concrete with anti-skid brakes. [22] The centre of gravity will be below the center of the fuselage, because the wing and engines are placed below the fuselage centreline. The centre of gravity height is calculated to be 3.3m.

The dynamic load on the nose gear is calculated to be 32.7kN. The design static load is obtained by dividing the dynamic load by a factor of 1.5 (for type VII tires) [22]. This value for the design static load is compared with the value found in section 13.2.1 and the higher value of these two is used to select the nose gear tires. Type VII tires [22] are selected, since they have a high load capacity. Dividing the dynamic load with a factor of 1.5 gives a static load of 21.8kN. The value found in section 13.2.1 is 16.9kN. In [22], the static loads are used to select the tires. Therefore, in order to select the nose gear tires a load of 21.8kN is used.

[22] does not provide an equation to calculate the dynamic loads for main gear. However, upon touchdown, the entire weight of the aircraft is supported by the main gear. The maximum landing weight is usually

Table 13.3: Specification of the chosen tires for the landing gear [22]

	Main gear	Nose gear
Tire type	VII	VII
Maximum load [kg]	10932	2812
Tire dimensions (diameter x width)[m]	0.76 x 0.20	0.46 x 0.14
Vmax [m/s]	110.9	122.9

80-90% of the MTOW. [22] Using 90%, the maximum landing weight is found to be 31908kg. Since the main gear consists of 4 tires, again using the safety factor of 1.07, each tire needs to support 81.4kN. This load is multiplied with the factor of 1.5 to obtain the dynamic loads acting on the main gear. This results in a dynamic load on each tire of the main gear of 122.1kN. The static load in this case is 81.4kN, which is higher than the value obtained in section 13.2.1. Therefore, this value is used to select the tire size.

13.2.3 Tire Choice

The design loads for the tires are the following:

- Main gear: 81.4 kN
- Nose gear: 21.8 kN

The tires are of the type VII. The type VII tires are universal tires with a high load capacity which are used in military and civil jets and turboprop aircraft. Using [22], the size of the tires are determined. The tire should be able to withstand the loads. The tires that are chosen are given in table 13.3. The maximum tire operating speed was calculated to be 53.8 m/s. As can be seen in table 13.3, the maximum tire speeds of the chosen tires are well above the maximum tire operating speed.

13.2.4 Shock absorbers

The oleo-pneumatic absorbers are chosen as shock absorbers since they have a relative high efficiency of 0.8. [22] Using oleo-pneumatic absorbers together with type VII tires result in the dimensions for the shock absorbers given in table 13.4. The equations used to calculate the required shock absorber stroke and diameter can be found in [13].

Table 13.4: Results of shock absorber sizing

	Main gear	Nose gear
Shock absorber type [-]	oleo-pneumatic	oleo-pneumatic
Shock absorber stroke [m]	0.20	0.12
Shock absorber diameter [m]	0.21	0.11

13.3 Green Taxiing

Improving the operational efficiency is an important aspect of the design philosophy. The operational efficiency of an aircraft operator can significantly be improved by green taxiing using an Electrical Green Taxiing System (EGTS). This reduces fuel and other taxi-related costs. Each wheel of the main landing gear is equipped with an electric motor to drive the aircraft. The APU generator is used to power these motors. This way, the aircraft can move without the use of the main engines. A 'Green Taxiing System' consists of the following components [36]:

- **Pilot Interface Unit:** Allows the pilot to switch on the EGTS and order the desired action motion forward or backwards.
- **EGTS controller:** Receives and converts actions into orders to the power electronics.
- **Wheel Actuator Controller Unit:** Converts current into instructions to the electrical motor proportional to the pilot's command as delivered by the EGTS controller.
- **Wheel Actuator:** Applies the required torque and speed proportional as received by the Wheel Actuator Controller Unit.
- **APU generator:** Generates power required for the EGTS.

The entire system weighs 320kg, but this value is expected to decrease by the time the system enters service in 2017[10]. Honeywell Aerospace estimates that the system reduces the fuel burn by 4.0%[11]. This means that due to green taxiing, 220kg of fuel is saved. However, it was calculated that the added structural weight increases the fuel burn again with 60kg. The total fuel saved is approximately 160kg, which is 2.9% of the total fuel weight. This electrical taxiing system offers aircraft operators other advantages, such as reducing noise in the airport environment and faster turn-around times due to autonomous pushback. The components of the EGTS are given in figure 13.7.
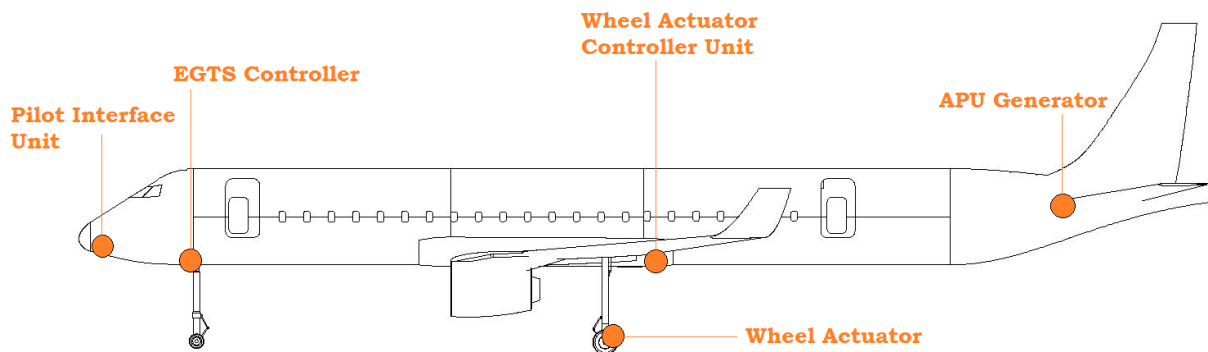
Figure 13.7: Components of EGTS

13.4 Recommendations

To fulfil the requirements stated in section 13.1, the landing gear height must be 2.61m, which is a rather high value for the landing gear height. The restricting parameter is the fuselage length. The upswept point of the fuselage starts at 8.05m from the end of the aircraft. The last 2m of the fuselage length are intended to hold the cargo, while the remaining cargo will be stored in the tail. However, it is calculated that it is possible to store all the cargo in the tail when the upswept point is moved towards the nose with 2m. This will significantly reduce the landing gear height. However, the project is in its final stage and a fuselage length decrease will have influence on all the calculations done so far. For this reason, the landing gear height is not changed. It is recommended to take a closer look at this issue for a redesign of the ARA in post DSE activities. Another recommendation is to look into the expansion of the length of the landing gear when it is unloaded after take-off. The landing gear was designed using requirements on the ground, so when the landing gear is fully loaded. After take-off no loads act on the landing gear anymore and therefore it will expand a bit. As this expansion was not taking into account during the positioning of the landing gear, more research has to be done to see what the length of this expansion will be and how the landing gear can be stored in the fuselage. One possibility is to make the wheeltrack larger. This influences the fuel tank sizing, so more investigation is required to see if this is a feasible possibility. Probably it is because there is space left in the wing. Another possibility could be to look more detailed into the retracting mechanism of the landing gear, such that the landing gear will be 'folded' and then retracted.

---

[10]url: http://www.airport-technology.com/features/feature-electric-green-aircraft-taxiing-takes-off/ [CITED: 18 June 2015]

[11]url: http://www.greentaxiing.com/benefits.html [CITED: 18 June 2015]

14 | Empennage

This chapter discusses the preliminary sizing of the empennage. In section 14.1 the method used for the horizontal stabiliser and vertical stabiliser sizing is discussed. Section 14.2 presents the results obtained from the preliminary empennage sizing.

14.1 Empennage Sizing and Wing Positioning

In this section the general outline of the method for determining the position of the wing and the tail surfaces adapted from [37], [38] and [18] are discussed. First, the loading diagrams for the ARA are generated and the most constraining centre of gravity range is identified. Secondly, the centre of gravity range for which the ARA is stable and controllable is determined. By combining the constraining centre of gravity range with the range of centres of gravity for stability and controllability an initial horizontal stabiliser surface area and wing position is obtained.

14.1.1 Loading diagrams

A loading diagram depicts the shift of the centre of gravity during the loading of the payload and fuel in the aircraft. In order to determine the range of stability for the ARA the most critical loading cases should be used. A MATLAB program is made based on the method presented in [37]. The MATLAB program is used to calculate the maximum forward and aft location of the centre of gravity for different load cases, for which two conclusions can be drawn. First, the class configuration does not have an influence on the most forward and most aft centre of gravity locations. Therefore, only the one-class configuration is considered. Secondly, there are two dominating load cases. The first case is for the harmonic range. For this case the maximum cargo mass is loaded in the cargo bay in the tail. Therefore, this case determines the most aft centre of gravity location. The second case is for the maximum range at MTOW with full fuel tanks and reduced payload (discussed in chapter 8). This case determines the most forward centre of gravity due to the loading of passengers. Therefore, both these cases are taken into account during the determination of the centre of gravity range in order to design for controllability and stability for all of the flight cases of the ARA.

In order to generate the loading diagrams, the fuel, cargo and passenger masses determined in chapter 8 are used. Furthermore, the OEW centre of gravity location ($x_{cg,\,OEW}$) is obtained from the subsystem weights and centre of gravity locations from table 8.3 in chapter 8. Three loading diagrams are made to determine the influence of the wing position on the centre of gravity of the aircraft. A loading diagram for x_{LEMAC} for the original wing position, a loading diagram when the wing is positioned 10% more forward and a loading diagram when the wing is positioned 10% more aft are generated. In figure 14.1 the loading diagrams for the harmonic range are shown for an x_{LEMAC} of 15.2 m. The bottom line is due to the cargo loading which shifts the centre of gravity in a straight line to the back. The first bubble in figure 14.1 represent the loading of the passengers at the window seats. One line represents the loading of the passengers from the back to the front and the other from the front to the back. Then the passengers at the aisle seats are seated which results in the second bubble. Lastly, the fuel is loaded and this shifts the centre of gravity in a straight line to the back. The top left diagram shows the loading diagram when the x_{LEMAC} is decreased by 10% (wing positioned more forward), the top right diagram shows the loading diagram for x_{LEMAC} (original wing position), the bottom left shows the loading diagram when x_{LEMAC} is increased by 10% (wing positioned more backward). The bottom right figure of figure 14.1 is the most aft and forward centre of gravity locations for x_{LEMAC} locations between $0.9 \cdot x_{LEMAC}$ and $1.1 \cdot x_{LEMAC}$ for both the constraining cases. Case 1 causes the most aft position and case 2 causes the most forward centre of gravity position. Note that the outer centre of gravity location boundaries are increased by 5% to account for in-flight and on ground centre of gravity shifts (e.g. moving cabin crew and moving passengers). [37]

14.1.2 Stability and Controllability

The required horizontal stabiliser area S_h is determined by stability and controllability requirements. The method discussed by [38] and [18] is used to determine the horizontal stabiliser area range as a function of the centre of gravity position for stability and controllability requirements. Furthermore, the landing gear position can also limit the allowable centre of gravity range due to tip-over. The tip-over restriction is determined by the position of the landing gear in the wing planform, determined in chapter 13.
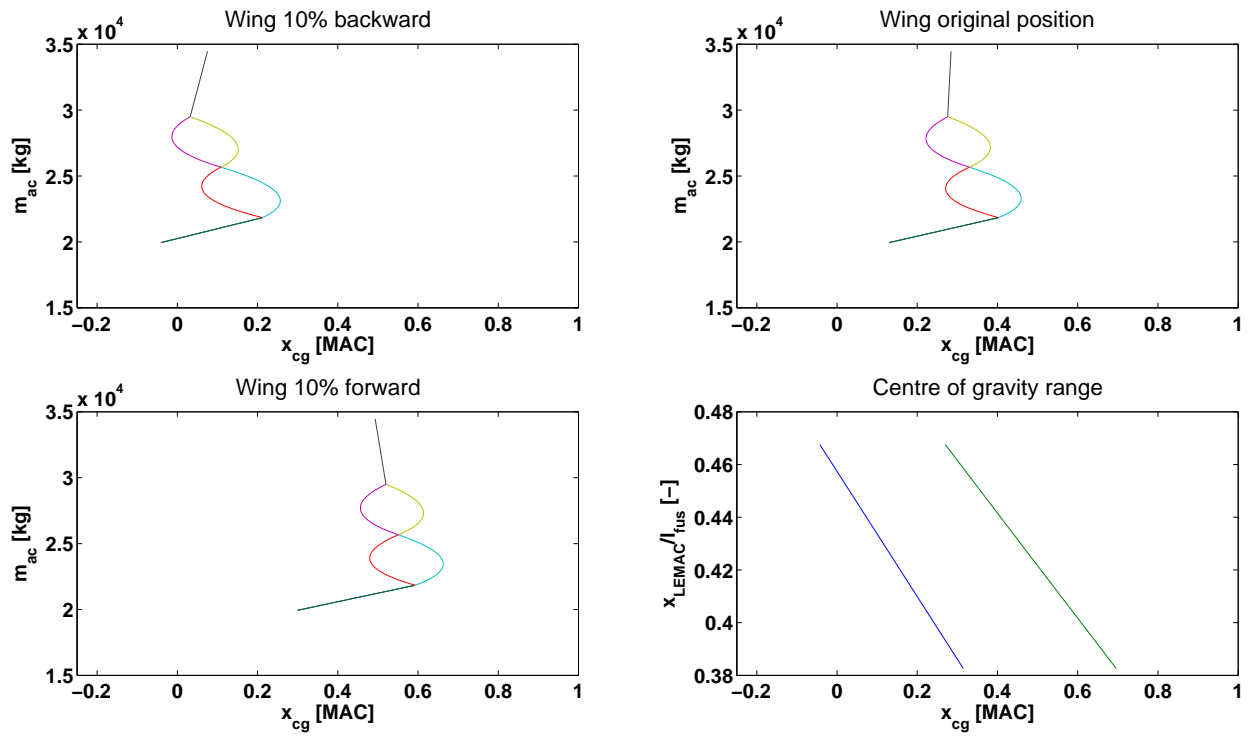
Figure 14.1: Load diagrams for the harmonic range and the extreme centre of gravity locations for the ARA ($x_{LEMAC} = 15.2m$)

In figure 14.2 the result of the stability, controllability and tip-over requirements on the horizontal stabiliser area and the location of the centre of gravity are shown. Furthermore, the areas where the aircraft is stable and controllable are indicated and the maximum allowable centre of gravity range is indicated.
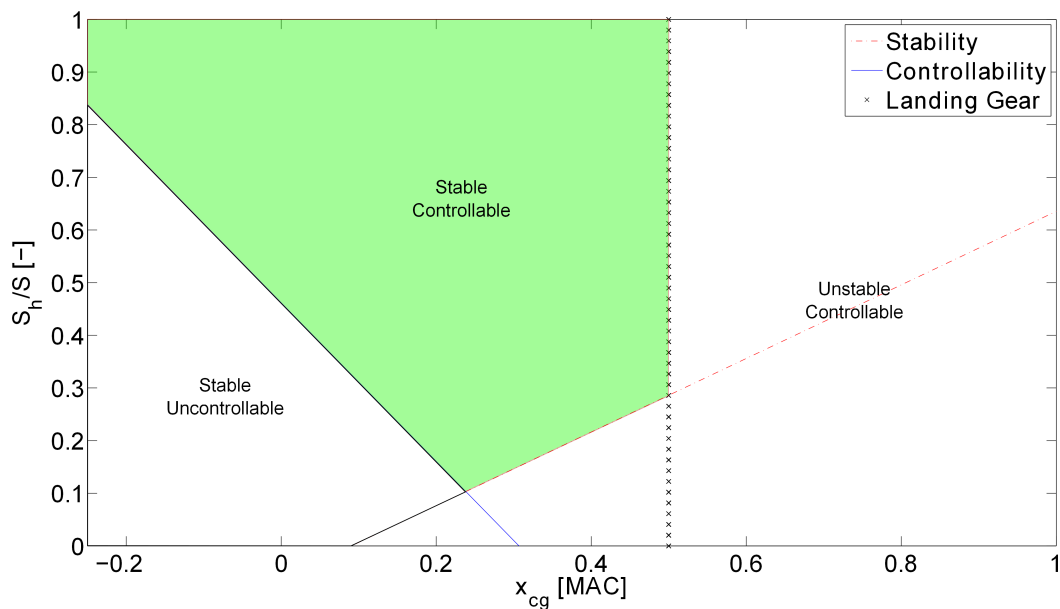
Figure 14.2: Worst case Centre of gravity range ($x_{LEMAC} = 15.2m$)

The graph of the maximum centre of gravity range (figure 14.1) obtained from section 14.1.1 is combined with the graph of the stability and controllability (figure 14.2) as shown in figure 14.3. The graphs are scaled with respect to each other such that the x-axis overlap and have the same scale. Then the maximum centre of gravity range graph is shifted along the y-axis in order to align the intersection points of the forward centre of gravity position with the controllability curve and the aft centre of gravity position with the stability curve. The aligned intersection points are indicated in figure 14.3 by the horizontal line. The

y-value of the maximum centre of gravity range graph indicates the position of the wing and the y-value of the controllability and stability graph indicates the minimum horizontal stabiliser area required to satisfy the controllability and stability requirement for the new wing position. In figure 14.3 the resulting wing position is approximately $0.425\ x_{LEMAC}/l_{fus}$ and the resulting horizontal tail area ratio is approximately $0.26\ S_h/S$. The wing position with respect to the nose and the horizontal tail area after the final iteration are given in table 14.1.
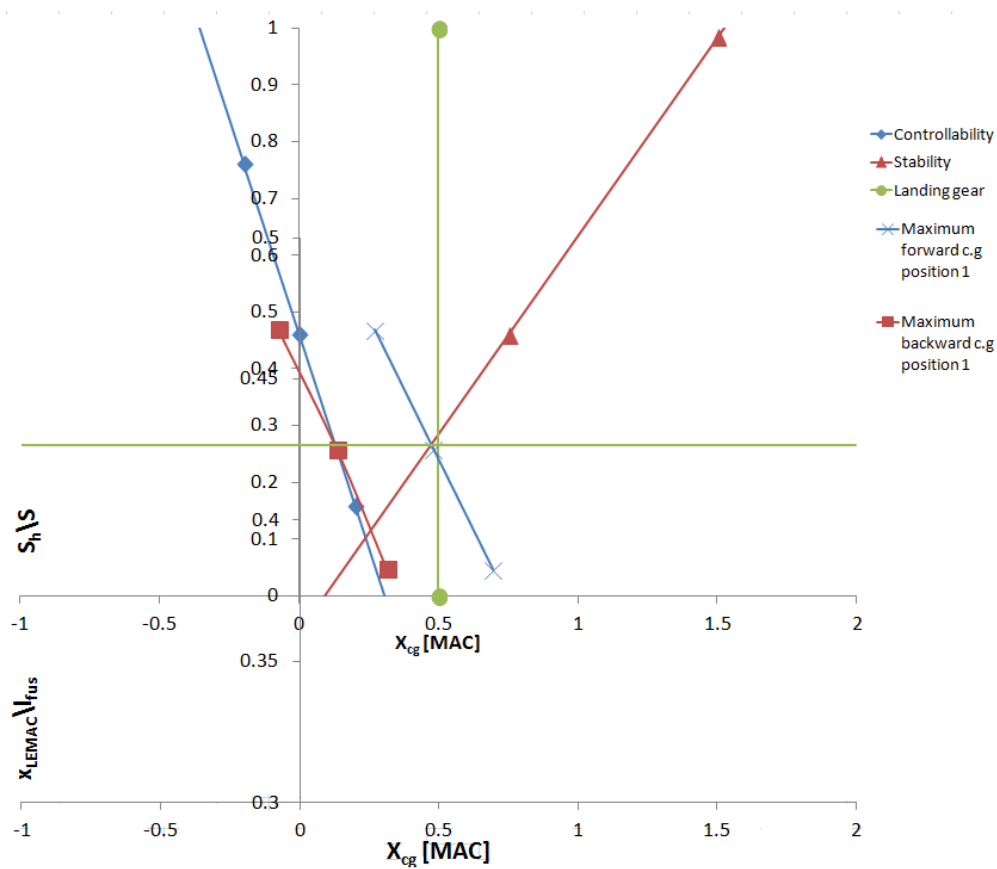
Figure 14.3: Combination of the extreme centre of gravity locations and controllability and stability graphs ($x_{LEMAC} = 15.2m$).

In order to obtain the right values for the horizontal tail surface and the corresponding wing position, both figures are placed on top of eachother and the corresponding parameters are obtained.

14.1.3   Vertical tail sizing

The vertical tail area is determined using reference data of aircraft with a conventional tail [12]. From reference data it is found that the ratio between the vertical tail area and the wing area is usually about 0.2. The resulting vertical tail area is given in table 14.1.

14.1.4   Airfoil and Sweep

For the horizontal and vertical tail wings an airfoil has to be chosen. Generally a symmetrical airfoil is chosen which is 10% thinner than the main wing, which resulted in the NACA 0007 airfoil. [39] This airfoil choice is required for the control surface sizing. The sweep of the horizontal tailwing also has to be determined. Generally, the main wing sweep angle is increased by 10°, to make sure it does not stall before the main wing. [18] This results in a leading edge sweep angle for the horizontal tailwing of 40°.

---

[12]url: http://booksite.elsevier.com/9780340741528/appendices/data-a/default.htm [CITED: 3 June 2015]

14.2 Empennage Characteristics

The results obtained from the method discussed in section 14.1 are shown in table 14.1. $x_{cg,aft}$ and $x_{cg,forward}$ are the most aft and most forward allowable centre of gravity locations for the ARA respectively. Furthermore, $x_{cg,OEW}$ is the operational empty weight centre of gravity location. The other parameters in table 14.1 are discussed in section 14.1. To verify the results the resulting wing position, horizontail tail area and vertical area are used to calculate the centre of gravity range with the equations from [38] and [18]. Furthermore, as this method is only a preliminary sizing based on semi-empirical equations, it is recommended that a detailed flight dynamics analysis is performed to determine if the tail areas suffice to guarantee controllability and stability of the ARA.

Table 14.1: Empennage sizing results.

Parameter	Value	Unit
S_h	27.3	$[m^2]$
S_v	21.0	$[m^2]$
x_{LEMAC}	15.2	$[m]$
$x_{cg,aft}$	17.0	$[m]$
$x_{cg,forward}$	15.7	$[m]$
$x_{cg,OEW}$	15.7	$[m]$

15 | Control Surfaces

Depending on the disturbance, an aircraft must be stabilised in the lateral, longitudinal and directional directions. Control surfaces are an essential part of the aircraft which allows the pilot to control the aircraft. Section 15.1 describes the types of control surfaces chosen and the assumptions made. Section 15.2 describes the sizing of the ailerons. In the section 15.3 the sizing of the spoilerons is described. Furthermore, the sizing of the rudder and elevator can be found in sections 15.4 and 15.5 respectively.

15.1 Roll Control Methods

Most aircraft use ailerons for lateral control. Examples of other control surfaces that are used for lateral control are flaperons and spoilerons. Before the sizing of the control surfaces is done, several assumptions have been made:

- The deflection of the control surface is instantaneous at t = 0s

- Damping is neglected

- The height of the c.g. is assumed to be at 3.3m from the ground.

- For the calculation of the mass moments of inertia the aircraft was divided into the following parts: wing, tail, engines and fuselage.

- The airfoil effective shape is assumed to be the same during the whole roll movement for spoileron deflection.

- Lift distribution variations due to changes in angle of attack during roll are neglected.

- When spoilerons are deployed, no lift is produced by the area of the wing behind the spoilerons.

Due to the simplicity and effectiveness of outboard ailerons, it is chosen to use outboard ailerons for roll control during take-off and landing. At a certain airspeed, a balance is reached where the lift gained due to aileron deflection is completely offset by the lift lost due to wing twisting. This speed is called the aileron reversal speed and at this speed the ailerons have no effect at all. Below the aileron reversal speed, the ailerons cause a rolling motion in the desired direction. When exceeding the aileron reversal speed, the effect of the ailerons is reversed. Aileron reversal is most likely to occur at outboard ailerons since the twist of the wing usually is bigger at the tip than at the root. For this reason, outboard ailerons will only be used at low speeds. The inboard ailerons are further away from the tip, so they stay effective at high speed. However, since the trailing edge of the wing up to the outboard aileron is dedicated to flaps, there is no room for inboard ailerons on the ARA. In order to be able to roll at high speed, spoilers will be used. Spoilers for roll control are called spoilerons.

15.2 Outboard Ailerons

Ailerons make the aircraft roll by increasing lift on one wing, while decreasing lift on the other wing. This additional lift is a direct result of the downward deflection of the aileron, whilst the decrease in lift is a direct result of upward deflection of the aileron. In this section the aileron sizing is described. First, the method used will be discussed. Afterwards, the results are discussed.

15.2.1 Method

The method used to size the ailerons is given in [40]. First of all, the aircraft class and critical flight phase for roll control have to be determined. Since the effectiveness of control surfaces is the lowest while flying at low speeds, the roll control in take-off or landing operations is the flight phase for which the ailerons are sized. The approach speed is equal to 58 m/s. With a MTOW of 34500 kg, the ARA is defined as a class III aircraft in [40]. From this it follows that an aircraft from Class III (see figure 15.1), flying under condition C (landing), at level 1 (passenger aircraft), should be able to roll over an angle of 30° in 2.5 seconds as can be seen in figure 15.2.

The first step in analysing the ailerons is to calculate the rolling moment coefficient derivative $(C_{l_{\delta_a}})$, which can be done using equation 15.1. Since the ratio of aileron to wing chord is 0.35, the aileron effectiveness

Class	Aircraft characteristics
I	Small, light aircraft (maximum take-off mass less than 6000 kg) with low maneuverability
II	Aircraft of medium weight and low-to-medium maneuverability (maximum take-off mass between 6000 and 30 000 kg)
III	Large, heavy, and low-to-medium maneuverability aircraft (maximum take-off mass more than 30 000 kg)
IV	Highly maneuverable aircraft, no weight limit (e.g., acrobatic, missile, and fighter)

Figure 15.1: Aircraft classes [40]

(c) Time to achieve a 30° bank angle change for Class III

Level	Speed range	Flight phase category		
		A (s)	B (s)	C (s)
1	Low	1.8	2.3	2.5
	Medium	1.5	2.0	2.5
	High	2.0	2.3	2.5
2	Low	2.4	3.9	4.0
	Medium	2.0	3.3	4.0
	High	2.5	3.9	4.0
3	All	3.0	5.0	6.0

Figure 15.2: Roll requirements for different phases and categories [40]

Category	Examples of flight operation
A	(i) Air-to-air combat (CO); (ii) ground attack (GA); (iii) weapon delivery/launch (WD); (iv) aerial recovery (AR); (v) reconnaissance (RC); (vi) in-flight refueling (receiver) (RR); (vii) terrain following (TR); (viii) anti-submarine search (AS); (xi) close formation flying (FF); and (x) low-altitude parachute extraction system (LAPES) delivery.
B	(i) Climb (CL); (ii) cruise (CR); (iii) loiter (LO); (iv) in-flight refueling in which the aircraft acts as a tanker (RT); (v) descent (D); (vi) emergency descent (ED); (vii) emergency deceleration (DE); and (viii) aerial delivery (AD).
C	(i) Take-off (TO); (ii) catapult take-off (CT); (iii) powered approach (PA); (iv) wave-off/go-around (WO); and (v) landing (L).

Figure 15.3: Flight phase categories [40]

parameter (τ), is determined to be 0.55 from figure 15.4. Figure 15.4 is used for the sizing of all the control surfaces. After having performed iterations, the inner edge and outer edge position of the aileron as a function of wing span are selected to be at 73% and 90% of the wing semispan respectively. Therefore, $y_i = 0.73 \cdot 30.71/2 = 11.20m$ and $y_o = 0.9 \cdot 30.71/2 = 13.82m$. The inputs for equation 15.1 are given in table 15.1.
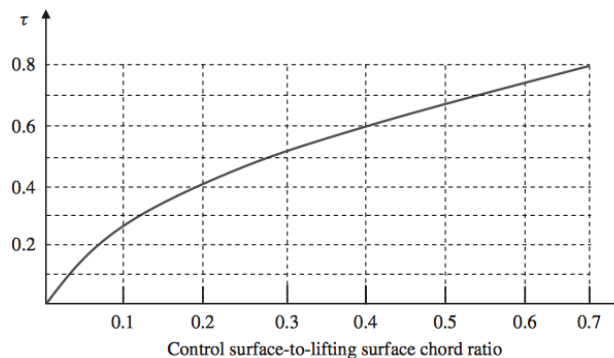
Figure 15.4: Aileron effectiveness parameter

$$C_{l_{\delta_a}} = \frac{2C_{l_{\alpha_w}}\tau c_r}{Sb} \cdot \left[\frac{y^2}{2} + \frac{2}{3}(\frac{\lambda-1}{b})y^3 \right]_{y_i}^{y_o} \tag{15.1}$$

After having obtained the derivative of the rolling moment coefficient, the rolling moment coefficient can be calculated using equation 15.2. When ailerons are deflected more than 20-25°, flow separation tends to occur and results in the ailerons decreasing in effectiveness. To prevent loss of roll control effectiveness, the maximum aileron deflection needs to be less or equal to 25°.[40] The maximum deflection angle is therefore assumed to be 25°.

$$C_l = C_{l_{\delta_a}} \cdot \delta_a \tag{15.2}$$

The next step is to calculate the rolling moment. The critical flight phase for roll control is at the lowest speed, the approach speed. The rolling moment can then be calculated with equation 15.3.

$$L_a = \frac{1}{2}\rho V_{app}^2 SC_l b \tag{15.3}$$

Table 15.1: Inputs to calculate $C_{l_{\delta_a}}$

Symbol	Description	Value	Unit
$C_{l_{\alpha_w}}$	Lift slope of wing	4.73	$1/deg$
τ	aileron effectiveness parameter	0.55	[-]
c_r	root chord	5.8	m
S	wing area	104.81	m^2
b	wing span	30.71	m
λ	taper ratio	0.3	[-]
y_i	inner edge location of aileron	11.20	m
y_o	outer edge location of aileron	13.82	m

Then the steady roll rate (P_{ss}) can be calculated with equation 15.4. The rolling drag coefficient (C_{D_r}) is assumed to be 0.9 and the drag arm is assumed to be at 40% of the wing span, so y_d is $0.4 \cdot 30.71/2 = 6.45m$. [40]

$$P_{ss} = \sqrt{\frac{2 \cdot L_a}{\rho(S_w + S_{ht} + S_{vt})C_{D_r} \cdot y_D^3}} \tag{15.4}$$

The steady roll rate can then be used to calculate the bank angle at which the aircraft achieves steady roll rate, with equation 15.5. In this equation the mass moment of inertia is used. To calculate the mass moment of inertia, the aircraft was simplified, as can be seen in figure 15.5. By adding the mass moments of inertia of the cylindrical and rectangular shapes, the mass moment of inertia was calculated to be 752713 kgm^2.

$$\Phi = \frac{I_{xx}}{\rho(S_w + S_{ht} + S_{vt})C_{D_r} \cdot y_D^3} \cdot ln(P_{ss}) \tag{15.5}$$
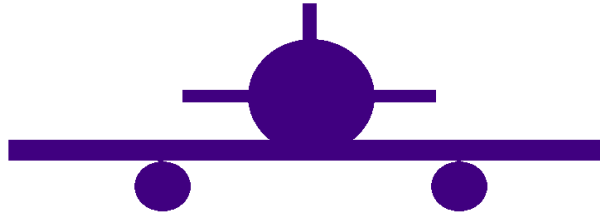
Figure 15.5: Simplified aircraft representation used for mass moment of inertia

An accelerated rolling motion can be expressed with equation 15.6. Assuming that the aircraft is initially at wing-level flight condition ($P_0 = 0$) and the new roll rate is the steady-state roll rate ($P_1 = P_{ss}$), the aircraft roll acceleration that is produced by the aileron rolling moment can then be calculated with equation 15.7.

$$P_1^2 - P_0^2 = 2\dot{P}\Phi \tag{15.6}$$

$$\dot{P} = \frac{P_{ss}^2}{2\Phi} \tag{15.7}$$

Now the roll angle can be calculated as a function of time with equation 15.8:

$$\Phi = \frac{1}{2}\dot{P} \cdot t^2 \tag{15.8}$$

15.2.2 Results Ailerons

The roll angle as a function of time is given in figure 15.6.

The time to roll 30° is calculated to be 2.48 seconds, which is indicated in figure 15.6. With these dimensions of the aileron the requirement is satisfied. The results of the aileron sizing are summarised in table 15.2.

Table 15.2: Results aileron sizing

Parameter	Description	Value
b_a	aileron span	2.6m
c_a	aileron chord	0.35c
δa_{max}	maximum aileron deflection	25°
t	time to roll 30°	2.48s
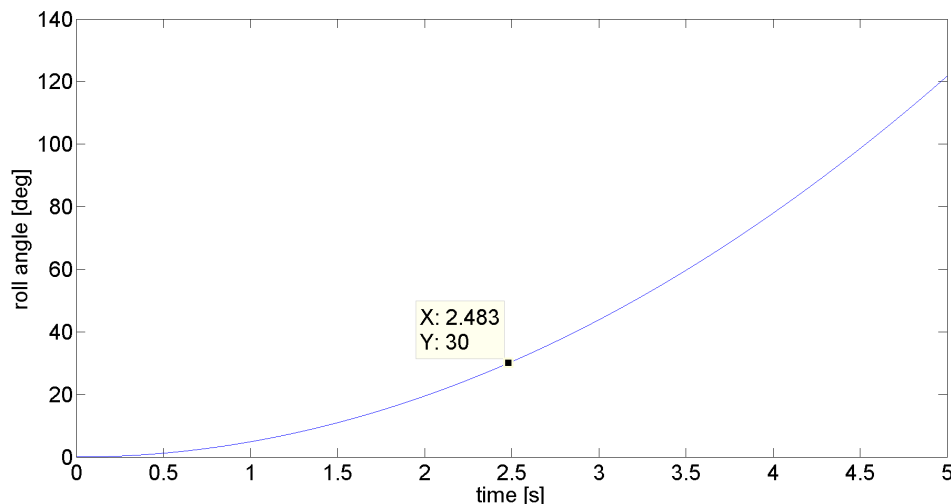
Figure 15.6: Roll angle using outboard ailerons

15.3 Spoilerons

Jet aircraft can have two sets of ailerons; a pair of outboard low-speed ailerons and a pair of high-speed inboard ailerons. The inboard ailerons can be used at high speed since the wingtips tend to twist with outboard aileron deflection at high speeds, as is explained in section 15.1. Since the trailing edge of the wing until the outboard aileron is dedicated to flaps, there is no room for inboard ailerons on the ARA. Therefore, spoilerons will be used to be able to roll at high speed. Spoilerons are panels located on the upper side of the wing, deploying (on one side) at an angle upwards to the longitudinal direction, causing a loss of lift over that section of the wing and additional drag.

15.3.1 Method

The influence of spoileron deflection on aerodynamic coefficients in the transonic flow field is mathematically difficult to model. Accurate results can only be obtained by conducting a windtunnel test or utilizing a CFD analysis. This is however outside the scope of this project. Therefore, the preliminary sizing of the spoilerons is done using a simplified approach which estimates the lift loss due to the deflection of a spoileron by looking at the Cp-distribution of the airfoil. In figure 15.7 the Cp-distribution of the airfoil is given at cruise angle of attack. The spoileron is placed at 60% of the chord from the leading edge. It is assumed that when the spoiler is deflected, there is no lift behind the spoiler any more. The Cp-distribution with spoilerons deflected is shown in figure 15.8. From this figure the difference in lift of the left and right wing can be calculated. The effect of the spoiler is estimated to decrease the lift with 18.37 %. Then the lift can be calculated with equation 15.9.

$$L = \frac{1}{2}\rho V^2 S C_L \tag{15.9}$$

$$M = L \cdot d \tag{15.10}$$

The moment around the centre of gravity is calculated with equation 15.10. After which the roll acceleration can then be calculated using equation 15.11. Finally, the roll angle is calculated using equation 15.12

$$\dot{P} = \frac{M}{I_{xx}} \tag{15.11}$$
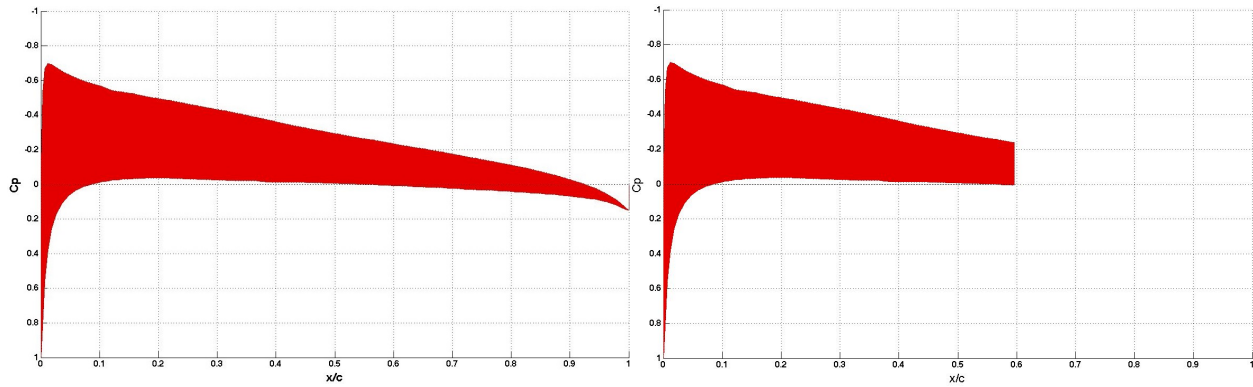
Figure 15.7: Cp-distribution at an angle of attack of 1.84deg with Re=$2 \cdot 10^6$ on clean surface

Figure 15.8: Cp-distribution at angle of attack of 1.84deg with Re=$2 \cdot 10^6$ with spoileron

$$\Phi = \frac{1}{2}\dot{P}t^2 \tag{15.12}$$

15.3.2 Results Spoilerons

In figure 15.9 the roll angle over time is given. Since the flight condition is now cruise (phase B), the aircraft should be able to roll an angle of 30° in 2.3 seconds. With a spoileron span of 5 meters and a spoileron chord of 0.20c, the time calculated to roll an angle of 30° at cruise speed with the spoilerons is calculated to be 2.2 seconds, so the requirement is satisfied. The results of the spoileron sizing are given in table 15.3. It should be noted that spoilerons are panels which can be placed on top of the wing skin, thus also partially on top of the high lift devices and fuel tank.

Table 15.3: Results of the spoileron sizing

Symbol	Description	Value
b_s	spoileron span	5 m
c_s	spoileron chord	0.20 c
t	time to roll 30°	2.2 s
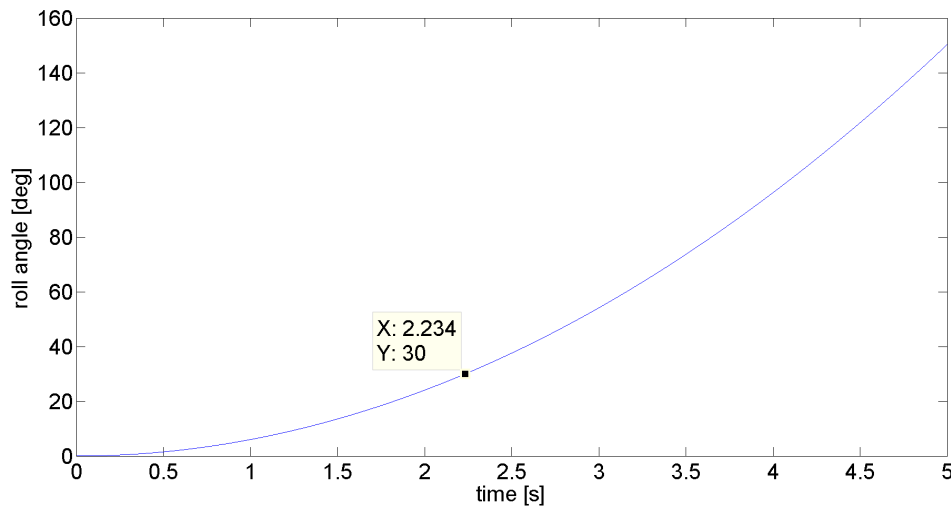
Figure 15.9: Roll angle using spoilerons

15.4 Elevator

In order to control the aircraft longitudinally, an elevator is designed. An elevator acts like a plain flap and allows the aircraft to be controlled longitudinally by providing an incremental lift force on the horizontal

tail. The requirement of take-off rotation is described in section 15.4.1. Additionally, the longitudinal trim requirement is be described in section 15.4.2.

15.4.1   Take-off Rotation

On an aircraft with a tricycle landing gear, the elevator must be powerful enough to rotate the aircraft about the main gear and lift the nose with specified angular pitch acceleration. Since the ARA has a MTOW of more than 30000 kg, from figure 15.3 it was determined that the ARA is a class III aircraft. For class III aircraft, the required pitch angular acceleration is 4-6 $\frac{deg}{s^2}$ with a rotation time of 3-5 seconds.

No.	Aircraft type	Rotation time during take-off (s)	Take-off pitch angular acceleration (deg/s^2)
1	Highly maneuverable (e.g., acrobatic GA and fighter)	0.2–0.7	12–20
2	Utility, semi-acrobatic GA	1–2	10–15
3	Normal general aviation	1–3	8–10
4	Small transport	2–4	6–8
5	Large transport	3–5	4–6
6	Remote control, model	1–2	10–15

Figure 15.10: Pitch angular acceleration and rotation time requirement [40]

It is assumed that the aircraft performs the rotation of 14.34° required for take-off when still in contact with the runway. Since the rotation is performed around the main landing gear, the moments are calculated about the main landing gear. The most critical condition for which the elevator is sized is found to be when the aircraft centre of gravity is most forward, as this condition requires the most negative elevator deflection (upward).

The method used is obtained from [40]. By taking moments about the main gear and using a pitch angular acceleration of 4 $\frac{deg}{s^2}$, the required moment produced by the horizontal tail is calculated (with equation 15.13). The mass moment of inertia around the y-axis is calculated using a simplified representation of the aircraft as can be seen in figure 15.11. The fuselage and engine are modeled as cylinders, while the wing and tail are modeled as beams. The speed that is used in the calculations is the minimum controllable speed as calculated with equation 15.18.

$$\sum M = -M_T - M_W + M_L - M_{ac} + M_{HT} = I_{yy}\alpha \qquad (15.13)$$

The values and description for each of these variables in 15.13 are presented in table 15.4.

Table 15.4: Parameters used for moment about main gear

Symbol	Value	Description
M_T	$2.25 \cdot 10^5 \ Nm$	Moment caused by the thrust
M_W	$4.73 \cdot 10^5 \ Nm$	Moment caused by the weight
M_L	$1.87 \cdot 10^5 \ Nm$	Moment caused by the main wing
I_{yy}	$7.22 \cdot 10^5 \ kgm^2$	Mass moment of inertia about y-axis
α	$4 \ \frac{deg}{s^2}$	Required pitch angular acceleration

The lift required from the horizontal tail is calculated to be 56.7kN. This results in a required elevator C_L of 0.77. Using a maximum deflection of 25°, the elevator effectiveness (τ_e) is calculated using equation 15.14. From figure 15.4, the required elevator chord is determined. An elevator effectiveness of 0.5 results in a c_e/c_h ratio of 0.27. The MAC of the horizontal tail is 2.56m, which leads to an elevator chord of 0.69m. The final elevator dimensions can be found in table 15.5.

$$C_L = C_{L_{\alpha_h}}(\alpha_h + \tau\delta_e) \qquad (15.14)$$
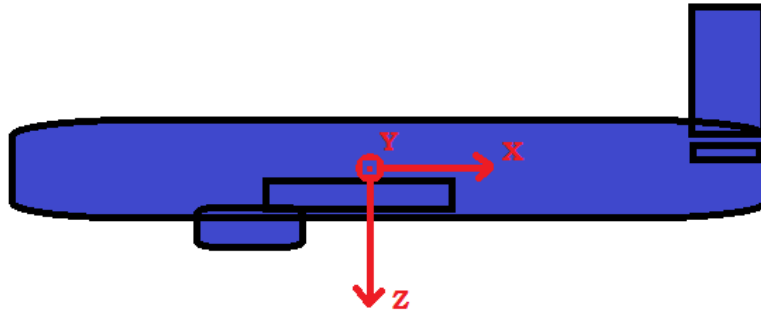
Figure 15.11: Mass Moment of Inertia about y-axis

Symbol	Description	Value [Unit]
c_e	Elevator chord	0.69 [m]
b_e	Elevator span	10.5 [m]
S_e	Elevator area	7.28 [m^2]
c_{h_r}	Horizontal tail root chord	3.6 [m]
c_{h_t}	Horizontal tail tip chord	1.1 [m]
b_h	Horizontal tail span	11.7 [m]
S_h	Horizontal tail area	27.3 [m^2]
δ_e	Maximum elevator deflection	0.32 [m]

Table 15.5: Elevator and horizontal tail dimensions

15.4.2   Longitudinal Trim Requirement

It is beneficial for the pilots to have the aircraft trimmed. When the aircraft is trimmed the pilot does not need to exert a constant pressure on the controls. The trim point is reached by adjusting the elevator deflection such that the moments (about the centre of gravity) and forces are in equilibrium.

$$\delta_e = \frac{(\frac{Tz_T}{qSC} + C_{m_0}) \cdot C_{L_\alpha} + (C_{L_1} - C_{L_0} \cdot C_{m_\alpha})}{C_{L_\alpha} C_{m_{\delta_E}} - C_{m_\alpha} C_{L_{\delta_E}}} \tag{15.15}$$

By solving the equation 15.15, an elevator trim angle of 2.9° is obtained (downward). It is beneficial to have this angle as small as possible to minimize drag. It is found that in order to meet the trim requirement, an increase in elevator size is not required.

15.5   Rudder

In order for the aircraft to obtain directional controllability and stability the rudder is sized. Since the vertical tail has been sized in chapter 14, it will be used for determining the rudder area with the Roskam method using [41] and [34]. The main criteria for sizing the rudder area for the ARA is the one engine inoperative condition. This will be done for the most critical condition. The moment caused by the operative engine is counteracted by a rudder deflection δ_r, providing a counteracting moment. This moment caused by having only one operative engine is calculated in equation 15.16.[34]

$$N_{t_{crit}} = T_{TO_e} y_t = 312 kNm \tag{15.16}$$

$$N_D = 0.25 N_{t_{crit}} = 78 kNm \tag{15.17}$$

Equation 15.16 comprises of a force(the engine thrust) and its arm to the fuselage centerline, y_t. The inoperative engine causes a moment due to the drag, with the equation for a jet-driven aircraft with high by-pass ratio shown in equation 15.17.[34]

The minimum control speed of the aircraft is the speed at which the rudder is still functionally operative. This speed is based off the stall speed and is shown in equation 15.18.[34]

$$V_{mc} = 1.2 V_s = 58.7 m/s \tag{15.18}$$

Using equations 15.16, 15.17 and 15.18 the required rudder deflection is computed. Considering the airfoil on the tail and a dynamic pressure distribution on the tail compared to the main wing of 0.85, as is an approximation for a fuselage mounted stabilizer, the remaining values for computing the rudder deflection are determined, such as $C_{n_{\delta_r}}$, the derivative of the yawing moment due to the rudder. [38] The required rudder deflection δ_r is calculated using equation 15.19.

$$\delta_r = \frac{(N_D + N_{t_{crit}})}{q_{mc}SbC_{n_{\delta_r}}} = 29.3° \tag{15.19}$$

It is now needed to check if this value for the rudder deflection is actually obtainable and makes sense. From reference data [39], a maximum rudder deflection of 30° is obtained and thus the rudder deflection of 29.3° is within limits.

The corresponding C_r/C_v ratio, the ratio of rudder MAC to vertical tail MAC, for these calculations is 0.275, resulting in a rudder MAC of $1m$. Furthermore with this value of the rudder chord, the rudder span is found to not exceed the whole vertical tail area span: a value of b_r/b_v of 0.80 is used resulting in a rudder span b_r of 5.1 m. The rudder area is found to be 5.1 m^2.

The general rudder parameters are shown in table 15.6. To give an overview of the overall vertical wing parameters, a CAD drawing of the vertical wing, including rudder sizing, is shown in figure 15.12.

Table 15.6: Rudder Parameters

Symbol	Description	Value [Unit]
λ	vertical tail taper ratio	0.3 $[-]$
S_v	vertical tail area	20.97 $[m^2]$
C_v	vertical tail MAC	3.65 $[m]$
b_v	vertical tail span	6.3 $[m]$
S_r	rudder area	5.1 $[m^2]$
C_r	rudder chord	1.0 $[m]$
b_r	rudder span	5.1 $[m]$
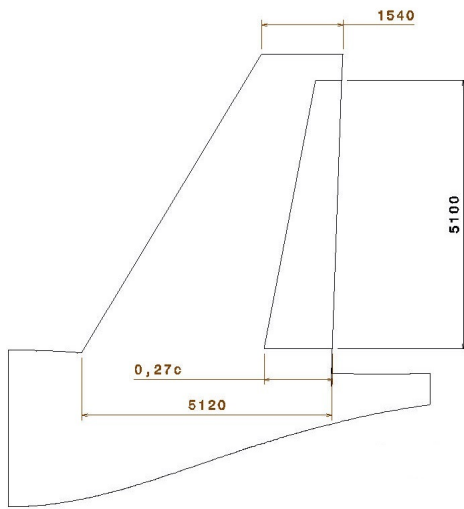
Figure 15.12: Vertical Tail Overview

15.6 Recommendations

The calculations performed to size the spoilerons and ailerons as described in this chapter are a rough estimate. The size of the spoilers can be optimised since a simplified approach was used to calculate the lift decrease, which underestimates the lift loss due to a deflection of the spoileron. The change of airfoil effective shape was not taken into account. The simplified approach overestimates the sizes of the required spoilerons. From the calculations it followed that a lift loss of 18.37% is caused by the spoilerons. This value is most likely to increase, resulting in smaller spoilerons. It is recommended to conduct a windtunnel test or CFD analysis in order to obtain more accurate results of the lift loss. Also, the mass moment of inertia could be calculated less simplified, resulting in more accurate dimensions for the control surfaces. Finally, it would be more beneficial for the longitudinal trim, to use trim tabs to trim the ARA instead of using the complete elevator.

Part III

Detailed Design

16 | Winglets

The driving factor when designing a winglet is fuel consumption. A winglet increases the aerodynamic efficiency of the aircraft, with the downside of adding structural mass. The winglet must be optimised with respect to these two parameters. To find out which wingtip device offers the optimal design, a Vortex Lattice Method (VLM) is used to analyse several different winglet concepts.

First, a literature study is performed to find promising concepts, the theory and the concepts can be found in section 16.1. To test the winglets, an aerodynamic analysis is done which is presented in section 16.2 after which a preliminary structural analysis is performed and shown in section 16.3. Finally, the best options are analysed and the overall optimal design is presented in section 16.4.

16.1   Winglet Theory

During subsonic flight, there are two main types of drag:

- Parasitic drag: due to the influence of viscosity, which is mainly due to skin friction

- Induced drag: due to the generation of lift

Winglets are used to reduce the induced drag of the wing. The wing's tip vortices create a sidewash which modifies the flow on the winglet, this can lead to winglet thrust, or negative induced drag. [42] Winglets distribute the lift over the wing more evenly which increases the effective span of the wing and consequently the aerodynamic efficiency[13]. Increasing the aspect ratio of the wing results in a large change in the vortex drag without a large increase in wetted area. Studies have shown that a vertical surface located at the wing tip is worth close to 45% of its height as span, if loaded in an optimal way. [42] This suggests that a wing extension is aerodynamically more efficient than a vertical winglet but will incur a stronger increase of the wing's root bending moment and will result in a heavier structure.

Design studies show that a winglet height of $\frac{h_w}{(b/2)} = x\%$ will lead to a vortex induced drag reduction of $x\%$, at a given lift. [42] Unfortunately, the structural penalty will increase when the height of the winglet is increased. When designing a winglet, one has to balance between aerodynamic benefits and structural penalties. Smaller winglets have less influence on the C_L/C_D value, but have less weight and cause less wing root bending moment due to aerodynamic forces when compared to a large winglet.

When designing a wingtip device, one has to take into account that the thickness of the airfoil should be as low as possible (typically 8%) and that the winglet should not stall before the wing itself. A drawback of a thin airfoil is that the operating Mach number of the wingtip is usually low. Typical Reynold's numbers are between 10^5 and 10^6. Winglets increase the chance of wing flutter. Another downside of adding a winglet is that twist and camber of a winglet must be optimised for one speed, this is usually the cruise speed, so at velocities other than the design speed, the wingtip will be less efficient. [42] Although for a short ranged aircraft, such as the ARA, optimisation for take-off and landing is possibly more efficient.

Increasing the chord length of the winglet results in higher winglet loading and will cause the outer part of the wing to stall earlier. The airfoil will require a large lift coefficient when the chord length is decreased. The height of the winglet is determined by the optimal induced drag and profile drag relationship, a taller winglet is often beneficial. [42]

Most existing winglets are upward pointed winglets, however it is possible to have a downward pointed winglet. A downward winglet produces more lift but has less drag reduction than a conventional winglet. Furthermore, the downward device shows low bending moment penalties due to it often having a smaller moment arm than an upward winglet. [43] This is because the wing has dihedral and a downward placed winglet has a lower arm between the lift force on the winglet and the root of the wing than an upward pointed winglet.

It is possible to combine an upward and a downward winglet. An example of this is the Whitcomb winglet, it has an upper winglet that starts at the maximum chord thickness and a lower winglet that ends just after the maximum chord thickness. The upper winglet has the same sweep as the wing but a larger camber. The lower winglet contributes little to the drag reduction and is often omitted. The optimum cant angle for Whitcomb's experiment was 15°url: `http://cms.education.gov.il/NR/rdonlyres/`

---

[13]url: `http://www.b737.org.uk/winglets.htm` [CITED: 16 June 2015]

D9F6FC7B-A508-43C8-BB34-5C6D8AE0346D/178686/Understanding_Winglets_Technology.pdf [CITED: 16 June 2015].

In contrast to other winglets, including the original Whitcomb design, winglets made by Aviation Partners Inc (API) are joined to the wingtip in a constant radius curve, rather than a relatively sharp angle junction. The smooth curve, according to API[14], reduces shock interference between the winglet and wing near the tip, thus allowing the winglet chord to be extended forward of the point of maximum chord thickness at the tip. Just as important, API uses supercritical airfoil sections in its winglets that have shock waves that are farther aft and weaker than those of the original wing. As a result, there is little interference between the two shock waves[15].

By a genetic algorithm that was designed to find a winglet configuration with fixed lift for minimum drag it was found that a C- or box-wing is the most aerodynamically efficient. These winglets are upward winglets that have a wing section sweeping back towards the fuselage of the aircraft[16].

A winglet could be a wing extension, currently there are four different aircraft that use raked wing extensions, the Boeing 767-400, 777, 747-800, and 787. These are all long range aircraft with long periods of cruise, for which these wingtips are highly efficient. Winglets are more efficient in climb as they produce lift and reduce the drag of an aircraft. Raked wingtips on the other hand do not generate lift, but only reduce the drag by redirecting the wingtip vortices more outboard and aft. They redistribute the lift across the wing, making the wing more efficient. However, for the ARA, it is more important to save fuel during take-off and landing due to its short range. Therefore, the raked wing extension does not seem a viable option for the ARA. However, a raked tip of the winglet could improve its efficiency.

Finally, since winglets increase the climb performance of the aircraft, it allows for a lower thrust setting, thus extending the lifetime of an engine and reducing the maintenance costs. Also, for a lower engine thrust setting, the noise of the aircraft can be reduced and regulations for noise are more easily met. When designed correctly, winglets will improve the aerodynamic efficiency and will therefore reduce the fuel consumption, which in turn reduces the emission of CO_2 and NO_x[17]. Furthermore, a winglet is eye-catching and will therefore be more attractive to potential customers. [42]

16.2   Aerodynamic Analysis

To design a winglet with the best overall performance, it has to be optimised for a single stage of the flight. For the design of the winglet, the program XFLR5 is used which is a vortex lattice analysis tool for airfoils and wings. XFLR5 is unable to model viscous effects and therefore it is chosen to optimise the winglet for take-off and landing, since these phases are influential flight conditions for the fuel burn of a short ranged aircraft like the ARA. In these phases the aircraft is flying at high values of C_L and therefore the results of the analysis are compared at a C_L of 1.4 which was found in chapter 12. Many different possible winglet designs are modelled in the program, for which it shows a $C_L - \alpha$ curve and a $C_L - C_D$ curve. Using these curves, the aerodynamically optimal winglet can be found.

Validation of XFLR5 is done by using AVL, which is a vortex lattice tool for airfoils and wings. Although the programs produce different numerical results for the same wing(tip) configurations, both programs show the same trend when a parameter is changed. Therefore both programs can be compared qualitatively but not quantitatively.

Some standard winglets are chosen for which the parameters are changed to find the optimal performing winglet. This is explained in section 16.2.1. Furthermore, using the theory explained above, some other wingtip devices are tested for their aerodynamic efficiency: a blended winglet, raked winglet, Whitcomb winglet and C-winglet. Also it is investigated what airfoil is the most efficient. This is explained in section 16.2.2.

16.2.1   Winglet Parameter Optimisation

To investigate which winglet has the best performance, six parameters are varied to find their optimal values as shown in figure 16.1. In figure 16.1 the wing is represented by the dotted line and the arrows indicate the positive direction of the parameters. A standard winglet is chosen for which the initial parameters and the results of the parameter tests are shown in table 16.1. These parameters are verified to gain knowledge

---

[14]url: http://www.aviationpartnersboeing.com/winglets_remc.php [CITED: 16 June 2015]
[15]url: http://cms.education.gov.il/NR/rdonlyres/D9F6FC7B-A508-43C8-BB34-5C6D8AE0346D/178686/Understanding_Winglets_Technology.pdf [CITED: 16 June 2015]
[16]url: http://aero.stanford.edu/reports/nonplanarwings/CWingTheory.html [CITED: 16 June 2015]
[17]url: http://www.aviationpartnersboeing.com/winglets_remc.php [CITED: 16 June 2015]

and to verify their influence on C_L, C_D and C_L/C_D. The optimal values are the optimum for that specific parameter while the other parameters are kept constant. Combinations of the parameters can result in even better C_L/C_D values and are explained in section 16.4
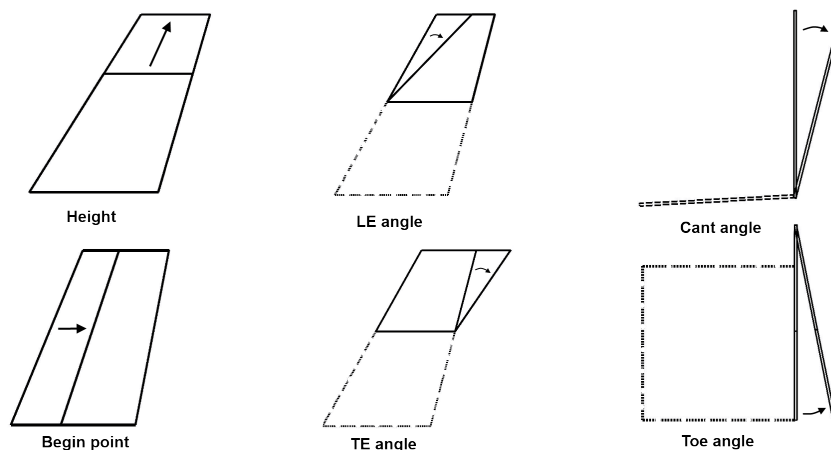
Figure 16.1: The six varied winglet parameters

Table 16.1: Parameters tested with XFLR5 with their initial and optimal values

	Height [% of half span]	Toe angle [degrees]	Begin point % [chord]	LE angle [degrees]	TE angle [degrees]	Cant angle [degrees]
Initial Design	10	0	0	10	0	0
Optimal Design	20 (max tested)	3	40	20	-10	90

Height
Increasing the height of the winglet will improve the C_L/C_D ratio. A taller winglet will always be more aerodynamically efficient, however this increase follows an inversed exponential curve. This means that by increasing the height of the winglet, the increase in aerodynamic efficiency will become less and at some point negligible. Furthermore, increasing the height of the winglet will bring structural penalties which will be explained in section 16.3.

Toe angle
Toe angles (or the sweep of the winglet) are usually kept small. By changing this parameter, the toe angle for optimal aerodynamic efficiency was found to be 3°.

Begin point
Tests with XFLR5 resulted in an optimal starting point of the winglet at 40% of the chord length. This is around the point of maximum thickness of the airfoil and thus where the speed of the air over the wing is the largest. When the winglet begins after this point, the peak pressure of the wing has less interference with the winglet.

Leading and trailing edge angle
Different sweep angles on the leading and trailing edge of the winglet have different efficiencies. The angles for optimal aerodynamic efficiency are 20° for the leading edge angle and -10° for the trailing edge, with respect to the the main wing's leading and trailing edge. It is found that the most optimum winglet planforms have an angle of around 10° between the LE and TE.

Cant angle
The cant angle or the dihedral of the winglet is a parameter for which 0° complies with a winglet which is straight up and 90° is a wing extension. Increasing the cant angle from 0 to 90° results in an increase in aerodynamic efficiency with an optimum at 90°, as expected from theory. Beyond 90° (a downward winglet), the aerodynamic efficiency decreases. Note that for cant angles of 90 to 180°, the lift coefficient is higher but the drag reduction is lower compared to the positive winglet with a cant angle of 0 to 90°. This complies with the theory.

16.2.2 Winglet Configurations

Different parameters of a standard winglet are investigated. Also, different overall winglet configurations which could lead to an improvement in C_L/C_D are investigated. Furthermore, the winglet airfoil is important

for the winglet effectiveness. The analysis of the configurations is shown in this section.

Winglet airfoil
The airfoil for the winglet is first assumed to be the same as the wing, the NACA-1408. The transition from wing to winglet is therefore smooth resulting in less drag. Afterwards, several different airfoils are chosen, changing in thickness, camber and position of camber. Furthermore, also symmetric airfoils are analysed. After analysis it is found that the most efficient airfoil is the NACA-1408. If the winglet has a cant angle, the winglet produces lift making the wing more efficient.

Blended winglet
Blended winglets are used on for example the Boeing 737-700 and are reported to be more efficient than conventional winglets [42], however XFLR5 showed the blended winglet to be less efficient than a conventional winglet. Validation using AVL showed the same trend. A blended winglet is therefore not included in the design.

C-winglet
The C-winglet is supposed to be an efficient winglet configuration having a relatively low induced drag. From analysis it is found that the C-wing does not reduce drag more than the conventional winglet and does not have a better C_L/C_D ratio. A C-winglet is therefore discarded for the ARA.

Raked tip
To optimize the winglet even further, the tip of the winglet is analysed. It is found that using rake on the tip of the winglet increases the aerodynamic efficiency by approximately 1% without having to increase the structural weight.

Whitcomb winglet
Modelling the downward Whitcomb winglet in XFLR5 shows positive results towards the aerodynamic efficiency of the aircraft. By placing a smaller downward winglet in front of a conventional winglet, the rotating airflow or induced drag, is most efficiently reduced[18].

16.3   Structural Analysis

Similar to the aerodynamic analysis, the standard winglet is used and the same six parameters are changed to see what effect they have on the total weight of the aircraft. This analysis is performed on a simplified model of the wing and the forces acting on it. The area of the winglet is used to calculate the normal force on the winglet, which is used to compute the moment around the root of the wing. To estimate the force on the winglet, the wing loading is used and multiplied with the winglet area. There are two different parameters that influence the structural weight due to a winglet. Firstly, the addition of weight by adding a winglet results in a bending relief of the main wing which is beneficial. Secondly, the winglet adds a moment to the wing. This results in a larger bending moment and an increase of the wing's structural weight. The weight of the winglet itself is included in the analysis, but since the winglet is small and thus has a small addition in weight, the bending relief due to the winglet weight is limited. For the most extreme case in which the winglet has a mass 100kg, the bending relief due to the winglet weight is in the order of 5%. The results of the analysis are explained below in a qualitative manner.

Height
When the height of the winglet is increased, the area of the winglet increases as well. An increase in area results in a larger force on the winglet. Both these factors result in an increased bending moment and therefore a heavier wing.

Toe angle
It is assumed for analysis that changing the toe angle does not change the area of the winglet. Since small angles are used for the toe angle, like the optimum for aerodynamic efficiency which was at 3°, this is a reasonable assumption. For the same reason, the change in arm with respect to the wingbox root position is small and therefore neglected. The toe angle does not increase the weight of the wing.

Begin point
The begin point of the winglet largely affects the change in wing weight. Moving the begin point further backward, decreases the area of the winglet and therefore reduces the force on the winglet and the weight of the wing.

---

[18]url: `http://cms.education.gov.il/NR/rdonlyres/D9F6FC7B-A508-43C8-BB34-5C6D8AE0346D/178686/Understanding_Winglets_Technology.pdf` [CITED: 16 June 2015]

Leading and trailing edge angle

Increasing the leading edge angle of the winglet results in a decrease in total area. The consequence is a lower bending moment and a smaller increase in wing weight.

Cant angle

Changing the cant angle does not change the area of the winglet, it does however change the direction of the force on the winglet and therefore changes the bending moment created by the winglet around the root of the main wing. The highest bending moment is reached at a cant angle of 90°, which is basically a wing extension. The force is directed vertically and therefore it has a moment arm which is the full span of the wing plus half of the winglet height. The moment is lowest at a cant angle of 0 and 180°. The force is then directed horizontally and only has a relatively small moment arm. With a cant angle of 180° the moment is even lower than at 0° because the point at which the force acts is moved closer to the point around which the moments are taken. This is due to the dihedral of the wing.

Different parameters

For the structural analysis the toe, LE and TE angle do not have a lot of influence on the structural weight, however they do have a significant influence on the aerodynamic efficiency. Therefore, these three parameters are determined by the aerodynamic analysis. The starting point and height of the winglet influence the wing's structural and aerodynamic efficiency inversely. Increasing the winglet's cant angle results in a larger moment and thus a heavier wing. Therefore, the structural and aerodynamic analysis have to be combined to find the optimal design. It is estimated that the winglet weight is approximately 40kg which is obtained from the reference area of the winglet in combination with a reference winglet from Boeing[19].

16.4   Design Choice

To optimise the winglet for both aerodynamic and structural efficiency, the percentage in structural weight increase was subtracted from the percentage in aerodynamic increase with a 7:6 ratio respectively. This ratio is obtained from the sensitivity analysis in chapter 21 where it is shown that 1% increase in aerodynamic efficiency results in a 0.6% decrease in fuel consumption and 1% addition in structural weight results in a 0.7% increase in fuel consumption.

16.4.1   Combining parameters

For the aerodynamic analysis, a combination of different parameters are tested which results in a design for the upper winglet. Next, the Whitcomb lower winglet is added to increase the aerodynamic efficiency and possbily the overall efficiency even further. Using the Whitcomb lower winglet, the entire winglet is optimised. Both the upper and lower winglet are fitted with raked winglet tips.

As can be seen in table 16.1, the optimal values are different from the initially set values for the parameters. When combining the parameters for an optimal winglet design these values change again. The most aerodynamically efficient upward winglet is found to have a begin point at 40% of the chord. This is around the point of maximum thickness, where the speed of the air over the airfoil is the largest. Having the winglet begin aft of this point increases the efficiency and reduces the interference. For the best height of the overall design, the aerodynamic and structural efficiency are combined and a cant angle of 15° is found to be optimal. This leads to optimum leading and trailing edge angles of 0 and -5°, respectively. This differs from the optimum values described in table 16.1, however the taper ratio is found to be relatively constant, approximately 0.4-0.5. The optimal toe angle is 3°, as was already found to be optimal previously.

Modelling the downward winglet shows improvement in the aerodynamic efficiency of the aircraft. The structural penalty due to the extra wingtip added is small, since the wingtip is pointed downward and has a smaller arm with respect to the point of rotation. During analysis it is found that increasing the downward winglet in length increases the aerodynamic efficiency while keeping the structural penalty relatively small and therefore increasing the overall efficiency. However, this length is limited because of ground operation considerations. Vehicles have to be around the aircraft during ground operations. To limit the possibility of one of these vehicles hitting the downward winglet, the tip has to have a ground clearance of 3 meters, where the height of refueler vehicles is the driving parameter.[20], [21]

It is assumed that the wing extension due to the winglet could have a maximum span increase of 5%. This is because the winglet is an addition to the wing, or the wing of another aircraft, and the addition should not exceed the wing span limit. Thus the wingspan extension is kept as little as possible. Together with the

---

[19]url: http://www.b737.org.uk/winglets.htm [CITED: 18 June 2015]
[20]url: http://garsite.com/jet-refuelers/10000-gallon/ [CITED: 17 June 2015]
[21]url: http://www.easternsupplies.co.uk/products-aviation-refuelling-vehicle.htm [CITED: 17 June 2015]

ground clearance consideration, this resulted in an upper winglet maximum cant angle of 15° and a lower winglet maximum cant angle of 50°. Both these angles were chosen because it was found that increasing the cant angle from 0 towards 90° constantly increases the overall efficiency of the winglet.

16.4.2 Final Design

After both the aerodynamic and structural analyses are completed, the configuration of the final design is shown in figure 16.2. The resulting design parameters are shown in table 16.2. The final winglet design does not look like conventional winglets and is not yet available on the market. This highly efficient winglet is named 'FLOTIN' after its creators, Floris and Martijn, as it is not yet an existing design.
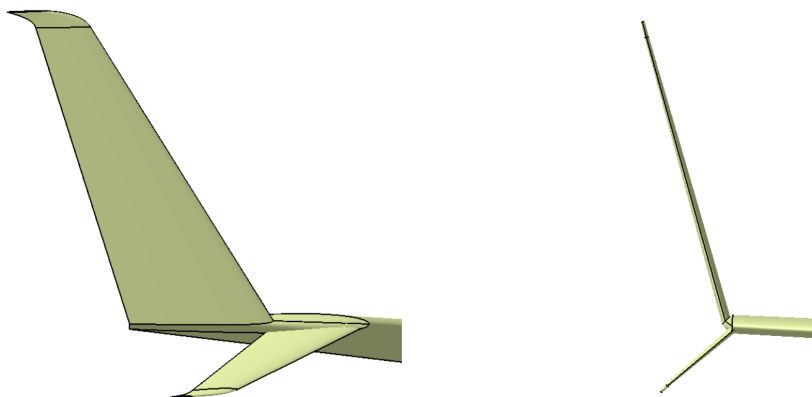
Figure 16.2: The FLOTIN winglet, the finalised winglet design

Table 16.2: Final design of the winglet

	Height [% of half span]	Toe angle [degrees]	Begin/end point [% tip chord]	LE angle [degrees]	TE angle [degrees]	Cant angle [degrees]
Upper winglet	15	3	40/100	0	-5	15
Lower winglet	5	3	0/40	25	20	50

The total aerodynamic efficiency of adding the FLOTIN winglet compared to only having a wing without a winglet is approximately 10.4%. The structural penalty related to adding a winglet to the wing is approximately 3.0% of the wing weight. Since improvement in aerodynamic efficiency is slighty less important than the addition of extra structural weight, the total fuel efficiency of the adding a winglet is approximately 6.1%.

Finally, not only the efficiency of a winglet is important but a winglet also has a certain commercial value. When customers see an aircraft with winglets, they automatically think that the aircraft is more advanced and more streamlined. So even for a winglet which brings 0% fuel redcution, the ARA will be more attractive for airliners due to the fact that the aircraft has winglets and will therefore also increase the aircraft sales[22].

16.5   Recommendations

For future winglet design there is still the possibility for improvement on the winglet, especially the lower winglet. By increasing the size of the lower winglet more overall efficiency can be obtained, but due to ground clearance considerations, not the full sized winglet has been used. When enough safety measures can be provided, an even more efficient winglet can be acquired in the future. Furthermore, for more accurate results on aerodynamic analysis, viscosity should be taken into account especially when the winglet is designed for cruise speed. Finally, for further investigation into the structural aspect of the winglet, the skin and stringer properties could be analysed to get a more accurate idea of the weight of the winglet and therefore have a better insight of the forces acting on the wing.

---

[22]url: `http://jetadvisors.com/winglets/` [CITED: 29 June 2015]

17 | Cargo Bay Structural Design

This chapter presents the detailed structural design of the cargo section of the ARA. The case study of the cargo section is used to determine the material type and topology of the fuselage section and predict the corresponding weight and fuel reductions. First of all, the constraining load cases have to be identified. The load cases are discussed in section 17.1. Secondly, two tools to analyse stresses for a given fuselage layout are created, one for metals and one for composites. These tools are discussed in section 17.2. Thirdly, these tools are used to optimise the fuselage layout with respect to stringers and skin thickness. Section 17.3 presents the results found from the analysis of section 17.2. Lastly, the conclusions and recommendations can be found in section 17.4.

17.1 Load Case Analysis

In this section the load cases that act on the fuselage are analysed. The used method is based on information found in [44] and the regulations from CS-25 [2]. Concerning fuselages, the regulations address four different load categories, i.e. ground loads, flight loads, flight loads combined with internal pressure and internal overpressure alone. The ARA must be able to withstand the described load cases in combination with the ARA operational configuration at the time of these load cases.

17.1.1 General Assumptions

The assumptions that have been made to simplify the fuselage geometry calculations are:

- The fuselage is modelled without centre wing box, instead it is assumed that the front and rear spar will transfer all the loads of the wings to the fuselage. Due to this assumption the stresses around the spars are higher than in reality. Therefore, this model cannot be used to design the fuselage section in proximity of the wings.

- The wing weight, main wing lift, main landing gear weight, thrust of the engines, drag of nacelle and pylons, as well as the loads carried by the main landing gear are transferred into the fuselage through the front and rear wing spars. Again this assumption will cause higher stresses in the fuselage in proximity of the wing spars.

- The airframe equipment and services weight are modelled to be distributed across the fuselage length as are the fuselage structural weight, the passengers and the cargo. This assumption will cause that the loads are more or less distributed as in reality.

- The empennage weight, the horizontal and vertical lift force, the nose landing gear weight, the avionics weight and pilot weights are modelled as concentrated forces. This assumption will cause higher stresses than in reality in the fuselage sections of the empennage and the cockpit where the concentrated forces are applied.

- When on the ground the normal force due to the nose gear is modelled as a concentrated force. This assumption closely simulates reality were the force on the nose gear is transferred by a nose landing gear strut to the fuselage structure.

- The fuselage is modelled without cut-outs (no windows, no doors). This assumption will cause that no additional stresses are considered in the design due to cut-outs.

17.1.2 Weight Distribution

From the class II estimation, weights of the aircraft subsystems and their corresponding centres of gravity as discussed in chapter 8 are obtained. For the loads acting on the fuselage, some weights are modelled as distributed forces such as the fuselage, cargo and passenger weight. The distribution of the aircraft weight components that are assumed to act on the fuselage are given in table 17.1. The locations are measured with respect to the nose of the aircraft. A sketch of the situation is presented in 17.1.

Table 17.1: Distributed weights acting on the aircraft

Distributed Loads	Weight Components	Range
Acting on fuselage:		
$q_{fus,etc}$	air-conditioning-, pressurisation- and anti-icing-systems, auxiliary gear, cabin crew, electrical systems, flight control systems, furniture, fuselage structure, hydraulic and pneumatic systems, oxygen system and paint	$(0m)$ - $(35m)$
q_{pas}	Passengers	$(6.4m)$ - $(24.5m)$
q_{cargo}	Cargo	$(24.5m)$ - $(31.0m)$
Acting on wing:		
q_{wing}	Wing structure	front spar$(14.3m)$- rear spar$(17.6m)$
q_{fuel}	Fuel	front spar$(14.3m)$- rear spar$(17.6m)$
q_{lift}	Lift	front spar$(14.3m)$- rear spar$(17.6m)$
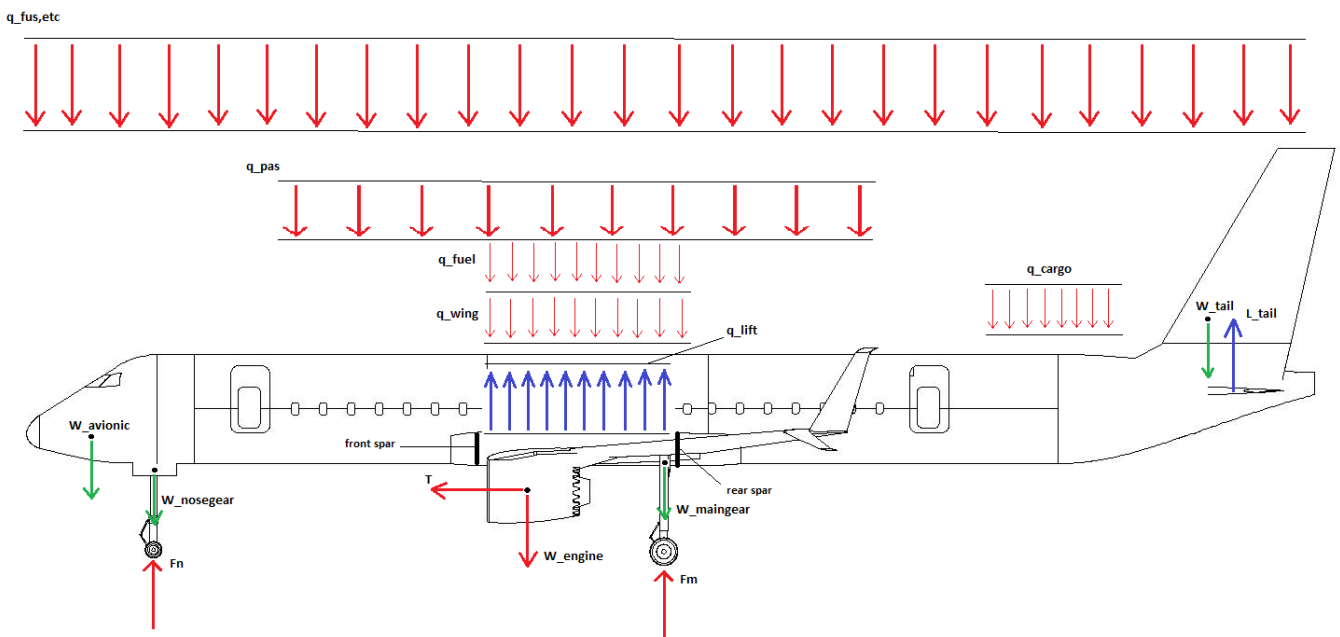
Figure 17.1: Weight and force distribution

17.1.3 General Method and Sign Convention

In order to optimise the fuselage structure, all the loads that act on the fuselage during the ARA's operational life are determined. The loads acting on the fuselage structure vary for different Unit Load Cases (ULCs). This results in different shear forces, bending moments and torques that the fuselage has to withstand. Furthermore, the Combined Load Cases (CLCs) are determined through the superposition of ULCs that can occur simultaneously during the operational life of the aircraft. The CLCs generally cause larger stresses than the ULCs and therefore the CLCs are used to optimise the fuselage structure. By dividing the fuselage into twelve sections, the shear forces are calculated over the length of each section starting from the nose. Each of the twelve sections starts from the beginning of a distributed force or concentrated force until just before the start of a new force, so that each section has a homogeneous force distribution. Each section is than divided into n subsections, where $n = \frac{section\ length}{dx}$. Where dx is the stepsize which is set to 0.0001 for the calculations.

The shear force in a section is computed by summing the shear force of the previous section with the distributed shear force in the present section. The moment in each section is computed by adding the moment of the previous section to the moment in the present section and by integrating the shear force in the present section over the length of the moment arm. The sign convention that is used for the calculations of the load cases is shown in figure 17.2.
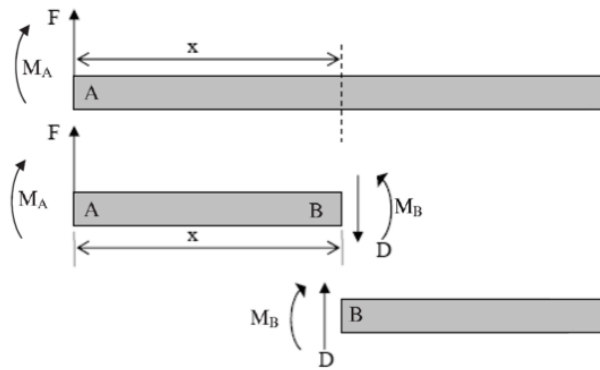
Figure 17.2: Sign Convention

17.1.4 Unit Load: Cabin Pressurisation

During flight the cabin of the aircraft is pressurised. The air pressure inside the cabin will be the pressure at an altitude of $2000m$[23] which is in the range of typical aircraft at a cruising altitude of $11000m - 12200m$. The maximum operating altitude of the aircraft is limited by the engine efficiency. As no information is available for the maximum operating altitude of the engine the maximum height is taken from a reference aircraft which uses the same engines, the MRJ-70. From the MRJ-70 a maximum operating altitude of the aircraft of $12000m$ is obtained [24]. The pressure corresponding to an altitude of $2000m$ is $79.5kPa$. The maximum operating altitude of the aircraft is $12km$, the outside pressure at this altitude is $19.3kPa$. The pressures are determined from the International Standard Atmosphere (ISA). The difference between the cabin pressure and the outside maximum operating pressure is equal to $60.1kPa$, for the fuselage this pressure difference is multiplied by 1.33 for aircraft operating below $45,000ft$ or $13.7km$ according to the airworthiness regulations. [2] Therefore, a maximum cabin pressure of $80kPa$ must be withstood. [2]

17.1.5 Unit load: Horizontal Force due to Drag and Thrust

The horizontal force acting on the fuselage structure is caused by the drag of the aircraft and the thrust delivered by the engines. The aircraft drag is divided in several drag components. It is assumed that the wing, fuselage, empennage, nacelle and pylons contribute to the drag of the aircraft during cruise. The total drag during cruise is equal to $22.7kN$ which is equal to the total delivered thrust. In table 17.2 the distributed drag forces of each drag component can be seen as a percentage of the total drag. These percentages are estimations based on the methods provided by [45]. In figure 17.3 it can be seen that all of the loads are distributed except for the thrust, the initial drag on the nose and the drag of the nacelles and pylons. The drag of the nacelles and pylons is assumed to be aligned with the thrust. The drag of the wings, pylons, nacelles and the thrust will be transferred by the front and rear wing spar to the fuselage structure. The resulting normal force distribution can be found in figure C.1 in appendix C.

Figure 17.3: Drag distribution on the aircraft

---

[23]url: http://www.who.int/ith/mode_of_travel/cab/en/ [CITED: 18 June 2015]

[24] url: https://janes.ihs.com/CustomPages/Janes/ReferenceHome.aspx [CITED: 23 May 2015]

Table 17.2: Distribution of drag on the ARA

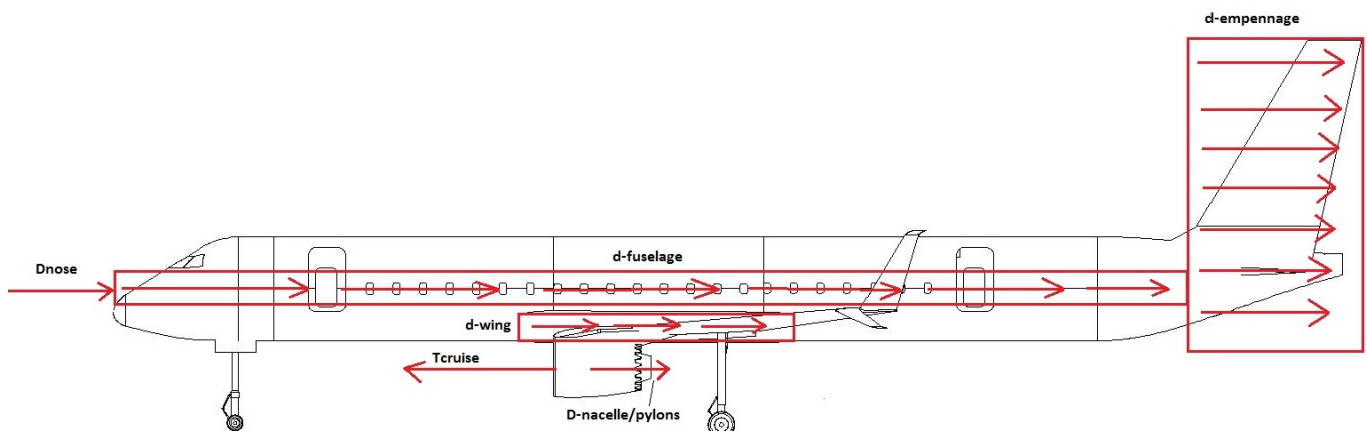| Distributed drag force	Range	Estimated % of total drag
$d_{fuselage}$	(0m)-(31m)	40
d_{wing}	front spar(14.3m)- rear spar(17.6m)	34
$d_{empennage}$	(31m)-(35m)	16
$D_{nacelle/pylons}$	engine(14.85m)	8
D_{nose}	(0m)	2

17.1.6 Unit Load: Flight Cases

Several load cases are considered as driving cases for the fuselage analysis. In this section the different unit load cases that occur during flight are presented.

Cruise 1g
This load case considers the cruise flight phase where all the forces and moments are in equilibrium. Drag equals thrust and lift equals weight. For the calculations the maximum weight during cruise is used, which is calculated to be $32914kg$ based on the fuel fractions in chapter 8, table 8.2. The different weights acting on the fuselage are explained in section 17.1.2. In cruise the lift generated by the wing and horizontal tail is 97.9% and 2.1% of the weight during cruise, respectively. The thrust in cruise equals approximately $22.7kN$. The thrust of the engines, the wing and fuel weights are transferred from the wing to the fuselage by the front and rear spar. The spars will therefore cause additional shear and moment forces on the fuselage. For this load case no torque is acting on the fuselage. The resulting shear forces and moments are plotted in figures C.2 and C.3 in appendix C.

Horizontal Tail Elevator Deflection
This load case considers that 100% of the maximum loading is acting on both sides of the horizontal tail. According to [44] the maximum horizontal tail load, L_h due to an abrupt elevator manoeuvre can be described by equation 17.1. This load can be considered to act upward or downward depending on the elevator deflection.

$$L_h = K_r \cdot \frac{1}{2} \cdot \rho \cdot V^2 \cdot S_h \cdot C_{L_{h_{\delta_e}}} \cdot \delta_{e_{max}} \tag{17.1}$$

In equation 17.1 $C_{L_{h_{\delta_e}}}$ is the horizontal tail lift slope as a function of the elevator deflection δ_e, S_h is the horizontal tail surface area of $27.3m^2$ (see chapter 14), $\delta_{e_{max}}$ the maximum elevator deflection of $0.32m$ (see chapter 15), K_r the aircraft response factor for abrupt elevator manoeuvres. According to [44] K_r ranges from 0.7 to 0.9. K_r is set to 0.9, the most critical condition. $C_{L_{h_{\delta_e}}}$ can be calculated using equation 17.2. Where S_e is the elevator surface area of $7.28m^2$ (see chapter 15).

$$C_{L_{h_{\delta_e}}} = C_{L_{h_\alpha}} \cdot \sqrt{\frac{S_e}{S_h}} \tag{17.2}$$

The horizontal tail lift slope as a function of the angle of attack α is estimated with equation 17.3. With A_h the horizontal tail aspect ratio of 5 and λ_h the horizontal tail sweep angle of 37° (see chapter 14). This leads to a $C_{L_{h_\alpha}}$ value of 3.59. Substituting this in equation 17.2 a value of 1.85 for $C_{L_{h_{\delta_e}}}$ is obtained.

$$C_{L_{h_\alpha}} = \frac{2\pi}{1 + \frac{3}{A_h cos \lambda_h}} \tag{17.3}$$

Substituting all the inputs in equation 17.1 gives the maximum loading on the horizontal tail of $149kN$. This loading will cause additional shear forces and moments in the fuselage in addition to the forces during the normal cruise condition. The results are plotted in figures C.4 and C.5 in appendix C for a downward horizontal tail force and figures C.6 and C.7 for an upward horizontal tail force.

Side Slipping Flight
The highest side slip angles are obtained when an in-flight engine failure occurs. The thrust is provided by only one engine which causes a moment around the centre of gravity. The pilot has to neutralise this with a rudder deflection, so that eventually a steady flight will be established. Maximum side slip angles are 8°,

but an over swing factor of 1.6 should be applied. [44] The tail force F_{tail} that causes a sideways bending moment in the fuselage is calculated with equation 17.4.

$$\sum M_{cg} = 0 \Rightarrow 0 = T \cdot y_{eng} \cdot F_{tail} \cdot cos\beta(x_{ac_h} - x_{cg}) \tag{17.4}$$

$$F_{tail} = \frac{Ty_eng}{cos\beta(x_{ac_h} - x_{cg})} \tag{17.5}$$

In equation 17.4 F_{tail} is calculated to have an absolute value of $17.3kN$, it is assumed that the force acts through the aerodynamic centre of the horizontal tail. F_{tail} will cause additional shear forces, bending moments and a torque inside the fuselage. A sketch of the situation is shown in figure 17.4. The resulting shear forces and moments are plotted in figures C.8, C.9 and C.10 in appendix C.
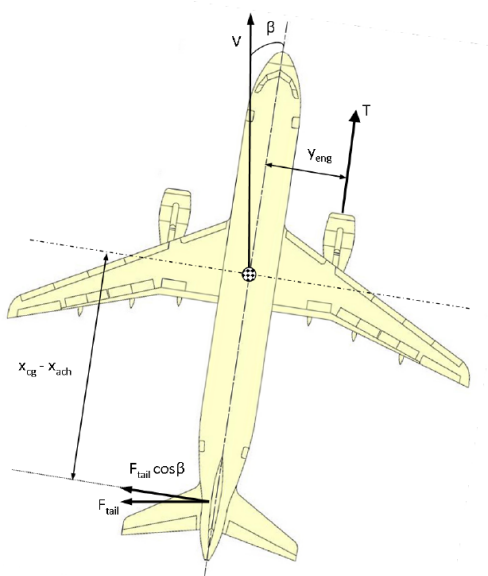
Figure 17.4: Forces during side slipping flight

Lateral Gust
The lateral gust loading on the vertical tail is calculated with equation 17.6. [44]

$$L_v = K_g \cdot \frac{1}{2} \cdot \rho_0 \cdot U_E \cdot V_E \cdot S_v \cdot C_{L_{v_\beta}} \tag{17.6}$$

In equation 17.6 L_v is the side load on the vertical tail, S_v is the vertical tail surface area of $20.96m^2$ (see chapter 14) and V_E is the equivalent cruise airspeed of $128.7m/s$ (see chapter 19). K_g is the gust alleviation factor and U_E is the equivalent gust velocity, the method to calculate both factors is explained in chapter 19. At cruise a value of 0.865 for K_g and $15.24m/s$ for U_E are obtained, respectively. The side lift slope with respect to the side slip angle β, $C_{L_{v_\beta}}$ is calculated with equation 17.7, where A_v is the aspect ratio of the vertical tail which is equal to 1.9 (see chapter 14) and λ_v is the sweep angle of the vertical tail which is equal to $28.6°$ (see chapter 14). Substituting all the values in 17.6 a value of 2.25 for $C_{L_{v_\beta}}$ is obtained.

$$C_{L_{v_\beta}} = \frac{2\pi}{1 + \frac{3}{A_v cos\lambda_v}} \tag{17.7}$$

Using equation 17.6 the side load on the vertical tail L_v is calculated which equals $16.9kN$ it is assumed that this force acts in the aerodynamic centre of the vertical tail. The side load on the vertical tail will also cause additional shear forces, moments and torque on the fuselage structure. The results are plotted in figures C.11, C.12 and C.13 in appendix C.

17.1.7 Unit Load: Ground Cases

In this section the ground load cases will be explained.

Static Ground Case 1g
The static ground case 1g can be described as the case where the aircraft is on the ground with no aerodynamic loads, pressurisation and thrust. In this case the only load acting on the aircraft is the weight which causes a load on the landing gear. This load is partially carried by the nose gear and partially by the main gear. The load carried by the main landing gear is then transferred to the rear and front spar of the wing. From there these loads are transferred to the fuselage structure. The load carried by the nose landing gear is directly transferred to the fuselage structure at the point where the nose gear is located. The resulting shear forces and moments are plotted in figures C.14 and C.15 in appendix C.

Three Point Level Landing
For the three point level landing case, the aircraft has contact with the ground simultaneously on the nose and main landing gear. Drag, thrust and pressurisation are neglected for the calculations of this case. A landing load factor of 2 is taken into account which means that the vertical acceleration of the weight of the aircraft equals 2g. Additionally, the weight with which the aircraft lands is assumed to be equal to the MTOW. This is slightly more then the most critical case, due to an aborted take-off, where the aircraft weight is slightly less then the MTOW. The resulting forces and moments for this case are shown in figures C.16 and C.17 in appendix C.

Two Point Level Landing
For the two point level landing condition the aircraft is assumed to first make contact with the ground through the main gear. Again, pressurisation, drag and thrust can be neglected. Just like at the three point level landing, for the two point level landing a landing load factor of 2 is taken into account. By looking at this condition the most critical vertical reaction acting at the main landing gear can be determined. This load causes a shear force at the front and rear spar and is subsequently transferred to the fuselage structure. The results are plotted in appendix C, figures C.18 and C.19.

Abrupt Ground Braking
With the abrupt ground braking case, the aircraft uses full braking power of the main landing gear. It is assumed that full breaking power is applied when the aircraft is in contact with the ground with both the main and nose landing gear. As a result, a pitch down nose acceleration is causing a moment around the main landing gear leading to a higher load being carried by the nose landing gear. Furthermore, it is assumed that the drag only consists of the friction of the tires with the ground. For the calculations a dynamic factor has been used which means that the aircraft is experiencing a pitch rotational acceleration during the braking. The results are shown in figures C.20 and C.21 in appendix C.

17.1.8 Combined Load Cases

The combined load cases are found by superposition of the unit load cases that could occur simultaneously during the operational life of the aircraft. A summary of the unit load cases is given in table 17.3 whereas the combined load cases that were considered during the design of the fuselage can be found in table 17.4.

Table 17.3: Unit Load Cases

Code	Unit Load Case (ULC)
ULC E1	Cabin pressurisation
ULC E2	Horizontal force due to drag and thrust
Flight Cases:	
ULC F1	Cruise 1g
ULC F2	Horizontal tail elevator deflection
ULC F3	Side slipping flight
ULC F4	Lateral gust
Ground Cases:	
ULC G1	Static ground case 1g
ULC G2	Three point level landing
ULC G3	Two point level landing
ULC G4	Abrupt ground braking

Table 17.4: Combined Load Cases (CLC)

Code	Combined Load Case	ULC Combination
CLC 1	g manoeuvre + cabin pressurisation	ULC F1+ ULC E1
CLC 2	-g manoeuvre + cabin pressurisation	-ULC F1+ ULC E1
CLC 3	2.5g manoeuvre + cabin pressurisation	2.5 · ULC F1 + ULC E1
CLC 4	lateral gust + cabin pressurisation	ULC F4+ ULC E1
CLC 5	-lateral gust + cabin pressurisation	-ULC F4+ ULC E1
CLC 6	side slip + cabin pressurisation	ULC F3 + ULC E1
CLC 7	-side slip + cabin pressurisation	-ULC F3 + ULC E1
CLC 8	horizontal tail force up + cabin pressurisation	ULC F2+ ULC E1
CLC 9	horizontal tail force down + cabin pressurisation	-ULC F2+ ULC E1
CLC 10	2.5g manoeuvre + h-tail force up + cabin pressurisation	2.5 ·ULC F1 + ULC F2+ ULC E1
CLC 11	2.5g manoeuvre + h-tail force down + cabin pressurisation	2.5 ·ULC F1 - ULC F2+ ULC E1
CLC 12	2.5g manoeuvre +side slip + cabin pressurisation	2.5 · ULC F1 + ULC F3+ ULC E1
CLC 13	2.5g manoeuvre -side slip + cabin pressurisation	2.5 · ULC F1 - ULC F3+ ULC E1
CLC 14	2.5g manoeuvre +lateral gust + cabin pressurisation	2.5 · ULC F1 + ULC F4+ ULC E1
CLC 15	2.5g manoeuvre -lateral gust + cabin pressurisation	2.5 · ULC F1 - ULC F4+ ULC E1

17.2 Structural and Material Analysis

In section 17.2.1 the analytical stress analysis methods are discussed. Furthermore, in 17.2.2 the dimensions of the stringers are discussed. Sections 17.2.3, 17.2.4 and 17.2.5 discuss the application of sandwich panels, metals and composites as materials in the fuselage, respectively.

17.2.1 Stress Analysis

The internal forces and moments obtained from the load case analysis are converted to local stresses throughout the fuselage cross-sections. The stresses which are taken into account in the model are: the bending stress in the x-direction due to M_y and M_z, the normal stress in the x-direction due to the normal force S_x, the hoop stress due to the pressure, normal stress in the x-direction due to the pressure, the shear stress in the yz-plane due to the shear forces S_y and S_z and the shear stress in the yz-plane due to the moment M_x. The stresses in the z-direction are neglected due to the assumption of a thin-walled fuselage skin. Furthermore, the effect of buckling is not considered. However, buckling is next to the analysis discussed in this section the most important failure analysis for the fuselage and stiffeners. Therefore, it should be kept in mind that the results found from the analysis presented in this chapter are lacking and that it is recommended to do a more elaborate analysis as discussed in section 17.4.

Before any stresses are calculated, the neutral axes locations and moments of inertia should be computed. The neutral axes locations can be calculated by using equations 17.8 and 17.9, where A_i is the area of a component of the cross-sectional area such as the skin (or a skin element) and the stringers and y_i and z_i are the y- and z-coordinates of the components respectively. The moments of inertia are calculated by using equations 17.10, 17.11 and 17.12.

$$\bar{y} = \frac{\sum_{i=1}^{n} A_i \cdot y_i}{\sum_{i=1}^{n} A_i} \tag{17.8}$$

$$\bar{z} = \frac{\sum_{i=1}^{n} A_i \cdot z_i}{\sum_{i=1}^{n} A_i} \tag{17.9}$$

$$I_{yy} = \int y^2 \, dA \tag{17.10}$$

$$I_{zz} = \int z^2 \, dA \tag{17.11}$$

$$I_{yz} = \int y \cdot z \, dA \qquad (17.12)$$

The bending stress in the x-axis direction throughout the cross-section is a function of the distance to the neutral axes and is calculated with equation 17.13. [46]

$$\sigma_{x,bending} = \frac{-M_y(I_{zz} \cdot (z - \bar{z}) + I_{yz} \cdot (y - \bar{y}))}{I_{yy} \cdot I_{zz} - I_{yz}^2} + \frac{M_z(I_{yy} \cdot (y - \bar{y}) - I_{yz} \cdot (z - \bar{z}))}{I_{yy} \cdot I_{zz} - I_{yz}^2} \qquad (17.13)$$

Furthermore, as at this stage it is not known of what material the stiffeners in the fuselage are composed of it is assumed that the stiffeners are from the same material as the fuselage skin. This implies equal strain throughout the cross-section and therefore the stress in x-direction due to the normal force S_x is calculated by using equation 17.14. These assumptions should be revisited when a detailed stringer design is performed.

$$\sigma_{x,force} = \frac{S_x}{A} \qquad (17.14)$$

The pressure causes a stress in x-direction and a hoop stress which are calculated by using equations 17.15 and 17.16, respectively. Where p is the cabin pressure, r is the radius of the fuselage and t_{skin} is the fuselage skin thickness.

$$\sigma_{x,pressure} = \frac{p \cdot r}{2 \cdot t_{skin}} \qquad (17.15)$$

$$\sigma_{hoop} = \frac{p \cdot r}{t_{skin}} \qquad (17.16)$$

The forces in the y- and z-direction and the moment M_x cause shear stresses in the yz-plane. First, the shear flow throughout the cross-section is calculated with equation 17.20 [46], where q_b is the basic shear flow, $q_{s,0}$ is the constant zero-twist shear flow and $q_{torsion}$ is the constant shear flow due to M_x. q_b is calculated with equation 17.17 [46], where y_{str} and z_{str} are the coordinates of the stringer location with respect to the cross-section axis system and A_{str} is the area of the stringer. Note that the addition of stringers increases the shear flow locally as can be seen from the terms $\sum_{i=1}^{n} A_{str,i} \cdot y_{str,i}$ and $\sum_{i=1}^{n} A_{str,i} \cdot z_{str,i}$ in equation 17.17. $q_{s,0}$ and $q_{torsion}$ are obtained by using equation 17.18 and 17.19, respectively.

$$q_b = -\frac{S_y \cdot I_{yy} + S_z \cdot I_{yz}}{I_{yy} \cdot I_{zz} - I_{yz}^2} \left(\int_0^s t_s \cdot y_{str} \, ds + \sum_{i=1}^{n} A_{str,i} \cdot y_{str,i} \right) -$$
$$\frac{-S_z \cdot I_{zz} - S_y \cdot I_{yz}}{I_{yy} \cdot I_{zz} - I_{yz}^2} \left(-\int_0^s t_s \cdot z_{str} \, ds - \sum_{i=1}^{n} A_{str,i} \cdot z_{str,i} \right) \qquad (17.17)$$

$$q_{s,0} = \int_0^s q_b \cdot t_{skin} \, ds \qquad (17.18)$$

$$q_{torsion} = \frac{M_x}{2 \cdot A} \qquad (17.19)$$

The shear stress due to shear flow is calculated from the total shear flow by using equation 17.21.

$$q_s = q_b + q_{s,0} + q_{torsion} \qquad (17.20)$$

$$\tau_{yz} = \frac{q_s}{t_{skin}} \qquad (17.21)$$

17.2.2 Stringer Design Choice

Ideally, a stringer is designed when the required cross-sectional area has been determined. However, it is beneficial to standardise the stringers to avoid the cost of manufacturing custom stringers for each section of the fuselage. Therefore, it is decided to limit the number of stringers to three different types. A choice is made between three different types of stringers: Z, L and hat stringers, which are shown in figure 17.5. These are selected based on the ease of manufacturability. Driving criteria for the stringers are the total height of the stringer. During the preliminary design $40mm$ was set aside for the thickness of the skin combined with the height of the stringer. [13] With the skin thickness realistically varying between 1 and $4mm$ it is decided to allow a maximum total height for the stringers of $36mm$.
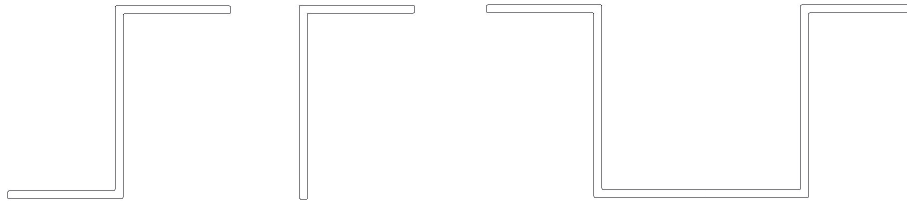

Figure 17.5: From left to right the Z, L and hat stringer

Stringers are inherently sensitive to buckling, with open cross-section stringers exposed to flexural-torsional buckling. [46] Hat stringers show a reduced influence to torsional buckling due to their closed cross sectional area. Additionally, when compared to L and Z stringers, they may have a lower height whilst maintaining a larger cross sectional area. However, when the width becomes too small, the stringer either does not accommodate for proper fastening to the skin due to a low contact area or becomes too tall and narrow (difficult to manufacture).

Based on analysis methods in [46] it is determined that the required cross sectional area of the stringers range between 100 and $300mm^2$. Three stringer cross-sections are designed based on the required areas (100, 200 and $300mm^2$). Both the $200mm^2$ and $300mm^2$ stringers are hat stringers to maintain flexural rigidity. The $100mm^2$ stringer is a z stringer due to the low area required and the constrained height of $36mm$.

17.2.3 Sandwich Panels

Sandwich panels are currently used on commercial aircraft in non-critical surfaces such as the vertical tail or fairings. In the midterm report it was commented that sandwich panels may be considered for the primary structure of the fuselage. [13] On further consideration, however, it is deemed that the use of sandwich panels is not a feasible option for regional jets. Firstly, operational costs are larger due to maintenance since sandwich panels are difficult and expensive to inspect and repair. Secondly, over time sandwich panels will increase in mass due to an accumulation of water in the core material. [47] This increases the fuel burn as the aircraft ages, again increasing operating costs. Thirdly, sandwich panels are impact sensitive. Especially for the underside of the fuselage this would result in increased mass to adequately protect the skin from Foreign Object Damage (FOD). [48] Since the ARA has a short range and low turnaround time it will often be exposed to these risks.

17.2.4 Metals

Structural analysis of the metal concepts is done by applying idealisation principles to the skin and stringers of the fuselage. [46] The following paragraphs outline the steps taken to analyse and optimise the design of the metal fuselage, and the assumptions made during the process.

It is assumed that all of the shear flow (due to torsion and shear forces) is carried completely by the skin. All hoop stresses due to pressure are assumed to be carried by the skin. Additionally, the skin is assumed to be 30% effective in taking normal stresses. This is due to the fact that the skin is prone to buckling when put under compressive normal stresses. [46] The stringers are assumed to be effective in taking only normal stresses due to bending, pressure and normal forces.

To facilitate a feasible structural analysis method the fuselage structure is idealised using the boom method. Firstly, the stringers are assumed to be discrete masses placed on the skin. Secondly, to facilitate the assumption that the skin is capable of taking some of the normal stresses, a fraction of the skin area adjacent to each boom is lumped into the respective boom. The implication of using a boom method to

analyse the shear flow is that only the average shear flow is calculated between each boom. This means that part of the skin will effectively always be failing in shear. To avoid this pitfall, the fuselage is later analysed with 2000 fictive booms (zero area) thereby the skin can be analysed for shear failure with a larger degree of accuracy.

The method used to optimise the fuselage cross section is to size the skin thickness so that it has no failure due to shear, this sizing is done for each combined load case to determine the minimum allowable skin thickness. Next, the booms are sized so that the entire fuselage does not fail due to any of the applied loads. Here, the load cases with large bending moments are critical drivers for the position and dimension of the stringers. The placement of the stringers is done manually between each iteration using a diagram that is created by the analysis program indicating the location of the failed booms. In section 17.2.1 the equations used to perform the structural analysis are presented.

Since metals show isotropic behaviour, the Von Mises failure criterion is calculated for the skin and booms. Which simplifies the failure analysis of the material. If the Von Mises stress exceeds the yield stress of the material (including a safety factor of 1.5) the structure fails. To account for fatigue due to the pressure cycles, the pressure input load is increased by a factor $f_p = \frac{YieldStrength}{FatigueStrength@n=10^5}$. For the chosen alloy (Al-7150) $f_p = 3.5$.

Metal Selection
The type of aluminium used for the stress analysis is dependent on two things: manufacturability and specific yield strength. Manufacturability includes the fact that the aluminium should be supplied as a sheet, not a billet. The specific yield strength is calculated using data from [49]. As is evident from the data in table 17.5 the price per kg of each material does not vary more than 13.5%. This difference is neglected in the choice of the material. The selected material is Al-7150-T61511. A detailed list of its properties is presented in table 17.6.

Table 17.5: Properties of different types of aluminium [49]

Metals	Price $[\frac{EUR}{kg}]$	Density $[\frac{Mg}{m^3}]$	Yield Strength [MPa]	Specific Yield Strength $[\frac{MPa}{\rho}]$	Specific strength at 10^5 cycles $[\frac{MPa}{\rho}]$
Al 2014-T6	2.00	2.83	324	114.49	37.45
Al 2024-T6	2.01	2.78	345	125.46	45.09
Al 5052 H38	1.80	2.7	221	81.85	36.67
Al 6061-T6	1.79	2.73	193	70.70	26.74
Al 6063-T6	1.77	2.72	200	73.53	26.84
Al 7050-T74	1.92	2.84	372	130.99	45.07
Al 7075-T6	1.86	2.83	359	126.86	43.11
Al 7149-T73	1.86	2.87	379	131.06	46.69
Al 7150-T61511	1.92	2.84	469	165.14	47.18
Al 7475-T6	1.86	2.81	407	144.84	59.43

Table 17.6: Material Properties Al-7150-T61511

Description	Value	Unit
Price	1.92	$(\frac{EUR}{kg})$
Density	2.84	$(\frac{Mg}{m^3})$
E	75.7	MPa
Yield Strength	469	MPa
Ultimate strength	510	MPa
G	29.4	GPa
Poisson's ratio	0.33	-
Fatigue Strength @ n= 10^5	134	MPa

17.2.5 Composites

Composite materials are orthotropic and thus require a more complex analysis and design procedure than metals. The procedure of the design of a composite fuselage is divided into multiple parts. First, the properties of the lamina and the laminate used for the skin are acquired. Secondly, the stress in each lamina for each laminate is calculated and each lamina is evaluated for failure. Furthermore, the iterative design method and philosophy for topology optimisation of the stringers and optimisation of the skin is discussed.

Next, the considered fibres and resin for the fuselage design and additional considerations of composite materials are discussed.

Lamina Properties

In order to analyse the stress in the skin, first the properties of a single unidirectional lamina need to be acquired. To acquire the longitudinal Young's modulus, transverse Young's modulus, major poisson's ratio and axial shear modulus a composite cylinder assemblage (CCA) model is used presented by [50] and adapted by [51]. The CCA model assumes that the fibres are circular in cross-section, spread in a periodic arrangement and continuous. For most composite lamina these are valid assumptions. However, it should be kept in mind that the effect of using different fibre cross-sections (which allows for a denser packing) cannot be evaluated by using the CCA model and is not in the scope of the analysis presented in this report. Also, it is assumed that there are no voids in the matrix. The density of the lamina is evaluated by using the method stipulated by [51].

Furthermore, the ultimate strengths for longitudinal tension, longitudinal compression, transverse tension, transverse compression and intralaminar shear have to be calculated for a single lamina. Note that the longitudinal compression failure mode can be due to fibre compression, delamination and/or micro-buckling. An analytical model to predict these failure stresses are lacking in accuracy as found from comparison studies such as [52]. Therefore, to predict these ultimate strengths the semi-empirical equations proposed by [53] are used.

Laminate Stress and Failure Analysis

A macro-mechanical analysis of the laminate and lamina is performed. First, the midplane strains and curvatures of the laminate are calculated with equation 17.22 [51]. Where $\underline{\mathbf{N}}$ consists of N_x and N_y which are the normal forces per unit length and N_{xy} which is the shear force per unit length. $\underline{\mathbf{M}}$ consists of M_x and M_y which are the bending moments per unit length and M_{xy} which is the twisting moment per unit length. The stress calculated in the stress analysis of section 17.2.1 is the membrane stress in the skin which is the average stress that acts at the skin. As no stress distribution acting at the skin is calculated, the moment around the midplane is zero. Therefore the entries of M_x, M_y and M_{xy} are zero. The $\underline{\mathbf{N}}$ parameters are obtained from the internal stresses from the stress analysis discussed in section 17.2.1 and the thickness of the laminate. Furthermore, the $[A]$, $[B]$ and $[D]$ matrices are the extensional, coupling and bending stiffness matrices respectively and depend on the top and bottom distance from each lamina to the midplane of the laminate and the transformed reduced stiffness matrix elements. A more detailed discussion and equations to calculate the entries of the $[A]$, $[B]$ and $[D]$ matrices are given in [51]. The outputs are the midplane strains ϵ_x^0, ϵ_y^0 and γ_y^0 and curvatures κ_x, κ_y, κ_{xy}, respectively.

$$\begin{bmatrix} \underline{\epsilon^0} \\ \underline{\kappa} \end{bmatrix} = \begin{bmatrix} \underline{A} & \underline{B} \\ \underline{C} & \underline{D} \end{bmatrix}^{-1} \begin{bmatrix} \underline{N} \\ \underline{M} \end{bmatrix} \tag{17.22}$$

Secondly, the global strain for each lamina (which is a function of the distance of the midplane to the lamina z) is calculated. The global strain is the strain in the directions of the laminate axis system as shown in figure 17.6 (the x- and y-axis). However, as $\underline{\mathbf{M}}$ is zero, the curvature $\underline{\kappa}$ is also zero. Resulting in the same global strains $\underline{\epsilon^0}$ at each ply. Now the global strains are known, the global stress at each lamina is calculated. The equations required to calculate the global strains and stresses for each lamina are given in [51].
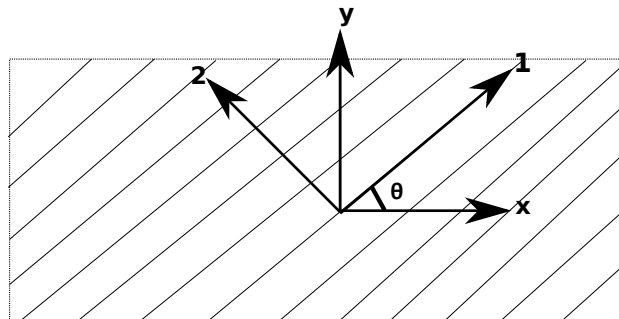
Figure 17.6: The definition of the local and global axes system for a lamina.

Furthermore, a macromechanical analysis of the lamina is performed. It is assumed that the lamina is thin, does not carry any out-of-plane loads and that plane stress conditions for the lamina can be assumed. Due to the low stiffness and strength properties in the transverse direction of the lamina, some laminas are placed at an angle to enable the laminate to also take the stresses in the transverse direction. In order to calculate the stresses in the lamina the global stresses are transformed to local stresses in the local axis system which

are the stresses in longitudinal and transverse direction of the fibre, respectively. The local (1- and 2-axis) and global axes (x- and y-axis) system of a lamina are shown in figure 17.6. The local stresses depend on the local strains of the lamina and the reduced stiffness coefficients. The coefficient of the transformed reduced stiffness matrix $[\bar{Q}]$ can be calculated by the sets of equations discussed and presented [51]. Furthermore, the equations required for calculating the local strains and the local stresses are given in [51].

Lastly, for each of the lamina a failure analysis is performed. The Tsai-Hill criterion is used to evaluate failure which depends on the ultimate strengths obtained from the lamina property calculations and the local stresses as is shown in equation 17.23. [51] Note that the ultimate strengths $\sigma_{ult,1}$ and $\sigma_{ult,2}$ depend on the sign of σ_1 and σ_2 as most of the composites have different ultimate strengths in tension and compression. Furthermore, n_{safety} is the safety factor induced on the stresses. For standard aerospace practice this value is 2 for composites. If the Tsai-Hill criterion is violated the lamina is considered to have failed. If a lamina has failed the preceding calculations have to be repeated, but without the contribution of the failed lamina. This way it can be checked if all of the other laminas also fail and therefore whether the laminate fails.

$$(\frac{\sigma_1}{\sigma_{ult,1}})^2 - (\frac{\sigma_1 \cdot \sigma_2}{\sigma_{ult,1}^2}) + (\frac{\sigma_2}{\sigma_{ult,2}})^2 + (\frac{\tau_{12}}{\tau_{ult,12}})^2 < \frac{1}{n_{safety}} \tag{17.23}$$

Iterative Design Method
The skin is discretised into a finite number of elements. For each element the local stresses at each of the lamina are evaluated and for each lamina of each element it is evaluated whether it will fail. First of all, the skin can fail due to the hoop stress and longitudinal stress due to the cabin pressure. As it is assumed that the skin takes all of the hoop and longitudinal stress due to the pressure, the skin is first designed for failure due to these stresses.

Furthermore, the skin elements can fail due to shear, bending and torsion stresses. First, an initial guess is made of which combination of the unit load cases discussed in section 17.1 is the most restricting. For this load case the fuselage cross-section is designed. To overcome these stresses the thickness of the skin should be increased or lumps of areas (stringers) should be added. The lumps of areas increase the moment of inertia of the fuselage cross-section which reduces the magnitude of these stresses. The stringers are modelled as lumps of area as the detailed design of the stringers is not considered in this report. The area of the lumps are set to one of three possible values at the beginning of the iteration as is described in section 17.2.2. The placement of the stringers is biased, as first the source of the highest stress contribution is identified and then the stringer is placed at the location which lowers this stress as much as possible. Also, if the design does not fail, stringers are removed systematically while continuously evaluating failure. This approach removes any redundant stiffeners, optimising the stringer topology and reducing the fuselage weight for a given composite material and stringer area. Secondly, the other combinations of unit load cases are evaluated with the design of the initial guessed combined load case. When it is found that failure of the design occurs for another combined load case the fuselage design is altered such that the failure is mitigated for the combined load case. After an alteration of the design all of the previous combined load cases are evaluated again to check if the altered design is still sufficient for the previous combined load cases. This process is repeated until a design is found which is sufficient for all of the load cases.

Composite Laminas for Fuselage Design
For the composite material for the fuselage of the ARA a variety of fibres and resins are considered. In table 17.7 the specific Young's modulus, specific strength and cost per kilogram are given for various fibres. The data is obtained from [49]. The most important criteria for a fibre for the ARA fuselage composite material is the specific strength. A higher specific strength fibre will result in a more weight efficient structure. Other parameters such as the flammability, thermal operating range, durability for environmental effects and cost per kg are checked for feasibility to be used in the fuselage of the ARA. For example, due to the high flammability of kevlar aramid fibres these types of fibres are not considered. Based on the specific strength and the feasibility of the other fibre properties it is found that Carbon Fibre (CF) is the best choice. The properties of the selected High-Strength Carbon Fibre (HSCF) are given in table 17.10.

Table 17.7: Data for various fibres [49]

	Carbon	Boron	Beryllium	Glass	Tungsten
Specific Young's modulus $(\frac{E}{\rho})$	122.3	153.7	163.4	34.4	198.0
Specific strength $(\frac{\sigma_{ult}}{\rho})$	2.5	0.8	0.4	1.9	1.1
Cost factor $(\frac{EUR}{kg})$	18.8-25.2	388-497	233-349	14.6-24.4	40.9-45

The main purpose of the resin is to protect the fibres, keep the fibres in place and take shear loads. As fibres have a weak shear resistance the ultimate shear strength of the composite is mostly dictated by the resin.

Therefore, the ultimate shear strength of the resin is identified as the most important selection property. Three types of resin have been considered: epoxy, bismaleimide and PolyEther Ether Ketone (PEEK) resins. Other resin types were found to be not suitable for the fuselage structural material of the ARA (too weak, too expensive or bad environmental resistance)[25],[26],[27]. [49] Data for different kind of resins for each considered resin type have been obtained from [49], the Cytec selector guide[26] and Hexcel[25]. Other resin producers such as Gurit[28] and Ten Cate[27] did not provide enough data for the resins and could therefore only be used as a reference for a limited number of mechanical properties of the resins. For each resin type a representative is selected and the corresponding properties are given in table 17.8. Cost estimates have been obtained from [49], however the values were deemed to be too inaccurate to be used in a trade-off. Therefore, the cost factor is not used in the selection of the resin as there are not sufficiently accurate figures available. Furthermore, for the CYCOM 5250-4 [54] and APC-2 [55] resins there is no ultimate in-plane shear strength available. However, the ultimate in-plane shear strength is provided for unidirectional tapes and laminas for certain fibres and the resins in question. Therefore, the fibre properties and the semi-empirical equations from [53] are used to calculate the in-plane shear strength for the resins.

Table 17.8: Data for epoxy, bismaleimide and cynanate resins. [49][56][54][55]

	Bismaleimide	Epoxy	PEEK
Type	CYCOM 5250-4	CYCOM 381 epoxy	APC-2
Density ρ $[\frac{kg}{m^3}]$	1250	1220	1320
Shear modulus G $[GPa]$	1.6	1.2	0.19
Shear strength $\tau_{xy,ult}$ $[MPa]$	97.5	90.2	117.5
Specific shear strength $\frac{\tau_{xy}}{\rho}$ $[\frac{MPa}{kg/m^3}]$	0.078	0.074	0.089

Based on the specific shear strengths of the resin given in table 17.7 and the feasibility of the other resin properties it is found that the APC-2 PEEK resin is the most appropriate choice. However, it should be taken into account that the PEEK resin requires a production temperature of 382° [55] which will result in higher production costs (more energy, specialised equipment, etc.). The properties of the APC-2 PEEK resin are given in table 17.10. Note that the worst-case properties of the APC-2 PEEK resin within the operational temperature range are used in order to account for thermal effects during the operation of the ARA.

Additional Considerations
For the lamina property calculations it is assumed that there are no voids in the matrix. However, in reality the composite will have some void content. According to [51] every 1% increase of void content can decrease the matrix-dominated properties by 2 to 10%. Therefore, it is important to keep the void content as low as possible. For state-of-the-art PEEK resin systems it is possible to achieve very low void content ($<1\%$) [57] and therefore mitigate the decreasing effect of void content in the matrix-dominated properties.

Furthermore, the matrix can absorb moisture increasing the weight. Moisture absorption of the composite increases the aircraft weight over its operational life-time. State-of-the-art PEEK resin systems can achieve a low moisture absorption reducing the weight increase of the aircraft. [57] For a CF PEEK composite the moisture absorption is between 0.4-0.55%. [49]

Lastly, fatigue of the composite should be taken into account. Composites are more fatigue resistant than metal, however composites still experience a decrease in mechanical properties after a number of cycles. For a variety of unidirectional CF composites such as CF PEEK, CF epoxy and HSCF bismaleimide it is found that after 10^7 cycles the ultimate tensile strength has decreased with the same rate indicating that epoxy shows similar fatigue characteristics as PEEK. [49] For 10^5 cycles no fatigue data could be found for CF PEEK composites. However, assuming that the carbon fibres show the same fatigue behaviour as other high strength fibres such as graphite, kevlar and boron it is estimated from [58] that the ultimate tensile strength is 85% of the original strength. Therefore, the safety factor n_{safety} in the Tsai-Hill criterion (equation 17.23) is increased to 2.3 ($2 \cdot 1.15$) to take into account the reduction in strength due to fatigue.

17.3 Results

By combining the ULCs from section 17.1 two constraining operating conditions for the fuselage are identified. First of all, a 2.5g manoeuvre with a pressurised cabin during cruise with a downward horizontal

---

[25] url: http://www.hexcel.com/products/aerospace/ [CITED: 18 June 2015]
[26] url: http://www.cytec.com/selector-guide/ [CITED: 18 June 2015]
[27] url: http://www.tencate.com/emea/aerospace-composites/products/default.aspx [CITED: 18 June 2015]
[28] url: http://www.gurit.com/prepregs.aspx [CITED: 18 June]

tail force (CLC11) is a dominating load case due to a large bending moment M_y and a large shear force S_z. Furthermore, a 2.5g manoeuvre with a pressurised cabin during cruise with sideslip (CLC12/13) is a dominating load case due to the large overall stresses this situation induces on the fuselage. An overview of these two dominating load cases is given in table 17.9.

Table 17.9: The two constraining operating conditions of the ARA with respect to the fuselage.

	CLC12	CLC13/14	Unit
$\mathbf{S_x}$	$5.9 \cdot 10^3$	$5.9 \cdot 10^3$	N
$\mathbf{S_y}$		$1.7 \cdot 10^4$	N
$\mathbf{S_z}$	$2.8 \cdot 10^5$	$9.2 \cdot 10^4$	N
$\mathbf{M_x}$		$5.5 \cdot 10^4$	Nm
$\mathbf{M_y}$	$1.6 \cdot 10^6$	$3.2 \cdot 10^5$	Nm
$\mathbf{M_z}$		$5.5 \cdot 10^4$	Nm
$\mathbf{P_{cab}}$	$8.5 \cdot 10^4$	$8.5 \cdot 10^4$	Pa

The properties of the HSCF-APC2 composite material have been calculated for a 60% fibre volume content and a 70% fibre volume content. It is found that the 60% fibre volume content provides the lightest structure as the 70% fibre volume content provides less shear and transverse strength and cause laminas to fail. In table 17.10 the density ρ, Young's modulus E, major poisson ratio ν, shear modulus G, ultimate axial compressive strength $\sigma_{ult,1C}$, ultimate axial tensile strength $\sigma_{ult,1T}$, ultimate transverse compressive strength $\sigma_{ult,2C}$, ultimate transverse tensile strength $\sigma_{ult,2T}$ and ultimate intralaminar shear strength $\tau_{ult,12}$ for the HSCF-APC2 composite with a fibre volume fraction V_f of 60% are given. Furthermore, the minimum operating temperature (T_{min}) is obtained from similar unidirectional carbon fibre PEEK composites from [49] and the maximum operating temperature is obtained from the APC-2 PEEK datasheet [55]. The laminate thickness t_{lamina} is estimated from UD tapes obtained from Hexcel[29] and the Cytec selector guide[30] It is checked if the calculated properties match properties from existing CF PEEK composites. The resulting properties are verified with HSCF PEEK composite data from [55] and CF PEEK composite data from [49] and [59].

Table 17.10: HSCF-APC2 composite properties

	Unit	HSCF	APC-2	HSCF-APC2
ρ	$[\frac{kg}{m^3}]$	$1.8 \cdot 10^3$	$1.3 \cdot 10^3$	$1.6 \cdot 10^3$
E	$[GPa]$	230	3.4	139
t_{lamina}	$[mm]$	-	-	0.13
ν	$[-]$	0.20	0.39	0.27
G	$[GPa]$	100	1.3	5.0
$\sigma_{ult,1C}$	$[MPa]$	$4.9 \cdot 10^3$	58	$1.2 \cdot 10^3$
$\sigma_{ult,1T}$	$[MPa]$	$4.5 \cdot 10^3$	58	$2.7 \cdot 10^3$
$\sigma_{ult,2C}$	$[MPa]$	-	58	37.5
$\sigma_{ult,2T}$	$[MPa]$	-	58	37.5
$\tau_{ult,12}$	$[MPa]$	-	126	105
V_f	$[-]$	-	-	0.6

Based on all of the combined load cases an optimised cross-section for an Al-7175 T61511 fuselage and a HSCF-APC2 fuselage have been found respectively. The mass per meter, the number of stringers and the skin thickness t_{skin} for both the configurations are given in table 17.11. The HSCF-APC2 skin consists of a 8x 0° and a 5x 90° orientation lamina. Lamina with ±45° orientation were evaluated but did not improve the structural efficiency. Further evaluation of the applied optimisation techique is required to confirm this cross-sectional layout.

Table 17.11: Results for aluminium and composites

	Al-7175 T61511	HSCF-APC2	Unit
Mass per meter	41.4	32.3	$\frac{kg}{m}$
No. of stringers	18	14	-
t_{skin}	1.20	1.85	mm

The optimised HSCF-APC2 cross-section is 22.0% lighter than the optimised Al-7175 T61511 fuselage cross-section. When including the worst case moisture absorption discussed in section 17.2.5 the difference reduces

---

[29] url: http://www.hexcel.com/products/aerospace/ [CITED: 18 June 2015]
[30] url: http://www.cytec.com/selector-guide/ [CITED: 18 June 2015]

to 21.9%. It is expected that the weight reduction with respect to the Al-7175 T61511 fuselage will be decreased further, when the fuselage is designed to comply with impact regulations. Furthermore, by including buckling, cut-outs and void content the difference is expected to be reduced even more. However, a weight reduction of 15% for the fuselage given in [23] and [24] seems achievable. The significance of reducing the fuselage weight with 1% is discussed in section 21.4. The final layout for the HSCF-APC2 cross-section is shown in figure 17.7. In figure 17.7 the stringers and skin thickness are indicated proportional to the fuselage radius. Furthermore, the inner radius is the cabin interior where the furnishing material, stringer height and outer skin thickness are included. Note that the stringers are depicted as lumps of area and that it does not depict the actual stringer cross-section.
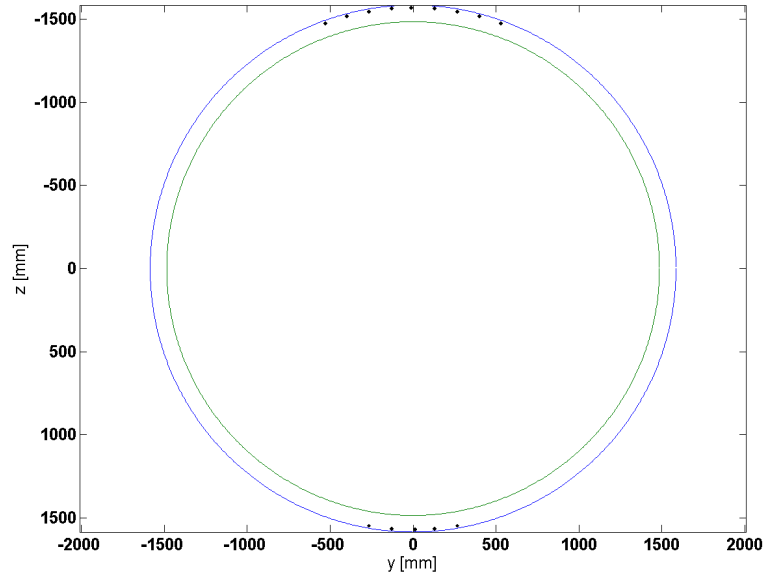

Figure 17.7: The structural layout for the HSCF-APC2 material with stringers shown as lumped areas.

17.4   Recommendations

An optimised HSCF-APC2 fuselage cross-section for the cargo bay section of the ARA has been calculated which provides a large weight reduction with respect to an Al-7175 T61511 fuselage cross-section. The model used for the calculations did not take into account the void content in the resin of the composite, failure of the stringers, buckling of the skin and impact regulations. It is recommended that these effects are included in a more detailed analysis to obtain a more accurate indication of the weight reduction by using composite materials rather than metals. Furthemore, it is recommended to do a detailed analysis of the effect of cut-outs on the metal and composite structure. Moreover, it is recommended to do a more thorough cost analysis including the manufacturing costs in order to determine if the reduction in operational costs due to the weight reduction outweigh the increase of initial costs due to material and manufacturing costs. Finally, the use of different materials for skins and stringers should be considered.

18 | Control Surfaces

In this chapter the last part of the detailed design will be discussed, the control surfaces. Mainly the design of an aileron will be discussed. First, in section 18.1, the design constraints for the aileron are investigated. Then certain methods for morphing structures, such as the use of compliant structures and their application in morphing structures, are looked upon in section 18.2. This culminates in section 18.3, which presents several concepts. In section 18.4 a trade-off is realised to come to one concept to further investigate and design in detail. This detailed design is described in section 18.5. The concept of vortex generators is discussed in section 18.6. The use of a fly-by-wire system and its improvements are discussed in 18.7. Finally, in section 18.8, further recommendations are presented.

18.1   Design Constraints

Before starting to design the control surfaces, one should know what the design constraints for these parts are. The design constraints are:

- Follow geometric constraints, such as sweep and taper ratios
- Deflect, within time constraint ($30°/2.5$sec), under actuation
- Do not deform more than 0.5cm under external loads
- Provide roll control when used
- Withstand 10^7 cycles, without fatigue occurring
- Deform the ailerons shape to reduce drag in each flight phase

With these in mind, the design project can continue. Certain methods should be looked upon in detail, as they seem to have promising features for complying with the requirements. Note that in the remainder of this chapter the emphasis will be on aileron design. The idea behind it is that the concept can be adjusted to be applicable for the elevators and the rudders as well.

18.2   Compliant and Morphing Structures

A monolithic joint-less mechanism which exploits the materials elasticity to produce a desired functionality, such as shape morphing, is a compliant structure. [60] Integrating actuators and sensors for transmission, within the compliant structure, makes it a compliant system. By eliminating flexural joints, which create stress concentrations, and distributing compliance, the maximum stress is lowered and thus the fatigue life is improved.

The incorporation of compliant structures is an interesting concept with respect to advancements in the field of control surfaces. This can lead towards having morphing structures, such as an aileron with an adaptable contour. Incorporating this provides promising outlooks, as are listed below:

- Reduced drag due to longer boundary layer attachment over the control surfaces
- Noise reduction
- Increased reliability as there are less joints in the mechanism of morphing the shape [61]
- Better controllability: Morphing surface can be designed to allow for continuous adjustments
- A reduced need for maintenance, as there are less moving surfaces which avoids friction and wear and is less susceptible to clogging and corrosion [61]
- No backlash

For the ARA, the idea of a morphing aileron is focused upon. The same steps can be undertaken for the elevators and rudder to achieve morph-able contours.

18.3   Concepts

Having completed an in depth literature study on the subjects involved; compliant mechanisms, smart morphing materials, actuators and skins, several concepts are generated.

- 1: *The Fishbone*
- 2: *The Topology Optimisation*
- 3: *The Balloons*
- 4: *The Spine*
- 5: *The Finger*

The Fishbone is a structure which utilises one semi-rigid beam in the middle of the aileron and has stringers going to the sides which are connected to the skin. The concept is visualised in figure 18.1. The deformation is actuated by a tendon which is connected to a pulley on the leading edge of the aileron and to both sides of the solid trailing edge.
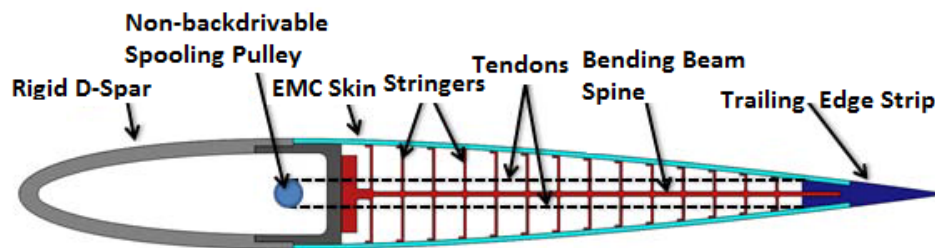

Figure 18.1: The Fishbone concept [62]

Topology Optimised can be best understood as a truss-structure. A computer program sets out a mesh and then calculates, using an algorithm, the most optimal and lightest structure using connections between the meshpoints. It incorpartes embedded actuators and sensors to make the morphing possible. In each of the selected shapes, the truss-structure will handle the static and dynamic loads. A result of topology optimisation can be found in figure 18.2.

The balloons morph by having inflatables underneath the skin which can be inflated by compressors and as such alter the camber of the aileron. A concept is shown in figure 18.3
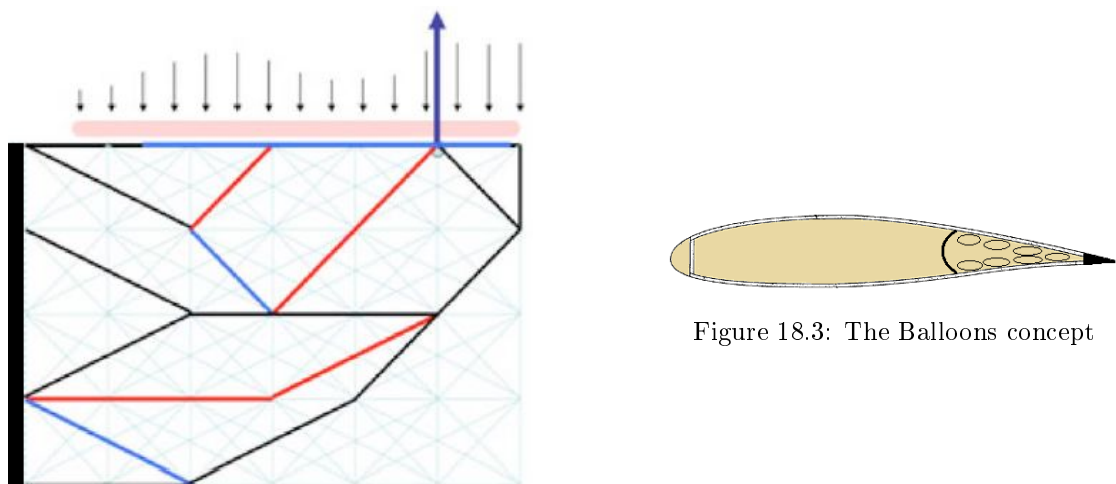

Figure 18.3: The Balloons concept

Figure 18.2: Topology optimisation [61]

The spine is opposite to a compliant structure and has segregation of functions. It is build up of several vertebrae which are interconnected. Making them deflect in a certain direction by an actuator will deform the outer shape. An option for a spine structure can be seen in figure 18.4

The finger is regarded as a combination between the spine and a compliant mechanism; it uses contraction to realise its needed deflections. In figure 18.5 the mechanism is shown for deflection towards one side. If it were to be used for the aileron, it would be altered to allow for deflections in both directions.
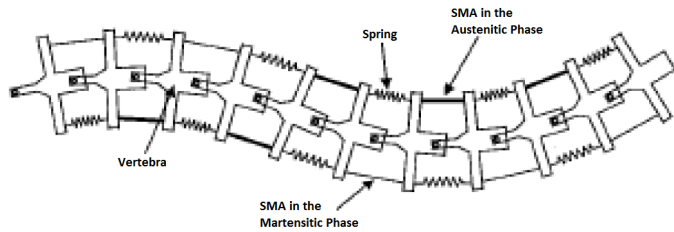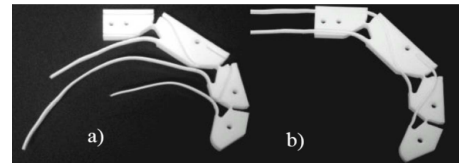
Figure 18.4: Spine structure [63]

Figure 18.5: Finger structure [64]

Something to consider for all these concepts is what kind of skin is applied on top of them and how the two are connected. Using an elastomeric material for a skin, which can stretch, is a solution. Problems with this are the skin acting as a membrane, which is not desirable from an aerodynamic perspective and the inability to effectively counteract forces which act out of plane, meaning the skin needs stiffening and thus increases the weight. Another possibility is the use of a thermoplastic which can realise high strains and be effective at cruise altitude. This is further looked into at the end of section 18.5.

18.4 Trade off

After the concepts are generated, a selection procedure should occur to end up with the best concept. This is done via a trade-off. In this trade-off, the topology optimisation concept is no longer considered. This concept proved too difficult to properly investigate without high-end topology optimisation programs. The publicly available programs showed some promising results, but nothing useful could be deduced from them.

First, the considered trade-off criteria are established:

Weight, Maintenance, Morph-ability, Development risk, Reliability and Noise

Second, qualitative scores are awarded to the trade criteria:

Extremely poor (1), Poor (3), Average (5), Good (7), Extremely good (9)

Third, weights are assigned to these criteria, ranging from 1 to 10. These are presented in table 18.1:

Table 18.1: Weight factors for the criteria for the aileron concepts trade-off

Criteria	Weight Factor
Weight	5
Maintenance	6
Morph-ability	10
Development risk	4
Reliability	8
Noise	2

Morph-ability is rated highest, with 10 points, as this is actually the reason for looking into the concept. Also, having something truly innovative will be a huge benefit from a marketing point of view. Furthermore, reliability is also rated high with an 8, as it is paramount that the aircraft maintains its ability to manoeuvre while in flight. Maintenance and Weight both embody recurring costs; Maintenance is also important in combination with reliability. As such they receive scores of 6 and 5 points respectively. The next intermediate score is for Development risk, receiving a 4, it is needed that the concept is realisable for the ARA, which has its maiden flight scheduled in 2021. Noise is rated low as most of the noise will be experienced during cruise/at higher altitude, as such it will barely have an effect for the population on the ground and the fuselage will shield the people in the aircraft from it.

At this point, the trade-off can be performed. Its results are displayed in table 18.2:

For the weight category, the Spine, scores very poorly, as it is 'build up' from 'building blocks' (including springs & Shape Memory Alloys (SMA's)) which are all dimensionalised equally, while the forces it has to handle are not. Adding unnecessary weight to the design. The Balloons also score poor, as there will be a need for compressors which will add considerable weight. The Finger scores good on weight, it combines the spine structure with a compliant mechanism. The Fishbone scores best in the weight category, it has no heavy components.

Table 18.2: Trade-off summary aileron concepts

Criteria(weight)⟶ Concept↓	Weight (5)	Maintenance (6)	Morph-ability (10)	Development risk/produce-ability risk (4)	Reliability (8)	Noise (2)	Score
The Fishbone	9	5	7	9	7	5	**247**
The Balloons	3	7	3	3	9	3	177
The Spine	1	3	9	5	5	5	183
The Finger	7	5	9	7	7	5	**249**

In the second category, maintenance, the worst score is again awarded to the Spine. It is difficult to maintain. Also it has many springs and actuators which may need maintenance. The Finger and the Fishbone score intermediate, the Fishbone is expected to need most of its maintenance on its tensor and the Finger has less parts to maintain as opposed to the Spine. The Balloons are expected to be low-maintenance, constructing them out of material which is unlikely to break. They are also rather reachable. There might be some maintenance needed on the compressors.

For morph-ability, the Balloons score poorly, they are constrained to their placement and should be pressurised to full pressure to withstand forces and as such can not achieve all the desired shapes. The Fishbone scores well, it can provide all the needed camber. The Finger and the Spine score even better. Their morphing capabilities include double curves.

Fourth, development risk/produce-ability, here the Balloons score poor as they need to be produced in long slender shapes and in- and deflate in the same manner many times, without losing their grip on the surrounding structure. The Spine scores slightly better, it is a relatively simple design, yet consists of many parts which need to be connected correctly. The Finger is somewhat easier, due to the need of less actuators and SMA's compared similarly to the Spine. The best score goes to the Fishbone, extensive research is available about the concept and its structure is relatively easy, as the name suggests, it resembles the skeleton of a fish.

Reliability is the fifth category. The least reliable is the Spine, as there are many locations at which problems can occur. The Fishbone and Finger are rated equally reliable. Initially, the Fishbone could be rated lower, but by adding redundancy by using more tensors, which is most prone to failure and holds the highest severity, its reliability is increased at a low weight penalty. As the finger is assumed to be easier than the Spine, its reliability is higher. The Balloons have the highest reliability as the inflatables are expected to be very resilient.

Finally, the last category is the noise. Most of the noise generated by the concepts will be when they are used on altitude. As such they will not pose a problem to people on the ground. Furthermore, as the aileron is placed at the wing, the fuselage will shield most of noise from the people in the cabin. Therefore all the concepts score adequate at noise. Except for the balloons, as the compressors might generate quite some noise, as well as the exhaust nozzle when deflating. Therefore this concepts scores lower on noise.

Concept selection
From the trade-off, the Fishbone and the Finger come out as prime candidates, with the Finger scoring less than a percent better than the Fishbone. The Finger scores better on morph-ability, because it can create a double-curved deflection. However this is not necessary for the aileron of the ARA. The Fishbone scores better on development risk. The ARA has to be ready for production withing ten years. Therefore the lower development risk is more important than better morph-ability. So the Fishbone concept was selected as the concept to design in detail for the ARA.

18.5 Detailed Design

The Fishbone concept makes uses of a compliant mechanism. This means that the beam, stringers and ribs will be made out of one piece. To design the compliant mechanism a MATLAB program is written. This program calculates all the needed dimensions of the different parts by making use of several requirements and failure modes. The requirements are that the deflection of the skin between two stringer may not exceed 0.5mm and the deflection of the beam may not exceed 5mm when fully loaded. The different failure types are: column buckling in the stringers and ribs, buckling in the skin, fatigue and maximum shear and bending stress in the beam and skin.

To start the design first all the loads on the aileron are determined. From XFLR5 it is concluded that the

highest forces act on the aileron when it is maximally deflected. Therefore the aileron design is based on two load cases: full deflection upwards and full deflection downwards. From the pressure distribution in XFLR5 the forces and moments are calculated. This pressure distribution is multiplied by a safety factor of 1.5.

Amount of stringers and stringer placement
The stringer placement is calculated using the requirement of maximum deflection in the skin. The required distance needed between two stringers is calculated using equation 18.1. [65]

$$L_{stringers} = \left(\frac{v_{max_{skin}} \cdot 48 E_{skin} I_{skin}}{P} \right)^{1/3} \tag{18.1}$$

In this equation $L_{stringers}$ is the required distance between two stringers. However the load on the skin between two stringers depends on the stringer placement. So the length of the aileron (from 0.65c to 1c) is discretised into 1000 elements. Then an iteration is performed. For the first stringer the calculations starts with the first element. If the required distance between two stringers is larger than the width of the element used then the calculation is repeated, but now with one additional element. This is repeated until the required distance is smaller than the width of the elements used, then the iteration is terminated. Having placed the first stringer, a new iteration is started for the next stringer, using the first element after the previously placed stringer.

Thickness of the beam
After the stringers are placed, the required thickness for the beam is calculated. This is done using the requirement for the deflection of the beam. The moment of inertia of the beam is calculated using equations 18.2 and 18.3. [65]

$$I_{beam} = \frac{w \cdot L_{beam}^4}{8 \cdot E_{beam} \cdot v_{max_{beam}}} \tag{18.2}$$

$$I_{beam} = \frac{w_0 \cdot L_{beam}^4}{30 \cdot E_{beam} \cdot v_{max_{beam}}} \tag{18.3}$$

Equation 18.2 is used for a constant distributed load and equation 18.3 for a linearly distributed load. As the distribution on the beam is not linear nor constant, multiple superpositions of these equations are used to approach the distribution acting on the aileron. From the moment of inertia, the thickness of the beam is calculated.

After the thickness required to withstand the load on the beam is known, three failure tests are performed. The maximum bending stress in the beam may not exceed the yield stress and may not exceed the maximum cyclic stress for which the material can survive 10^7 cycles. Also the shear stress in the beam may not exceed the maximum allowable shear stress of the material. So the calculated thickness is tested against for these failure modes. If the beam fails, the thickness is adapted such that the beam passes all the failure tests and can carry all the loads.

Rib placement
The position of the ribs is determined using skin buckling. The stress at which skin buckling occurs is calculated using equation 18.4. [66]

$$\sigma_{cr} = K_c \cdot E \cdot \left(\frac{t}{b} \right)^2 \tag{18.4}$$

K_c is determined using line 1 in figure 18.6 (all ends of the skin are clamped). In this figure K_c is the compression buckling coefficient, a is the distance between two stringers and b is the distance between two ribs. However K_c is only known when b is known. To solve this problem of two unknowns with one equation, the line in figure 18.6 is approximated using different linear lines. For each stringer spacing, MATLAB calculated all the possible b's for the different values of K_c. Then the critical stress is calculated to see whether this stress is lower than the stresses which occur in the skin. If the critical stress is too low, thus allowing buckling, this combination of b and K_c is discarded. From the feasible possibilities the largest b is chosen. After the largest b is calculated for all the different stringers distances, the minimum value of b is chosen to be the final rib placement, to ensure that skin buckling does not occur.
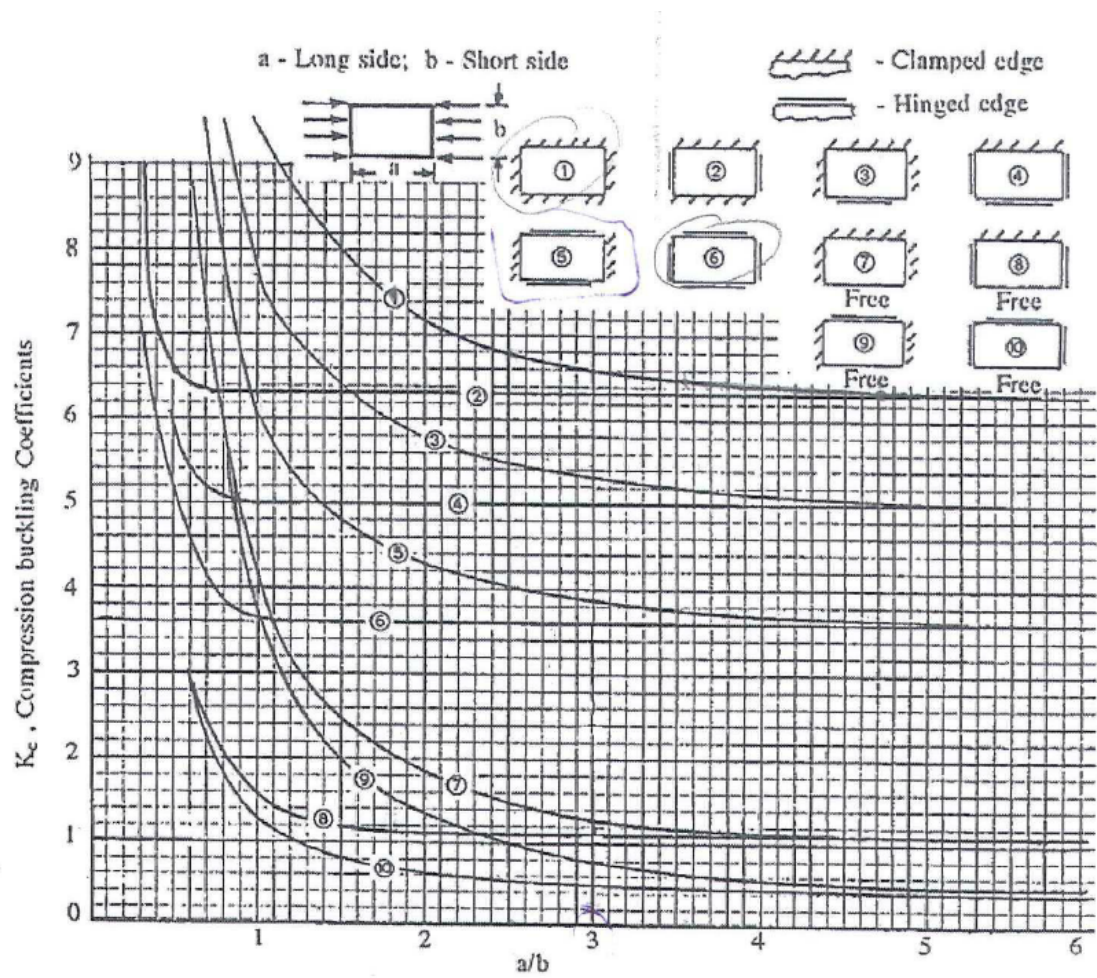
Figure 18.6: Skin buckling coefficient [66]

Thicknesses of the ribs and stringers

The thicknesses of the ribs and stringers are determined using column buckling. The moment of inertia of the ribs and stringers can be calculated using equation 18.5. [66]

$$I = \frac{F_{cr} \cdot L^2}{c \cdot \pi \cdot E} \tag{18.5}$$

In this equation F_{cr} is the load at which the stringer or rib fails and c is the column end fixity coefficient. The column end fixity coefficient depends on whether the ends are fixed, pinned or free. In the case of the aileron the column end fixity coefficient is 4, as both ends are clamped. [66] To determine which part of the force acts on the stringers and which part on the ribs an assumption is made that the force acting on a stringer or rib is proportional to the length of the stringer or rib. An example is given in figure 18.7. In this figure the lengths of the stringers and ribs are 4 and 6 cm, respectively. It is then assumed that $\frac{1}{5}$ of the force is acting on one stringer and $\frac{3}{10}$ of the force acting on one rib. Now everything is known to calculate the moment of inertia of the stringers and ribs and thus the thickness. If a thickness is less than 1mm a requirement is set that the minimum thickness should be 1mm. The reason for this is safety and producibility. As the stringers and ribs are made out of one piece no joints are needed.
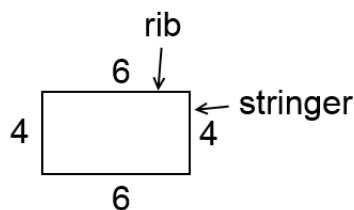

Figure 18.7: Force distribution for stringers and ribs

Skin thickness
All the calculations mentioned before are done for different skin thicknesses varying from 0.5mm to 5mm with steps of 0.1mm. The skin had to pass three failure tests. The maximum bending stress in the skin may not exceed the yield stress and maximum cyclic stress for which the material can survive 10^7 cycles. Furthermore the shear stress may not exceed the maximum shear stress of the material. If the skin did not pass these tests, the design based on this thickness is discarded.

Sizing of the trailing edge
The trailing edge of the aileron is too small to place any stringers, ribs or beams. Therefore, the end of the aileron is made solid. It is necessary to determine where this solid section starts. This is done by looking at the thickness of the beam. The stringer closest to the trailing edge which is bigger than the beam is where the solid section starts. Because if one stringer later is chosen, the beam will be thicker than the airfoil which is not feasible.

Weight of the aileron
When all the dimensions are calculated, the next step is to calculate the weight. As different designs are made based on various skin thicknesses, the final design can be chosen by selecting the one that is the lightest.

Tendon
The final step is to determine the torsion that has to be delivered by the actuator to morph the aileron. The rigid-beam theory cannot be used because the deflection of the beam will be too large. Therefore the Pseudo-Rigid-Beam-Model will be used. [67] This model represents the beam by using a torsional spring placed at 16% of the beam and a rigid part instead of the flexible beam. The stiffness of the torsional spring can be calculated using equation 18.6. [67]

$$K = \frac{2.25 \cdot E \cdot I}{L} \tag{18.6}$$

As all the dimensions are known the stiffness can be calculated. Multiplying this stiffness with the required deflection gives the torsion needed for the actuators.

Material
The aileron has specific needs with respect to the incorporated material. These needs differ for the parts of the aileron. For example, the skin and the transition region connecting the outboard parts of the aileron with the wing must withstand a great number of load cycles (fatigue), strain, water and a broad temperature range. Using CES EduPack 2014 [49], possible materials are evaluated. The best match for the transition region is found in the ultra high molecular weight polyethylene (PE-UHMW). It has an elastic strain of around 15% [68], which is sufficient because the sideflaps need around 10% strain. Having a density of about 931 $\frac{kg}{m^3}$ it is lightweight. For the skin it is decided to use the same material as is used for the transition region between the wing and the aileron. Because this material can elastically deform in the required temperature range. To make the torsion needed as small as possible to morph the aileron, the material of the beam, stringers, rib and trailing edge (which will be made out of one piece) must have a Young's modulus as small as possible for more flexibility. Also the fatigue stress must be high, to make sure that the material can handle all the cycles needed. Using CES EduPack 2014 it is found that Epoxy Unidirectional Composite (Glass Fiber) is the best material to meet these requirements. It has a density of 1.95 $\cdot 10^3 \frac{kg}{m^3}$ [49]

Result
The final results can be seen in table 18.3 and figure 18.8. The final layout with the dimensions of the stringer placement is presented in appendix D figure D.1.
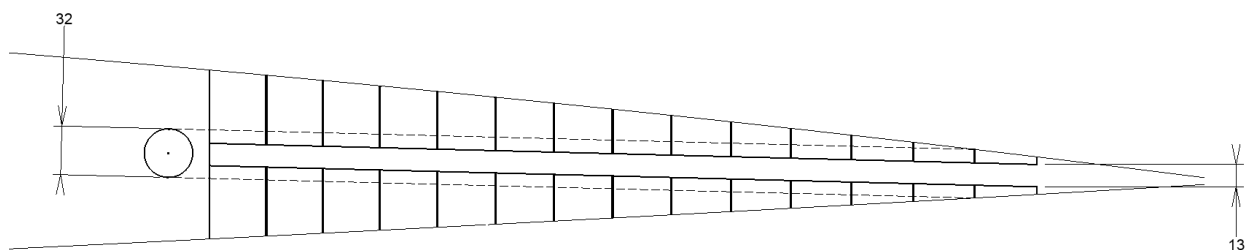

Figure 18.8: Final layout of the aileron mechanism

As can be seen, the torsion needed to actuate the aileron and deform it is high. However, this torque will be divided over multiple smaller actuators. This will decrease the torsion needed per actuator and it gives

Table 18.3: Final results ailerons

Parameter	Value	Unit
Skin thickness	3.6	[mm]
Number of stringers	13	[-]
Stringer thickness	1.0	[mm]
Number of ribs	77	[-]
Rib spacing	33.9	[mm]
Rib thickness	1.0	[mm]
Beam thickness	13.3	[mm]
Torsion needed for actuation	34.9	[kNm]
Weight aileron	47.8	[kg]
Begin of trailing edge solid	94	[% chord]

the possibility to twist the aileron if needed (in this case the inner edge has a different deflection than the outer edge of the aileron). Furthermore it turns out that all the stringers and ribs can have a thickness smaller than 1mm. However, due to the minimum thickness requirement the stringers and ribs have the same thickness of 1mm.

18.6 Vortex Generators

Vortex Generators are a type of aerodynamic enhancements that are used to influence the airflow over the aircraft by delaying separation. Generally a vortex generator is a small vane mounted upwards. In commercial aircraft it is mainly used on the engine nacelles, the leading edge of the wing or on the tail section. While highly sensitive to placement, if implemented correctly it may increase the stall angle and allow for a lower stall speed. An example of vortex generators is shown in figure 18.9.

Figure 18.9: Nacelle Vortex Generators [69]

The increased performance by vortex generators can lead to a decrease of stall speed up to 5 knots and a landing field length of 250 ft, as is for the Boeing 767-200. [69] Since the ARA is a much smaller aircraft, this effect will not be as significant. It is, however, worth investigating, since it is a relatively cheap and convenient approach to boundary layer control. Care should be put into the actual deployment of such devices since it does slightly deteriorate performance during cruise due to increased drag. To determine the right positioning and sizing a Computational Fluid Dynamics (CFD) analysis is required, and thus a true quantitative analysis of this feature is beyond the scope of the current project. However, its use is demonstrated on reference aircraft and can be explored more in post-DSE activities using advanced computing resources. For now, the addition of vortex generator are included in the design on the nacelles, wing and empennage, but the advantages will not be taken into calculations, but instead be used as a way for pilots to have more clearance for the landing distance assuming half the effects for the Boeing 767-200, thus a decrease of 1.5 m/s and a landing field length decrease of 38 m. Again, for post-DSE design and for further improvements after a CFD analysis for future versions of the ARA, this will be taken into account.

18.7 Fly-by-Wire

A fly-by-wire system is a system which is used to electronically control an aircraft using electrical inputs transmitted by wires to actuators and from sensors back to the system. This way the aircraft can automatically respond to changes in aerodynamic conditions using electrical signals from the sensors and consequently send out signals to the control surfaces to adjust accordingly. The system not only reduces the work load for the pilot, it also opens up possibilities of designing aircraft with a wide variety of aerodynamic configurations, such as statically unstable aircraft (fighter aircraft for example). This way the static stability can be reduced to increase the manoeuvrability of the aircraft and give it artificial stability.[70]

A distinction can be made between analogue and digital fly-by-wire systems. An analogue system uses voltage levels to transmit inputs and outputs based on for example the desired or measured deflection of a control surface. Digital systems on the other hand use binary signals to transmit in- and outputs. Both systems have advantages and disadvantages. The main advantages of an analogue system are that the system is simple yet reliable. The main disadvantages are that it is more susceptible to noise in the signals, due to the nature of the signals, and adjustments to the system are not easily made, but require rebuilding of the entire system.

The main advantages of the digital system is that due to the use of a binary signal, a wide variety of signals can be transmitted and received while being easily readable by a computer and the system is easily reconfigured by adjusting the software. The main disadvantages are that if the system fails due to for example a software failure, it fails entirely, thus needing multiple backup systems to retain safety [31].

For the ARA, a digital fly-by-wire system is used since the use of binary provides a more precise system that is easily readable by a computer.

In response to the chosen fly-by-wire system, several recent improvements will be implemented in the ARA, as explained in fly-by-optic, power-by-wire and Intelligent Flight Control System (IFCS).

Fly-by-Optics
The Fly-by-Optics system (sometimes referred to as fly-by-light) replaces the wires of a fly-by-wire system with optic cables. The main advantages are that the optic cables have increased data transfer speed and bandwidth and that the system is immune to electromagnetic interference while weighing less than a fly-by-wire system. This system has however not been fully implemented yet outside of testing. Reasons for this are that fibre optic systems are not yet readily available and more expensive than fly-by-wire systems, however it is expected to be feasible within ten years. [71]

Power-by-Wire
The power-by-wire system replaces hydraulic circuits in the fly-by-wire system with electrical power circuits. The big advantages of these systems are a reduction in weight and a reduction in maintenance costs due to the absence of hydraulics. This system is recently used in the Lockheed Martin F-35 and in redundant systems of the airbus A-380. [72]

Intelligent Flight Control System
The intelligent flight control system extends the use of the fly-by-wire system to cope with damage during flight such as the failure of an engine or the loss of control surfaces. Whereas normally the pilot would have to immediately take over, the intelligent flight control system reacts accordingly without delay. This system has mainly been in the testing phase and incorporates a change in the software of digital fly-by-wire systems, but is expected to be readily available for commercial use within ten years.[72]

The use of mainly electrical wiring warrants a necessary redundancy. The use of 4 on board computers capable of operating the fly-by-wire system is required and the wiring should have a redundancy by using redundant wires that run across different sections of the aircraft. The use of more electric wiring, which is implemented using the fly-by-wire and aforementioned improvements, reduces the maintenance load and any problems in the system or wiring are automatically recorded and can be communicated to maintenance crews, whereas with hydraulics this is left up to just inspection.

18.8 Recommendations

Some recommendations can be made to further improve the design of the aileron. First of all more failure tests must be done in order to make sure that the aileron is capable of withstanding all the loads. For example the Von Mises stress must be calculated and checked if this does not exceed the maximum allowable stress. Another recommendation is to look into more detail into the stringer design. For example if a I-, Z- or

---

[31]url: `http://www.ausairpower.net/AADR-FBW-CCV.html` [CITED: 24 April 2015]

other stringer type is best for this design. Also the influence of the transition region on the aileron has to be investigated further, because these will influence the flow over the aileron. Furthermore a recommendation is to look into more detail into the material selection. Due to limiting time there has not been an elaborate research into the possible materials. As such, there could be materials which are lighter and better in performance. The production process was also not taken into account. Production techniques to produce the design should be looked into, to come up with the best method. Lastly research should be done to find out whether the design of the aileron can be scaled to an elevator or rudder, the concept will probably need a few adaptations for the specific application. Finally, by running a CFD analysis, the control surfaces can be optimised and the usage of vortex generators can be investigated.

Part IV

Aircraft Performance

19 | V-n Diagrams and Flight Envelope

In this chapter the V_{EAS}-n diagram for manoeuvring and gusts are determined after which the combined diagram is plotted, that can be used to determine the extreme combinations of airspeed and load factor. The last section in this chapter deals with the flight envelope.

19.1 The V_{EAS}-n Diagram for Manoeuvres

The boundaries of operational use of the ARA are partly determined by the boundaries of the V_{EAS}-n diagram. This means that the aircraft must fly within a certain range of velocities and load factors to operate safely. In this section the velocities and load factors that can occur during manoeuvring are determined and explained. The obtained V_{EAS}-n diagram can be seen in figure 19.1. At the low speed side of this diagram the boundary is the stall curve for both positive as well as negative loadfactor. The light blue curve is the stall curve for when the flaps are extended downwards. At the high speed side the boundary is determined by aerodynamic instability which has a degrading effect on the flight controls. The upper and lower boundary are determined by selecting the proper load factors. The equations used to determine the V_{EAS}-n Diagram can be found in [73].
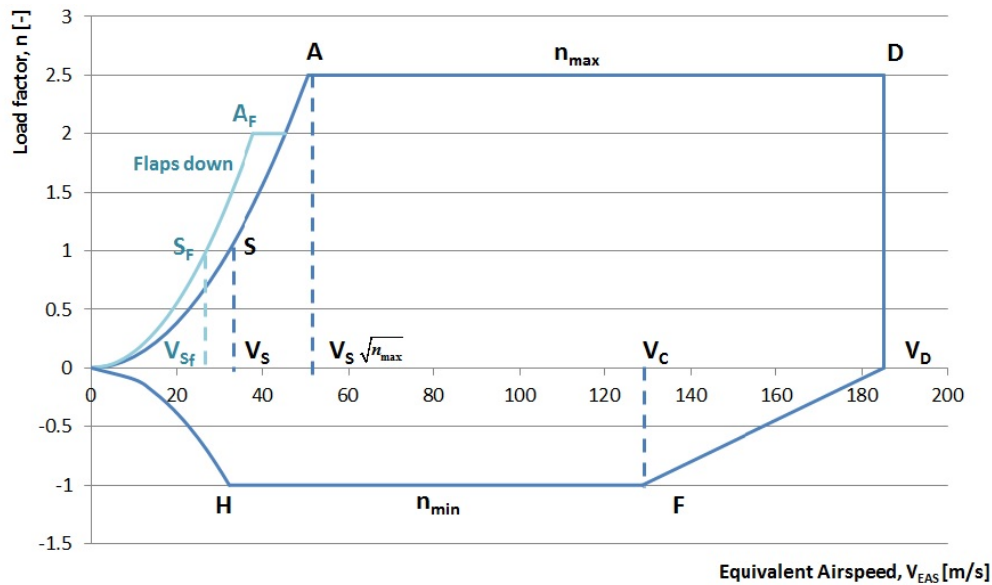

Figure 19.1: The V_{EAS}-diagram for manoeuvres

19.1.1 Establishing n_{max} and n_{min}

The values for the maximum and minimum load factor, n_{max} and n_{min} depend on the aircraft weight as can be seen in table 19.1, they are prescribed by the Certification Specifications (CS-25). [2] The MTOW of the ARA has been estimated to be 34610kg or 76302lbs. When looking at the table for a weight higher then 50000lbs a maximum load factor n_{max} of 2.5 and a minimum load factor of -1 should be selected.

Table 19.1: Maximum and minimum load factors for manoeuvres [73]

MTOW	n_{max}	n_{min}
$W \geq 50000$lbs	2.5	-1
W 4100lbs $\leq W < 50000$lbs	$2,1 + \frac{24000}{10000+W}$	-1
$W < 4100$lbs	3.8	-1

19.1.2 Velocities

In this section all the speeds are determined that will be used to construct the manoeuvring loading diagram. It is important to note that all the speeds should be plotted as equivalent airspeeds (EAS). Most of the airspeeds were previously determined as true airspeeds (TAS), they should be converted to EAS by using equation 19.1, with $\rho_0 = 1.225\ kg/m^3$ and ρ(at 11km cruise altitude) $= 0.364\ kg/m^3$.

$$EAS = TAS \cdot \sqrt{\frac{\rho}{\rho_0}} \tag{19.1}$$

Stall Speed V_S The true stall speed in clean configuration and landing configuration(with extended flaps) at cruise altitude was previously determined to be 58.72m/s and 48.90m/s. Converting this to equivalent airspeeds gives a stall speed V_S of 32.01m/s for clean configuration and a stall speed for when the flaps are extended downwards V_{S_f} of 26.67m/s. Both stall speeds are indicated in figure 19.1.

Design Manoeuvring Speed V_A The design manoeuvring speed represent the minimum manoeuvring speed at the maximum load factor. This speed can be determined with equation 19.2. Filling in the stall speed for clean configurations and the maximum load factor gives a V_A value of 50.61m/s (EAS) in clean configuration. Therefore point A in the figure can be plotted using the value of V_A at n_{max} of 2.5.

$$V_A = V_s \cdot \sqrt{n_{max}} \tag{19.2}$$

The curve connecting the origin and point A is plotted using the stall curve equation 19.3.

$$n_s = \left(\frac{V}{V_s}\right)^2 \tag{19.3}$$

The same method can be used for the 'flaps down' case, namely for point A_f, where the stall speed with the flaps extended should be used as an input for equation 19.2 and 19.3. The maximum load factor for when the flaps are extended is prescribed in CS-25 to be n=2. [2] This gives $V_{A_f} = 37.72$m/s (EAS).

From the origin till point H the stall speed is plotted for negative lift, where point H has the value of n_{min} of -1. When using equation 19.3, the speed at point H could be determined to be 32.01m/s (which is the same value as the stall speed in clean configuration).

Design Cruise Speed V_C The cruise speed (TAS) of 236.10m/s is converted to EAS; $V_C = 128.70$m/s.

According to [73] it could be concluded that the airspeed of point F indicated in figure 19.1 coincides with this cruise speed.

Design Dive Speed V_D Point D is found by calculating the design dive speed, which is the maximum speed the aircraft can achieve. The design dive speed must be selected so that it satisfies relation 19.4. Where M_C is the cruise mach number of 0.80 and M_D is the design dive mach number 0.92, which was previously determined. Using these values V_D is determined to be 185.00m/s (EAS).

$$\frac{V_C}{M_C} < 0.80 \cdot \frac{V_D}{M_D} \tag{19.4}$$

All the different velocities in both TAS and EAS are summarised in table 19.2.

Table 19.2: Calculated velocities as EAS and TAS (at cruise altitude of 11km with $\rho = 0.0369\frac{kg}{m^3}$)

Velocity	TAS [m/s]	EAS [m/s]
V_s	58.72	32.01
V_{s_f}	48.93	26.67
V_A	92.84	50.61
V_{A_s}	69.19	37.72
V_C	236.10	128.70
V_D	339.38	185.00

19.2 The V$_{EAS}$-n Diagram for Gusts

The gust diagram shows the maximum load factors the ARA will encounter when gusts occur. The magnitude of the gusts that will occur during flight depend on the speed and altitude. The gust diagram in this report is evaluated at 6.1 km. This is not the cruise altitude of the ARA, but at this height the load factors due to gust will be most critical. [73]

The load factors due to gust are evaluated at three different speeds. The 'bad weather' speed, the cruise speed and the design dive speed. The latter two were determined in the midterm report. The 'bad weather' speed is calculated using equation 19.5.

$$V_B = V_S \sqrt{1 + \frac{K_g U V_c a}{w}} \tag{19.5}$$

The V_S is the stall speed at the considered height, K_g is the gust alleviation coefficient, U is the gust speed that occurs at the considered speed (V_B, V_C or V_D), V_C is the cruise speed, a is the 3D lift slope coefficient and w is the wing loading W/S. The gust speed is obtained from table 19.3. The gust alleviation coefficient can be calculated using equation 19.6. The other values are known from the midterm report.

Table 19.3: Gust speeds for different velocities at an altitude of 6.1km [73]

	V_B	V_C	V_D
U	20.12 m/s	15.24 m/s	7.62 m/s

$$K_g = \frac{0.88 \mu_g}{5.3 + \mu_g} \tag{19.6}$$

The μ_g in this equation can be calculated as follow:

$$\mu_g = \frac{2w}{\rho \bar{c} a g} \tag{19.7}$$

In this equation w is the wing load W/s, ρ is the air density at the considered height, $\bar{c}$ is the mean aerodynamic chord, a is the 3D lift slope coefficient and g is the gravitational acceleration.

It is assumed that before the gust the aircraft is flying at a load factor of one. The difference in load factor due to the gust can be calculated and is then be added to one for positive gust and subtracted from one for negative gust, see equation 19.8.

$$n_g = 1 \pm \Delta n_g \tag{19.8}$$

The change in load factor Δn_g can be calculated using equation 19.9.

$$\Delta n_g = \frac{1}{2} \frac{\rho_0 a}{mg/S} U_{EAS} V_{EAS} K_g(\mu_g) \tag{19.9}$$

In this equation ρ_0 is the sea-level density, a is the 3D lift slope coefficient, mg is the weight of the aircraft and S is the wing area. Furthermore U_{EAS} is the gust speed that occurs at the considered speed, V_{EAS} is the considered speed (V_B, V_C or V_D) and K_g is the gust alleviation coefficient.

Now everything is known to calculate the load factors for each speed at the critical altitude of 6.1 km. The results are shown in figure 19.2.

From the previous equations it follows that for a given gust speed U the gust load versus airspeed in the diagram is a straight line, the different gust lines are indicated in the diagram with the dotted lines. Points one to six indicate the minimum and maximum gust loads evaluated for the different speeds. The two values at each point indicate the speed and load factor, respectively. Point one and six correspond to the 'bad weather' speed, two and five to the cruise speed and 3 and 4 to the design dive speed. The contour lines of the diagram are constructed by connecting points one to six and the origin.

19.3 The Combined V$_{EAS}$-n Diagram

In figure 19.3 the loading diagrams for gust and manoeuvres are combined. From this diagram the critical combinations of load factor and airspeed can be obtained for which the aircraft has to be designed so that it can operate safely. There are two critical load factors which are driving for the design, the maximum and minimum load factor. The maximum load factor is due to gust and has a value of 2.61. The minimum load factor is due to manoeuvre and has a value of -. These are the largest values that the aircraft has to resist.
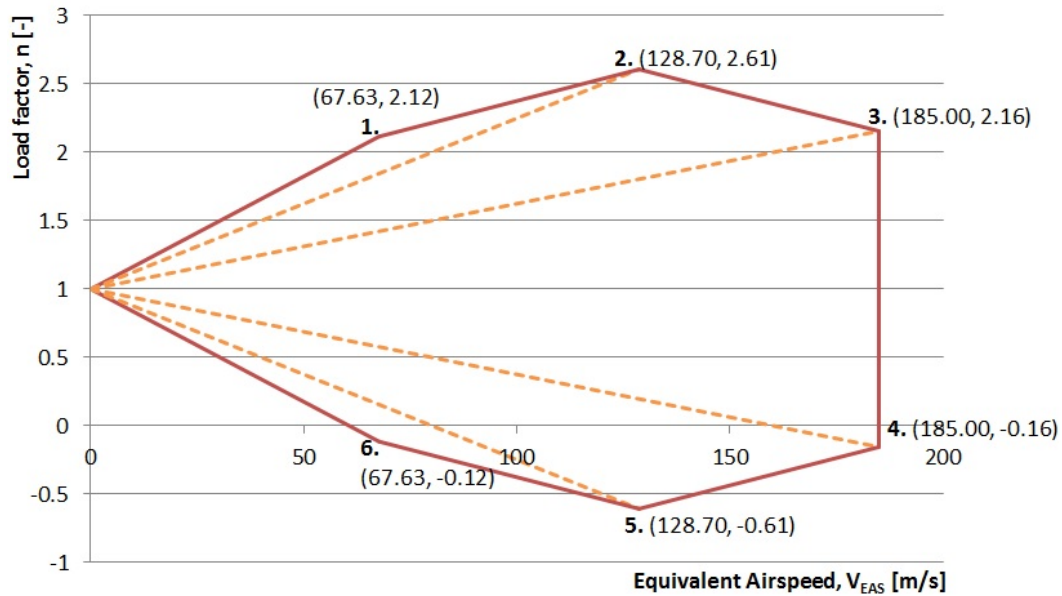
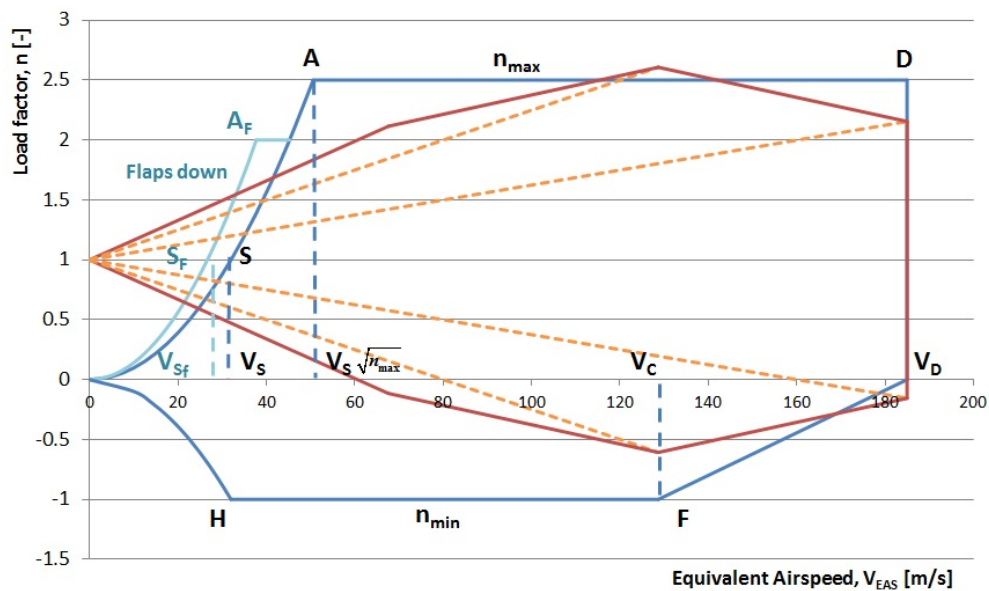Figure 19.2: The V_{EAS}-diagram for gusts

Figure 19.3: The combined V_{EAS}-diagram

19.4 The Flight Envelope

The flight envelope consists of six curves which put constraints on the altitude and speed of the ARA. Below every constraint is discussed separately. All the equations are obtained from [74].

Minimum Speed

The stall speed puts a constraint on the minimum speed that ARA can fly at each altitude. The minimum speed can be calculated using equation 19.10.

$$V_{min} = \sqrt{\frac{W}{S}\frac{2}{\rho}\frac{1}{C_{L_{max_{cruise}}}}} \tag{19.10}$$

As the density differs at each altitude, the stall speed varies as well. The higher the altitude, the higher the stall speed. The stall speed, V_S is indicated with line nr.1 in figure 19.4.

Design Dive Speed The design dive speed puts a limit on the maximum speed of ARA. In the midterm it

was set on 0.92 Mach at 11 km. Using the speed of sound, this Mach number can be converted to a speed. Equation 19.11 was used to calculated the design dive speed at every altitude, using the known speed at 11 km.

$$V_D = \sqrt{\frac{\rho_{11}}{\rho}} \cdot V_{11} \tag{19.11}$$

The design dive speed, V_D is the absolute maximum speed at which the aircraft can fly. It is indicated in figure 19.4 with line nr.3.

Maximum operating speed

The maximum operating speed, V_{MO} is the maximum speed at which ARA is allowed to fly under normal conditions. It was set in the midterm on 0.825 Mach on 11km. The corresponding maximum operation speeds for each altitude are calculated the same way as the design dive speed. The constraint is shown in figure 19.4 with line nr.5. Using the maximum operating speed as constraint gives a safety factor of 1.12 before the aircraft reaches its absolute maximum.

Maximum Mach Number The maximum Mach number, M_{max} is calculated using the Mach critical of the airfoil. It is the same for every altitude. However the speed of sound differs at each altitude. Therefore the corresponding speed will also differ. The maximum Mach number is indicated by line nr.2 in figure 19.4.

Maximum Operating Mach Number

The maximum operating Mach number M_{MO} is 0.825. Converting this Mach number the same way as the maximum Mach number gives line nr.6 in figure 19.4. This Mach number may not be exceed during normal flight conditions.

Maximum Height The maximum operational height is etermined in chapter 17 and is found to be 12 km. The maximum height is indicated by line nr.4 in figure 19.4.

Result
The result can be seen in figure 19.4. The highlighted area are the possible combinations of altitude and speed at which the ARA can fly.
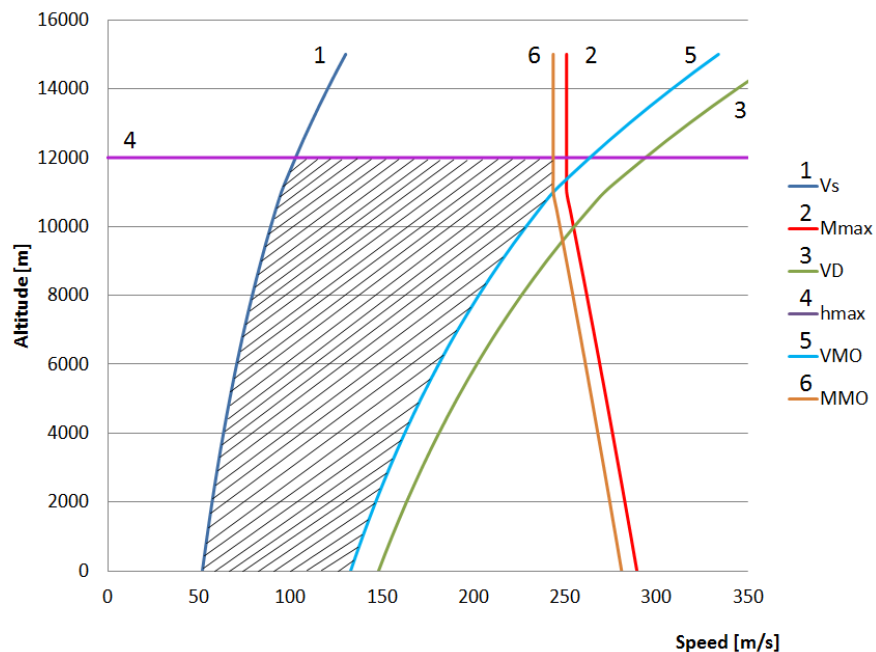

Figure 19.4: Flight envelope of ARA

20 | Configuration and Innovation

The ARA is a state-of-the-art aircraft which has a design range of 2000km. The aircraft has short take-off and landing characteristics allowing the ARA to land on many different airfields. Moreover, the aircraft is able to transport 90 passengers enabling the ARA to achieve the largest possible market share of the regional jet market. The configuration of the ARA can be seen in figure 20.1. A more detailed overview of the ARA is given in figure E.1 in appendix E.

Figure 20.1: Configuration of the ARA

A conventional tail is chosen for which the size depends on the centre of gravity and the moments created around the centre of gravity of the aircraft. Furthermore, a tricycle landing gear configuration is chosen.

Fuselage Layout
The layout of the cabin and the cross section of the fuselage can be seen in figure E.2 in appendix E. As can be seen in figure E.2 the ARA has 23 seat rows, 2-2 abreast. Furthermore the seat pitch is 30 inches (762mm). There are two lavatories for passenger comfort and two galleys. There is one row with only two passenger seats, with a storage compartment on the other side of the aisle. This storage compartment is used to store cabin crew luggage and auxiliary gear. Subsystems are stored between the cargo floor and the passenger floor. Furthermore there is a cargo bay behind the passenger section which continues partly in the empennage, in which all the cargo can be stored. This cargo bay position allows for faster loading as only one cargo bay needs to be loaded and the airport crew are able to stand inside the cargo bay. This decreases the turn-around time of the aircraft. Stability and controllability requirements are met for the ARA for this cargo bay positioning making the aft-cargo bay configuration feasible. Moreover, the ARA has the option for a two-class configuration so an operating airliner can choose between a single economy class layout with 90 passengers or a combined business and economy class with 81 passengers. Finally, to have a clear overview of the doors inside the aircraft (emergency exits and cargo door), the cut-outs have been left open. The ARA has two type A and two type 1 emergency exits and a cargo door.

Engines
The ARA features a conventional wing with innovative GTF engines housed in chevron nacelles with state-of-the-art aerodynamic design and noise reduction technology, which significantly cuts the fuel consumption and noise emissions resulting in lower operating costs. GTFs improve the fuel efficiency by 16% with respect to conventional turbofans. [28]

Winglets
To increase the aerodynamic efficiency of the ARA an investigation has been performed on the most effective winglet. The designed winglet increases the effective lift of the wing as well as reduces the induced drag and the incurred weight penalty. The winglet features both an upward and downward winglet with raked tips to optimally reduce the wing's tip vortices. The winglets increase the fuel efficiency by 6.1%.

Advanced Composite Materials

By using advanced composite materials for the fuselage, wing and empennage, an increase in fuel efficiency of 5.2% can be achieved. The ARA fuselage will be made out of a HSCF-ASC2 composite. This composite is self -extinguishing and has favourable environmental resistance, low void content, low moisture absorbtion and excellent mechanical properties. Combined with a topology optimised stringer layout the aircraft's empty weight has been significantly reduced compared to a metal design.

Morphing Control Surfaces

The aircraft features morphing ailerons. Using the elasticity of materials, the control surfaces morph the wing rather than deflecting a separate hinged surface. Incorporating these morphing control surfaces provides benefits such as reduced drag, noise reduction and increased controllability.

Green Taxiing

The operational efficiency of an airliner is significantly improved by green taxiing using an Electrical Green Taxiing System (EGTS). The electric motors on the main landing gear will provide power to enable the aircraft to perform its own pushback without the assistance of a tug and taxi towards the runway without the main engines running. This ultimately leads to faster turnaround times.

Overall Aircraft Efficiency

The ARA is compared to the Embraer E-Jet on fuel efficiency. The Embraer is a full metal aircraft with conventional turbofans and without winglets. The increase in efficiency that has been calculated for the different subsystems of the ARA are with respect to these features. The increase in efficiency of the engines, the winglets and the fuselage result in a total increase in efficiency of 24.3% with respect to the Embraer-175. Even if the Embraer is equipped with similar GTFs as for the ARA an increase in fuel efficiency of much more than 10% is achieved.

21 | Sensitivity Analysis

A sensitivity analysis investigates the change of the subsystem or overall aircraft design when a parameter is adjusted. A sensitivity analysis can be used to check the feasibility of the design. There are several design options that have an influence on the aircraft, which is investigated in this chapter. Section 21.1 discusses the sensitivity of the design when the weight is increased. In section 21.2 the sensitivity is analysed for a requirement change. Furthermore, in section 21.3 the sensitivity is analysed for changes regarding the stability and controllability and finally some numerical examples show the actual sensitivity of the ARA.

21.1 Weight Increase

One of the most common and most severe changes of the major design parameters is a change in the overall weight of the aircraft, especially if its an increase. An unforeseen structural liability could be the cause of an increase in weight in a (sub)system. This has cascading consequences for the other associated subsystems. The different consequences are explained in this section.

21.1.1 Engines

An increase in the weight requires an increase in the thrust to maintain the T/W design point. However, if the engines were already selected in an earlier stage of design, an increase in thrust is not easily fixed. Either weight has to be saved in other (sub)systems or a new engine has to be selected. Furthermore, this usually leads to heavier engines, which in turn requires more thrust, leading to a snowball effect. Also other subsystem designs based on the selected engine, for example the nacelle design, have to be altered for the new configuration. Since all these situations are very undesirable, effort should be made to keep them from occurring. It has to be noted that designing for an unforeseen increase in weight is nearly impossible, since this would only lead to a self-fulfilling prophecy.

Another possibility, during the design option trade-off phase, is a choice between two different types of engines, for example a GTF and an ORE. Both have vastly different layouts and characteristics such as a different optimal cruise Mach number. An ORE generally has an optimal Mach cruise number of 0.75, while the GTF is most efficient at a Mach number of 0.8. Thus, choosing a different engine may not only lead to a different fuel consumption or layout, but also to a different value of the cruise Mach number and indirectly the travel time. The bottom line is that a change in a major parameter could have very large consequences to the engine choice in the design option trade-off and thus should be carefully evaluated and avoided if possible. However, since the GTF engines produce more thrust then required(37 kN excessive), there is a safety margin to cope with an increase in weight to remain at the same thrust to weight ratio.

21.1.2 Lift

A direct consequence of a weight increase is a shift in the required lift for a selected design point. Either the generated lift is increased by increasing for example the surface area of the wing, flying at a different angle of attack or changing the airfoil, however these are only viable options in the early stages of the design. Furthermore, if the increase in weight results in worse take-off and landing performance, the high lift devices may have to be redesigned as well.

21.1.3 Landing Gear

If the aircraft weight increases, the load on the landing gear increases. This may cause a redesign of the landing gear, since the selected tires cannot withstand the loads anymore. However during every design and production, the maximum take-off weight of the aircraft increases which results in a higher load on the landing gear. If the aircraft weight increases excessively, the landing gear needs to be modified or even redesigned. Increasing the load on the nose gear by 10 kN would cause the current design to be insufficient and Increasing the load on the main gear by 25 kN would cause the current design to be insufficient.

21.2 Requirement Change

A change in the requirements can result in a change of (sub)systems of the aircraft. For instance a change in the take-off length of the runway can result in a change in maximum take-off weight of the aircraft of which the result has been explained in section 21.1. Another possible requirement change could be the range of the aircraft, which may result in a different configuration. For instance, if the maximum range is lowered, then the engine choice could be changed which is explained in section 21.1.1 and the weight decrease because there is a change in fuel needed on board of the aircraft. This causes a snowball effect again. Also if the range is decreased, the choice for a turboprop engine becomes interesting since at short range the speed of the aircraft is less important and turboprop engines are more efficient. Furthermore, a change in the requirement of amount of aircraft per month that need to be produced have an influence on the production method of certain parts. Finally, when there is a requirement change in noise and emission, the engine type has to be changed or the engine has to be redesigned if it does not comply with the regulations. This change can only be done in an early stage of the design as the engine type can change the entire configuration of the aircraft.

21.3 Stability & Controllability

Especially in civilian transport aircraft, the comfort of the passenger is of high importance, which should be taken into account during the design option trade-off. To accommodate for passenger comfort, the aircraft needs to be stable, which can be accomplished by the horizontal tailplane. Too much stability on the other hand makes the aircraft uncontrollable

For controllability a fly-by-wire system is commonly used, a change in configuration should be programmed accordingly and the system itself should be in compliance with other (sub)systems and sensors in order to function properly. It is important to size the horizontal tailplane to be stable and to simultaneously have controllability over the aircraft.

21.4 Numerical Examples

To get a better indication of the actual sensitivity of the design, some calculations are made to see the influence of changing certain parameters. These are obtained using the programs and sheets used during the class I and II weight estimations. Below the most important changes have been listed:

- **Decreasing the fuel density by 10%** Increases the weight of the electrical system by 0.6% and the fuel system by 3%. This allows to compare the effect of using different fuel types. If the fuel type is changed to bio fuel the effect on the design can be identified.

- **Fuselage drag** By decreasing the fuselage diameter by 10 %, 1.5-3% less profile drag can be realised.

- **Change in centre of gravity position** The maximum change in centre of gravity position due to weight increases or position changes of subsystems is 4% more aft during loading. If the centre of gravity position would change to be more aft the aircraft could become unstable and a different subsystem lay-out, wing position or empennage size may be required.

- **Wing position effect on empennage sizing** Relocating the wing's centre of gravity position 10% more aft causes a change in the empennage horizontal wing area of 11.3%

- **Winglet efficiency** To optimise the winglet for both aerodynamic and structural efficiency, the percentage in structural weight increase is subtracted from the percentage in aerodynamic increase with a 7:6 ratio respectively. This ratio is found from the class I weight estimation in which it is shown that 1% increase in aerodynamic efficiency and structural weight results in respectively, 0.6% decrease and 0.7% increase of fuel consumption.

- **Metal or Composite Aircraft** Using a composite aircraft rather than a metal aircraft reduces the OEW by 7.39 % and the fuel weight by 5.21%

- **Increase of Composite weight reduction factor of fuselage** Increasing the composite weight reduction factor by 1% for the fuselage with respect to a metal fuselage is 0.28% for the OEW and 0.19% for the fuel weight

The main cause of changes in aircraft design is due to a weight increase. The effect of a weight increase on several other parameters is shown in figures 21.1, 21.2 and 21.3. From these figures a change in the weight of the aircraft results in changes to the given parameters as shown in the figure. Prefered is a flat curve,

since that indicates a low sensitivity to a weight change: the growth of weight during the design phase and during the aircraft lifetime is inevitable, and its effect is deminished if the effect on other aircraft parameters is small.
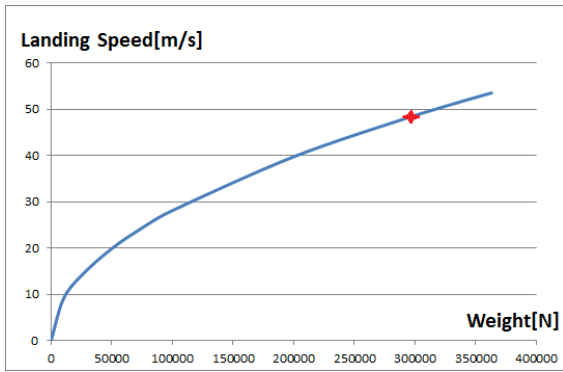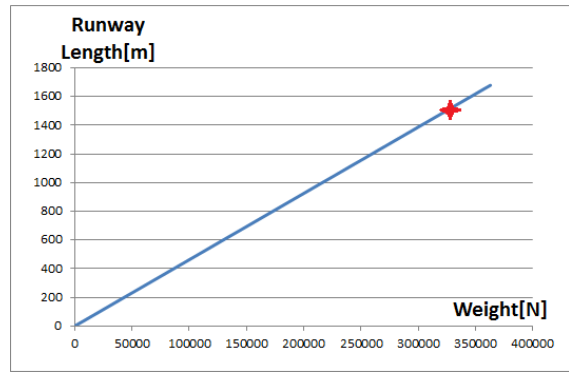

Figure 21.1: Landing Speed Sensitivity

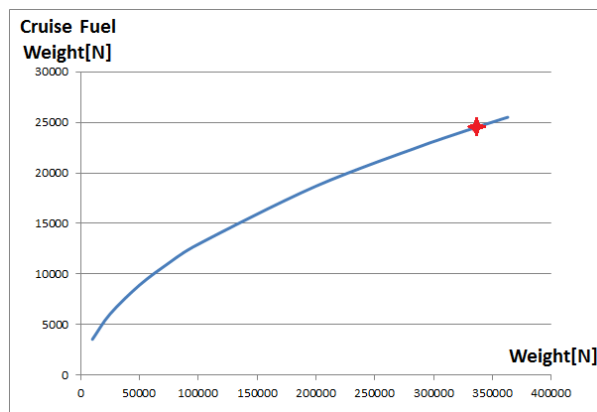Figure 21.2: Runway Length Sensitivity

Figure 21.3: Fuel Weight Sensitivity

In each of the figures the chosen design point for the ARA is shown with a cross. Any changes in weight will thus happen from that point. However, not only a result of a weight increase can be observed: a weight descrease due to fuel burn and its impact on other parameters is shown.

Part V

Production, Life and Investment

22 | Verification and Validation

Verification and validation is a vital part of the process of designing an aircraft. It is used to check if the product satisfies the specifications and if it matches the demands and wishes of the customer and aircraft safety regulations. In a world where technological advancements follow each other in rapid succession, verification and certification is very important. Therefore, especially when working on an Advanced Regional Aircraft, the use of verification is necessary to ensure a well developed design. [75] In section 22.1, the verification is discussed, followed by the validation in section 22.2 and the compliance matrix in section 22.3.

22.1 Verification

Verification is split in two parts. The first part is about determining whether all the used numerical and computer models are correct. A way to check these is by testing all the separate function units, or individual sections of the program. The units are checked by comparing the programs output with the analytical output. From this, it can be concluded whether they perform as they should. If the separate sections of the program work as intended, the program as a whole is checked in a system test. Furthermore all discrepancies should be explained and accounted for. In the second part it is made sure that the product matches the specifications.

The verification process is also used to check codes and programs used. Every program or code has been redundantly checked by multiple people. Therefore, it is assumed that both the calculations and the models are correct and useful for verification. The verification process can be performed by cross-checking the chosen method for the program with other methods or tools that are available. [76] Verification will mainly be focused on checking if the aircraft and its subsystems meet specifications.

In the aircraft industry, verification is performed to make sure manufacturers are producing products that actually meet the specification they are specifying. For that reason, verification on set regulations is done by an independent company that is licensed to do so by governmental bodies such as the European Union, such that it is performed by a neutral party. An example of a verification subject is the emission. Companies need to pay for emissions expelled by aircraft in operation. For this reason, an accurate emission profile for their aircraft is required, and this is verified by the aforementioned independent companies licensed to do so. The same applies to the payload distance.

Furthermore, the aircraft dimensions are verified during the manufacturing process. Many parts will be designed using computer software, and for the assembly it has to be made sure that these parts are manufactured with the required dimensions. This is done by quality control and is most important during early manufacturing, since any possible flaws in either assembly or manufacturing can be discovered here, which could influence full scale production.

Since a lot of different parts and systems are worked on at the same time, there should be an overview of the aircraft status as a whole. Every group should be on the same page and this should be checked by a quality control group with regular meetings where all parties are involved. This way the internal design structure can be verified.

22.2 Validation

Besides the verification, a validation process should be performed. This is a final check for the system to make sure it fulfils the set of requirements as stated in 2.1.

The ultimate goal of validation is to generate evidence that the system is accurately modelled. This can be done by comparing the validation data with the simulated computational predictions. For this to be successful, a clear definition of the intended use of the model is needed and the verification process should have been completed already. Note that the obtained validation data might differ from that what is required for validation.

22.2.1 Validation Processes

Validation is obtained by clearly showing that the demands and wishes are met. This is done in several ways. First of all, by checking the finalised design to compliance with the set requirements, as stated in section

2.1. This is initially done by checking the results from the simulation of the design and comparing with the initial set of requirements. In later stages real life testing will have to be performed to show compliance with the airworthiness regulations. For example, flight tests and full scale stress testing will be performed. For this several prototypes will have to be build. This way it provides a way of obtaining an airworthiness certificate by for example testing the engines for endurance and performance, testing the wings for strength and yielding and ensuring proper fuselage pressurisation. These tests are referred to as ground testing. Later on actual flight tests will be required. In these flight tests flight test pilots will test characteristics like range, stall characteristics and characteristic speeds as well as take the aircrafts to their limits to display the boundaries of the aircraft's flight evelope. Furthermore, any further customer requirements that can be tested will be done accordingly.

For the ARA several requirements as described in section 2.1 have to be validated after the design is completed. Each of these requirements are discussed below and for each of them it is explained how validation is obtained:

- **Pr-req2** First thing to note here is that there will be a ramp up time before this level of production can be achieved. Thus in the first few years of production 100 aircraft per year will not be achieved. Furthermore, since the production is greatly depended on the amount of orders, measuring the production by reflecting on for example the last month of production does not necessarily represent the production capabilities of the facility. Thus, this requirement should be monitored based on orders and expanded whenever the need arises.

- **O-req1** This requirement is checked after the design is completed and prototypes are build. First of all the sizing for the fuselage will be checked to see if it can actually accommodate the specified amount of passengers. Secondly, during safety testing for for example emergency exit time, it will be checked if the amount of passengers can actually safely leave the aircraft in the allotted time.

- **O-req3,4** First of all, the runway length should be evaluated again at the end of design to make sure that after each iteration in the design process the runway length requirement is still satisfied. The runway length requirement itself will be validated during extensive flight tests for obtaining airworthiness certificates.

- **Pe-req1+R-req4,5** This requirement will be checked during test flights for obtaining airworthiness certificates

- **Pe-req2** During flight testing operations the fuel burn will be measured and documented. It will then be compared to the direct competitor with the largest market share, the Embraer E-Jet.

- **R-req2,3** The emission requirement will be checked by licensed third party companies, as explained in verification, and should comply with regulations. The noise requirement will be checked by measuring in both ground operations for the engines as well as during flight testing.

- **R-req6** A prototype will be used to perform an ultimate strength destruction test and will be loaded on the wings until failure. This is a requirement for airworthiness certificates and should be performed to check if it can sustain the required loads.

22.2.2 Certification

Since the design of the Advanced Regional Aircraft features new technologies, these new technologies have to be certified for the JAR-21 requirements before they are eligible for use on a commercially flying aircraft. Before certification is assured, a part or system undergoes a series of tests to obtain an improved qualification, as is shown as an example for the GP7200 engine in figure 22.1.

In the design process the ORE was seriously considered as a candidate for engine implementation. However, the technology is not matured enough to be implemented within 10-15 years and the certification of the ORE has not yet been approved. Furthermore, a method of its certification has proven difficult under current regulations of for example blade out criteria.

The GTF however, has been certified in December 2014 for the Airbus A320 Neo[32]. Furthermore, the design has been tested thoroughly and is ready for implementation.

---

[32]url: http://www.purepowerengines.com/press/14121900.htm [CITED: 12 May 2015]

Figure 22.1: Engine certification [76]

22.3 Compliance Matrix

The compliance matrix, as can be seen in table 22.1, is used to show if the set requirements, as described in section 2.1 have been met. Should a certain requirement not be fulfilled, an explanation will be given and a modification to comply with the requirement will be suggested.

Table 22.1: Compliance Matrix

Req.	Met	Result
Pr-req1	Yes	10 Years
Pr-req2	No	8 per month
		100 per year
O-req1	Yes	90 pax single class
		81 pax two class
O-req2	Yes	9550kg
O-req3	Yes	1500m
O-req4	Yes	1500m
O-req5	Yes	Complies with requlations
D-req1	Yes	32m
D-req2,3	Yes	Complies with regulations
Pe-req1	Yes	2000km
Pe-req2	Yes	24.3% lower
R-req1-6	Yes	Engines and aircraft meet regulations

Requirement Pr-req2 has not been met. The ARA will be produced at a rate of 100/year instead of 25/month and thus 300/year. 25 aircraft per month would deliver all projected orders within four years, which is unnecessarily short, since orders are gradually placed over the years. 100 Aircraft per year fits the reflected order amount better. When the amount of orders is larger than 1100 adaptations can be made such that the production rate is sufficient.

Passenger comfort is assured by using advanced seats that are thinner but do not decrease comfort, as well as optimizing the space for passengers without increase seat pitch. Airworthiness is obtained by successfully completing ground and flight tests. Furthermore, certification for the GTF engines is completed thus ready for safe use.

23 | Risk Assessment

In this chapter the concepts and methods concerning risk assessment that will be used in the project are explained.

23.1 Risk Management

Throughout the design process risks should be constantly evaluated and managed accordingly. Proper risk management reduces the chance of project delay, exceeding the budget and/or reduction in technical performance of the final product. The complete view obtained from the risk management can be helpful while planning development activities and allocating resources.

Figure 23.1: The systems engineering universe [77]

The definition of risk is: "*Risk is a measure of uncertainty of attaining a goal, objective, or requirement pertaining to technical performance, cost, and schedule.*" [77] As can be seen in figure 23.1 the system engineering universe is established by technical performance, cost and schedule. All three are connected via risk. For example when the technical performance is near the limits of state-of-the-art, this can result in technical performance risk. When the available funding is limited this has a big influence on the cost risk. Note that all three dimensions are connected, for example if one wants to lower the schedule risk, this probably will increase the cost (risk) and/or the technical performance (risk) and vice versa. Note that risk cannot be removed completely, but can be made manageable.

For the ARA the systems engineering universe plays an important role. First of all, the cost of an aircraft needs to be as low as possible in order to compete with other regional aircraft on the market, this brings along some risks because products are produced as cheap as possible bringing along problems in achieving the required performance. Customers are interested in a technologically advanced aircraft and they want the aircraft to be ready to fly within a certain time. If 'The Company' produces a technologically advanced aircraft, the subsystems which are highly advanced, probably bring more risk to the aircraft. The break-even point of "The Company" is set to 400 aircraft, while a total of 1100 aircraft are expected to be sold. If for any reason less aircraft are sold, there is still a safety margin for the total profit. For instance if only 700 aircraft are sold, "The company" will still have a profit on the ARA.

During the design process and manufacturing, risk management is implemented in several ways. Firstly, an overview of the time scheduled is maintained per design element and any delay is reported. While the risks of delays can not be eliminated, these can be managed, by properly reporting and anticipating before hand. For example designers can be reallocated to better fit the proposed time schedule. Secondly, by making periodic reports of cost resources used, supervisors are able to keep an overview and check if they get out of hand. This could indicate either flawed methods or inefficiency, which can be coped with if noticed timely. Thirdly, the technical performance aspect of the ARA should be considered. Risk of technical performance can be reduced by having proper verification and validation throughout the process and making sure it follows prescribed requirements, rules and regulations. Again, using supervisors that ensure these characteristics is vital to minimize the overall risk.

The "advancements" of the ARA carry a risk in particular: technologies or techniques in development have yet to prove their full upsides as well as downsides (that are possibly overlooked beforehand). A particular risk for the ARA is the morphing control surface integration. It is a concept which is still in the testing phase, and while showing promising results and improvements, there are uncertainties of the implementation on larger aircraft. While this risk could be minimised by cooperating extensively with the manufacturer (since the production of the aileron is outsourced), it is difficult to make an estimate of the actual results.

Should the morphing control surface fail to meet demands, there can always be resorted back to "standard" control surfaces, however this leads to redesigns of the actual control surfaces itself and should be avoided if possible.

23.2 Risk Map

The term risk comprises technical risks as well as non-technical risks. Technical risks are the risks due to the subsystems and components of the aircraft. The non-technical risks are independent of technical aspects such as cost risks, schedule risks, human error and bird strikes. Risk can be seen as the product of the likelihood and the impact of an event. The general approach for the risk map is presented. From now on this method is referred to as the Risk Map Approach (RMA).

Step 1 Define clear categories for the likelihood and the impact of an event. For example a category for the likelihood could be "high" and a category for severity could be "catastrophic: mission failure or significant reduction in performance". Furthermore, a score is given to each category, where the lowest category (low chance of occurrence or small impact) has a score of 1 and for every higher category the score is increased by 1.

Step 2 Determine for every risk of interest in which categories they fit. Based on the risk categories a risk map can be created, where the risks are placed accordingly. The top right corner represents the most likely occurrence and harshest impact. The low left corner represent the least likely occurrence and mildest impact. With the risk map the highest risks can be found visually. See figure 23.2 for the risk map.

Step 3 Risk mitigation is performed which means that measures are taken to lower the highest risks in order to minimize the total risk. Some measures could be choosing a different technology, add/increase margins or redundancy and changing the way the product operates.

Step 4 In the last step, the risk items are tracked and the status of the risks and the mitigation is checked regularly.
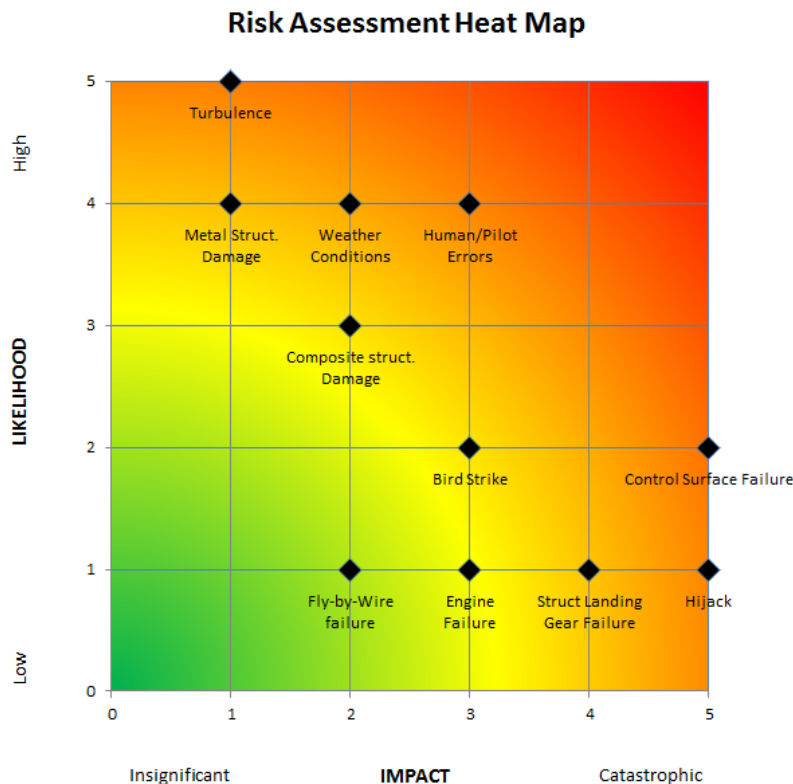

Figure 23.2: Risk Map

A classification of major causes of aircraft incidents and delays is shown in figure 23.2, which was done using aerospace engineering knowledge and FAA reports and manuals. [78] The most critical risks are human and pilot errors, weather conditions and control surface failure. Risk mitigation for each of these:

- Human and Pilot Errors: The largest cause of incidents is human error. The cause of this however differs; pilot fatigue, insufficient training, improper conduct or disregarding of rules, influence of medication, narcotics or alcohol, personal issues or other distractions and lack of communication (with ground control) have all been identified as causes of aircraft incidents in the past. [78] Most of these issues can be dealt with by providing pilots with better health support and regular physical as well as psychological check-ups.

- Weather Conditions: Weather conditions play a big part in aircraft safety, especially during take-off and landing. A lot of incidents can be avoided by enforcing strict weather condition rules for take-off, and thus putting less emphasis on preventing delays. Furthermore, 70% of all delays are caused by weather conditions. [79] While this is not necessarily a safety risk, it is a risk towards costs made by the airliner, thus deserving a high position on the risk map.

- Control Surface Failure: Since control surfaces are vital to maintain a controllable aircraft, a control surface failure can have disastrous consequences. Complex and innovative control surfaces might be deemed as fuel efficient, however, it can lead to a lower reliability and thus a safety risk. In the end, while the performance of the control surfaces might be increased, it may not be worth the increased risk, choosing a proven and simpler design reduces the risk of control surface failure.

Besides individual causes of risk as shown in figure 23.2, there are also risks related to the ARA program as a whole.

- Lack of Investors: For a project as big as designing a new aircraft, a financial backing is needed. Since this financial support is given even before any aircraft parts are produced, the investors could be taking a big risk. For this reason, failing to find sufficient investors and partners could be a concern. However, market analysis has shown that the demand for regional aircraft is rising in the next decades and the current regional aircraft are due for replacement, such that the regional aircraft market is a sound investment sector. While the global economic situation plays a role regarding interest rates and financial downfalls, the current economic situation is improving. For this reason, difficulties in finding investors does not appear to be extremely likely, but would have a huge impact, since a lack of investments causes a (temporarely) stop of the program. Should a lack of investors become an issue, the deal for the investors could be sweetend by giving more guarantees and possibly lowering the profit share of 'The Company'.

- Failure to meet requirements: The ARA is designed with certain requirements in mind and should meet them. There is however a risk that this does not happen. During the design phase the requirement should be kept in mind and if meeting them becomes a difficulty, the design should be adjusted accordingly. For example should the weight increase such that the runway length requirement cannot be met, a weight savings programme should be initiated. It should always be kept in mind that requirements can be reasoned with by discussing them with the customers to reduce the impact of this risk.

- Lack of Orders: The ultimate goal of the design of a new aircraft is getting as many orders as possible. In order to realize this, the design needs to compete with other manufacturers on the market. A lack of orders can have multiple causes: Economic decline, having poorer specifications when compared to the competition and/or unimpressive marketing strategies. This is a substantial risk for the ARA, and can have a massive impact. Not only can it lead to a lower profit or even a loss, it directly affects funding for further designs of the ARA. In order to avoid this, the design should be regularly evaluated with regards to the competition. Furthermore, promising marketing opertunities, such as large airshows, should be used as tools for meeting potential buyers.

24 | Operations and Logistics

An aircraft requires not only a profitable and efficient design, but also operations and logistics in order to function throughout its lifespan. In this chapter the many different aspects of these actions are explained with a focus on aircraft operations. Each subsequent section provides a more detailed approach towards a subset of aircraft life with regards to operations and logistics and is used to demonstrate the important role maintenance and safety operations play on aircraft downtime. Lastly, the scheduled and unscheduled maintenance requirements are explained, followed by the complete reliability, availability, maintainability and safety (RAMS) analysis.

24.1 Life Cycle Operations and Logistics

During its lifetime an aircraft will have endured a very large amount of flights and thus many operations and logistics related actions. A general life overview of an aircraft is shown in figure 24.1.
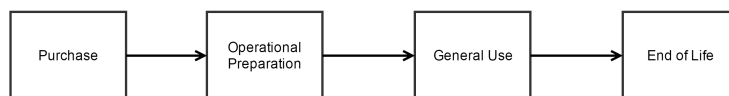

Figure 24.1: Aircraft Life Operations and Logistics

24.2 Flight Cycle Operations and Logistics

In this section a closer look will be taken at the flight cycle of an aircraft, which includes all operations and logistics before, during and after flight. This flight cycle is shown in figure 24.2.
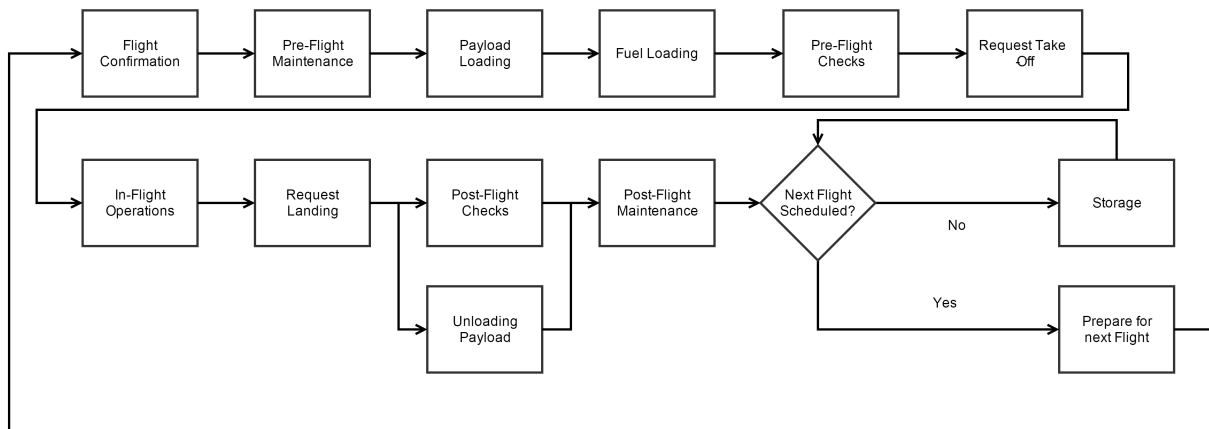

Figure 24.2: Aircraft Flight Operations and Logistics

When flight confirmation has been given, which means the scheduled flight will take place (within the time span of a day), the pre-flight maintenance occurs. Once the maintenance on the aircraft is performed, the aircraft can start the loading of payload and fuel. The pilots follow the check-list as prescribed for the given aircraft by the Original Equipment Manufacturer (OEM) before requesting take-off. The in-flight operations are more thoroughly described in section 24.3.

When the aircraft has landed, the post-flight checks, as prescribed by the OEM, are performed as well as unloading of the payload. Afterwards post-flight maintenance is performed. Major maintenance check ups are prescribed by regulations.

24.3 In-Flight Cycle Operations and Logistics

In this section a closer look will be taken at the in-flight cycle of an aircraft, which includes all the on-board and ground operations. In figure 24.3 the in-flight cycle operations and logistics of an aircraft are presented.
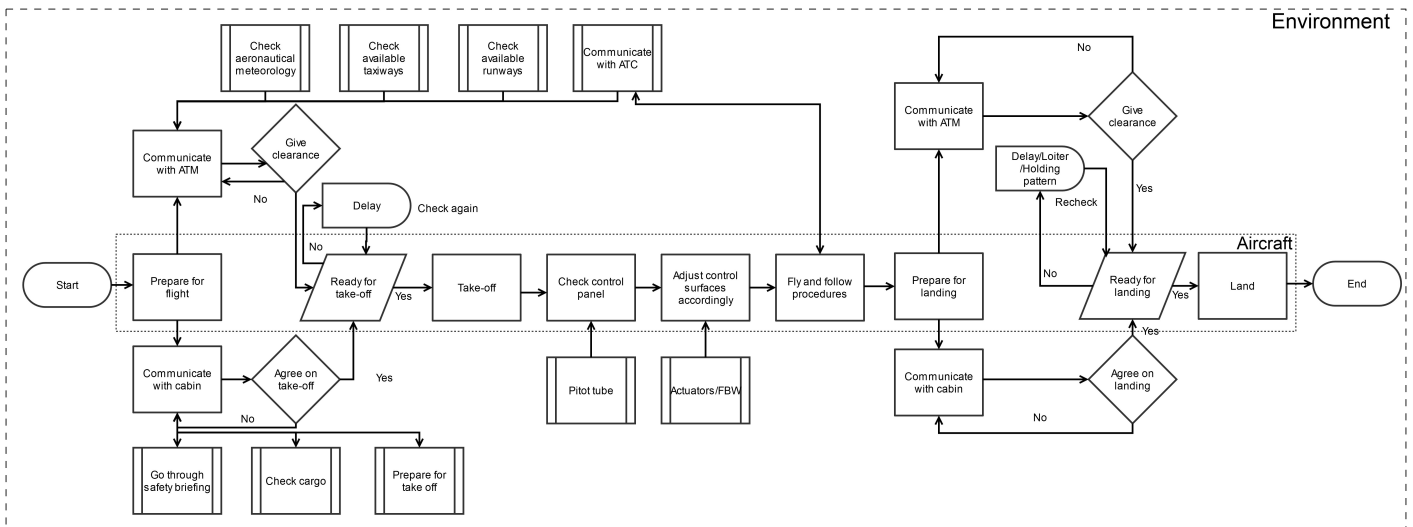
Figure 24.3: Aircraft In-Flight Operations and Logistics

Every step, check and guideline of an aircraft flight is presented and provides a guideline towards understanding the operations process.

The (co)pilot(s) are in control of the aircraft. Before they commence with the flight and take-off, they communicate with the cabin crew as well as the Air Traffic Management(ATM). The pilot will start the take-off when both indicate that they are ready. At all times during flight, granted there are no insurmountable issues, the (co)pilot(s) will have a direct communication link with Air Traffic Control(ATC). Whenever either the (co)pilot(s) or the ATC has a need for communication with the other, they will do so and follow procedure accordingly. All the internal in- and outputs the (co)pilot(s) process, such as changing the pitch angle, are not further processed in detail within the flow diagram, as they are considered handled without external communication. For landing a similar procedure is followed as was for take-off. The (co)pilot(s) will again communicate with the cabin and the ATM, not proceeding until given clearance from both. As long as no clearance is given by the ATM, the (co)pilot(s) will bring the aircraft to loiter in a holding pattern. In severe cases a decision might be made to divert to a different (nearby) airport or to proceed with an emergency landing, both options are not incorporated in the flow chart. Further communication after landing is not considered in the flow chart either.

24.4 Reliability, Availability, Maintainability, and Safety characteristics

In this section the Reliability, Availability, Maintainability, and Safety (RAMS) characteristics is discussed. It addresses a list of safety critical functions, the redundancy philosophy applied, the expected reliability and availability and an outline of scheduled and nonscheduled maintenance activities. As is shown in figure 24.4 from [18], the RAMS are interconnected with each other.
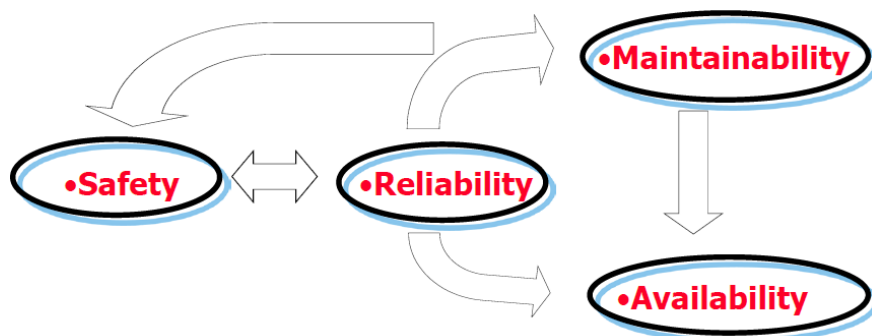

Figure 24.4: Relation between Reliability, Availability, Maintainability, and Safety characteristics

24.4.1 Maintainability

With respect to engineering, the degree of maintainability is a measure of the ease with which a product can be maintained, so that it can keep on functioning as required. Both the maintainability as the maintenance are discussed.

There are two types of maintenance, scheduled and unscheduled maintenance.

The first type is divided in five different sub categories of maintenance, commonly known as PS (Periodic Service), A, B, C and D checks. [80] They are arranged in increasing order of magnitude.

- PS Check: Performed every 2-3 days and takes less than 2 man hours
- A Check: Performed every 7-9 days and needs 10-20 man hours to complete
- B Check: Executed about every 2 months after 500-600 flight hours, using 100 man hours
- C Check: Scheduled every 15-18 months, 2000 man hours (3 days) planned to finish
- D Check: Taking place every 5-6 years, 20000-30000 man hours (3-6 weeks) planned to finish

The values in this list are generic for aircraft, varying based on the specific conditions the aircraft has been under. They are obtained for aircraft that are mostly made of metals. The ARA will consist of composites for a large part and as such its intervals between maintenance will be bigger, reducing the impact and cost of maintenance as a whole. It is reported by Boeing for the 787, that the needed maintenance due to fatigue had been significantly reduced, since composite handle tension loads better then standard aluminium application. Thus by introducing composites to tensile-loaded sections, the maintenance could be shifted to greater intervals. Furthermore, when comparing maintenance on the empennage of the Boeing 787 to the Boeing 777, while the size of the empennage of the Boeing 787 is 25 % greater then that of the Boeing 777, the required maintenance time reduced by 35%. Boeing reported this reduction resulting due to a reduced risk of corrosion and fatigue of composites compared to metals. [81] On this issue, it has to be noted however that maintenance on composites is still fairly new. A report of the Government Accountability Office (GAO) in 2011 on composite maintenance states that for composite maintenance four safety-related issues can be identified:

1. The information on composite structure behavior in aircraft is limited
2. There are technical issues with respect to the characteristic properties of composite materials
3. There have been difficulties in standardisation of repair materials and techniques
4. The training and awareness for maintenance crew with respect to composite material maintenance is relatively new

Regarding these issues, most are due to large scale implementation of composite materials being fairly new. Recent implementation on other aircraft that are largely made up of composites, such as the Boeing 787, have diminished this problem and have caused an increase in experience and knowledge regarding working with these materials for both manufacturers and maintenance crew. However, since there are a large amount different composite materials in the aircraft industry, the specifications for the ARA will have to be communicated with maintenance crew and training will be provided. This will be further explained in chapter 25.

The second type, unscheduled maintenance, takes place when during inspection issues arise that require immediate care. For aircraft more than 40% of the maintenance will be unscheduled. [82] Due to the implementation of composites, the unscheduled maintenance time will be reduced: Boeing reports that unscheduled maintenance for composite structures in aircraft not only happens less often due to corrosion and fatigue risk reduction, repair operations for composites, such as bonded composite repairs, take less time then aluminium repair operations and result in a less deteriorated aircraft with respect to aesthetics and aerodynamics. [81] The analysis of maintenance on composites has thus greatly influenced the decision of choosing a mainly composite aircraft for the ARA.

24.4.2 Safety and Reliability

Besides the general risk map as shown in figure 23.2 in section 23.1, a safety analysis for the software system is needed as prescribed by the FAA System Safety Handbook. [83] Systems that mainly use software should have a sufficient reliability to ensure safe transport for both passengers and pilots. Using fly-by-wire systems a reliable software (and hardware) system is needed since the main controls of the aircraft are software based. By providing a well executed verification and validation analysis the reliability of the aircraft as a whole can

be ensured as discussed in sections 22.1 and 22.2. Furthermore a certain degree of redundancy should be present, especially for vital parts of the aircraft which need to remain operative, such as the (actuation of) control surfaces. Replacing pneumatic and hydraulic systems by electrical systems with sufficient redundancy where applicable, as is done for the ARA, has increased the reliability in reference aircraft and is an increasing trend in civil aviation. [81]

24.4.3 Availability

As can be seen from figure 24.4, the availability of the ARA results from its reliability and maintainability. Having discussed both the reliability and maintainability, a prediction for the availability can be given. Assuming that the technically advanced features of the ARA ensure a high reliability, as all the incorporated innovative parts have passed certification and should thus not have high reliability risk, and the maintainability is improved due to quicker maintenance options for composites compared to metals, a high availability is prospected.

25 | Production Plan

The purpose of the production plan presented is to make the first steps in planning the infrastructure concerning the manufacturing and logistics of the ARA. The production plan can be applied to the entire production. The fuselage is used as a study case throughout this chapter to illustrate the adaption of the production plan for a specific sub-assembly. In section 25.1 the relevance of outsourcing subsystems of the ARA is discussed. Section 25.2 the in-house production is discussed which includes the part, sub-assembly and final assembly manufacturing. Furthermore, section 25.3 discusses the transport and information infrastructure during the manufacturing of the ARA. Lastly, section 25.4 discusses the quality management and assurance systems.

25.1 Aircraft Subsystem Outsourcing

Due to the large capital investment involved in the production of the aircraft it is convenient to reduce the risk during both the design and production phases. This can be realised by dividing the subsystems of the aircraft and distributing them among partners or subcontractors, so called outsourcing. Two types of outsourcing can be distinguished. First of all, there are built-to-print subcontractors which only manufacture the components based on a given design. Secondly, there are subcontractors which are responsible for the design and manufacturing of the part or sub-assembly. The latter is inherently more invested in the project and usually share more of the risk than built-to-print subcontractors. Furthermore, outsourcing parts of the design is especially convenient when certain subcontractors have more experience and better in-house technology than 'The Company' for certain subsystems.

The landing gear is a candidate for outsourcing as companies such as UTC Aerospace systems[33] and Messier-Bugatti-Dowty[34] are leading in the design and manufacturing of landing gears. Therefore, these two companies are good candidates for outsourcing of the landing gear due to their experience and in-house technology.

25.2 In-house Production

Two main categories of in-house production are distinguished: Part and sub-assembly manufacturing which is discussed in section 25.2.1, and assembly and integration which is discussed in section 25.2.2.

25.2.1 Part and Sub-assembly Manufacturing

'The Company' is responsible for the final assembly line and therefore it is important that the most critical components are managed by 'The Company'. Therefore, certain sub-assemblies will be manufactured in-house. The fuselage is a candidate for in-house production as the fuselage design uses an advanced composite material (see chapter 8 and 17). Therefore, it may not be possible to outsource the fuselage since the technology, experience and quality assurance for the manufacturing of such a structure might be limited. Furthermore, the transport costs for a large sub-assembly such as the fuselage can be high and therefore it can be decided to produce the fuselage sub-assemblies close to the final assembly-line.

The parts for the sub-assemblies which are manufactured in-house can partially be obtained from suppliers such as fasteners and adhesives. Parts such as stiffeners, ribs and frames which are used for an in-house sub-assembly can be manufactured in-house. Especially, if the parts consist of advanced materials or if the delivery rate of the parts is critical. For example, the fuselage sub-assembly is critical for the final assembly of the ARA. Therefore, an independent (from external influences such as subcontractors) stiffener and frame delivery rate is desired in order to minimise the risk and let 'The Company' keep control of the fuselage sub-assemblies production rate. Other areas of in-house manufacturing may also include metal additive manufacturing[35,36] and out-of-autoclave composite part manufacturing[37,38] as the technology and experience might not be available among subcontractors.

---

[33] url: http://utcaerospacesystems.com/cap/systems/Pages/landing-gear-business.aspx [CITED: 22 June 2015]
[34] url: http://www.safranmbd.com/landing-gears [CITED: 22 June 2015]
[35] url: http://www.norsktitanium.no/en/Topmenu/Our%20technology.aspx [CITED: 30 June 2015]
[36] url: http://us.dmgmori.com/products/lasertec/lasertec-additivemanufacturing/lasertec-65-3d [CITED: 30 June 2015]
[37] url: http://www.hexcel.com/Innovation/Documents/Product-Process%20Development%20For%20Out-of-Autoclave.pdf [CITED: 30 June 2015]
[38] url: http://www.tencate.com/emea/Images/TCAC_OutofAutoclave_Web_021214_tcm28-23023.pdf [CITED: 30 June 2015]

The location of the manufacturing sites for in-house production will depend on work force availability, transport costs and plant operation costs. Building a new manufacturing plant with expensive machinery and training skilled and semi-skilled labourers is a large investment. Investing in versatile machines with multiple applications and similar operator requirements is a possible area to reduce costs.

25.2.2   Assembly, Integration and Warehousing

Deciding the final assembly location of the ARA will be based on a trade-off between: transport costs of the sub-assemblies to the plant, construction and operational costs of the plant, location to customers and workforce availability. Managing the logistics of the assembly line will depend on how the aircraft has been divided into sub-assemblies. Various joining techniques are likely to be used, requiring careful planning of the order in which sub-systems and components are assembled. Deciding the order in which sub-assemblies are integrated into the main assembly depends on the configuration of the aircraft and the required accessibility to the integration area. This in turn will effect the order in which sub-assemblies are delivered to the assembly plant which is a part of the logistics management. Integration of sub-assemblies is dependent on the allowable manufacturing tolerances. During the prototyping phase this will be tested to ensure a smooth process during full scale manufacturing operations. Since the just-in-time philosophy is never fully achieved, there is a need to store shipped parts near the assembly facility.

25.3   Production Logistics

The logistics aspect entails the transport infrastructure and the communication infrastructure. Both are discussed in this section.

25.3.1   Transport

In today's globalised manufacturing environment, parts and sub-assemblies may be produced all over the globe. During the assembly stage these components must be brought together through the use of an extensive transport network. Additionally, materials used in the in-house production are to be shipped by suppliers. One, or several, third party transport networks may be used to maintain a continuous production. In case of unavailability of one transport provider, there must be sufficient redundancy to ensure that the part is delivered on time to the required location. Additionally, communication between the transport provider and 'The Company' must be as direct and up-to-date as possible to ensure fast solutions to eventual problems. For transporting over-sized parts such as the fuselage over large distances an in-house transport service may be a viable solution.

25.3.2   Communication Framework

During the production and assembly phase, communication between the different entities involved in the process is vital. Therefore, a communication framework should be established in which efficient communication between the entities is possible. The network framework consists of three main entities: Transport, Partners and 'The Company'. The Transport entity has already been discussed in subsection 25.3.1. The 'Partner' entity contains all the subcontractors and risk-sharing partners. 'The Company' entity is subdivided into three parts: the 'Admin', which is responsible for the administration of a centralised network, the 'Management', which is responsible for the risk management, budget management and other management tasks and the 'Assembly, In-house Production and Storage' which focuses on the assembly and production of the product.

The primary means of communications is direct communication between all entities. Furthermore, a digital environment is provided which can be used as a secondary means of communication. The three main groups all give feedback to and receive feedback from a centralised network which enables concurrent production and production management. The centralised network is a dynamic framework which allows for a rapid adaptation to process changes (including delays, unsatisfactory production quality, etc.). Every entity is responsible for the correctness of their own feedback. In order to maintain such a dynamic and complex network 'The Company' assigns an administrator to make sure all the entities use the same feedback format, solve problems in the centralised network and to manage the centralised network in general. The information shared through the centralised network is stored and can be used later on to assess and back track problems arising in the production process which allows for adaptions to obtain a more efficient production process and framework. As the centralised network is a secondary means of communications, there will be a primary functioning communication framework in case of a technical failure of the centralised network. In order to

minimise the risk of technical failure the centralised network is located on cloud servers. Therefore, when one of the servers is non-operational the digital environment is still functional.

In figure 25.1 the proposed framework is schematically shown. Direct communication (primary means of communication) is shown by the dashed line arrows. The communication using the digital environment (secondary means of communication) is shown by the solid line arrows. Furthermore, in figure 25.1 the direct communication between the Transport and Partners with the smaller entities of 'The Company' is depicted by dashed line arrows to 'The Company' entity.
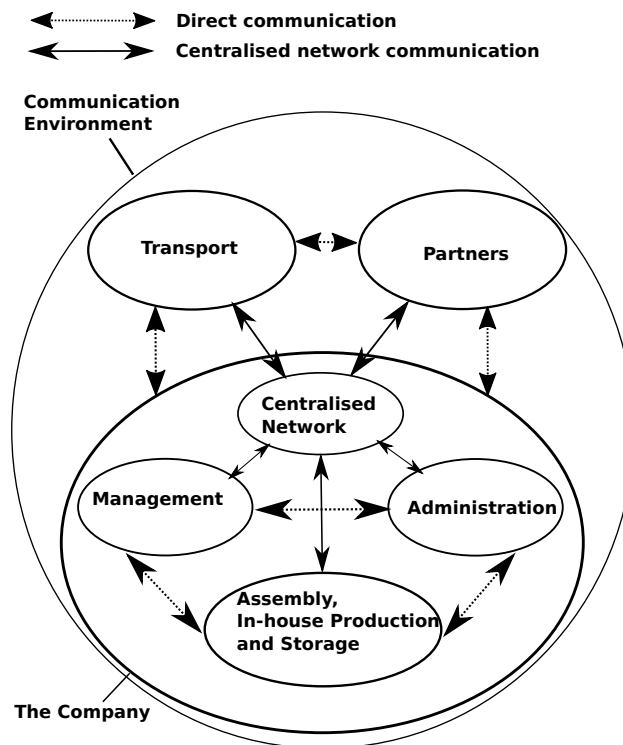

Figure 25.1: The communication network framework.

25.4 Quality Assurance

The entire production chain will comply with the AS9100 standard in order to ensure the quality of the final product. The AS9100 is an international standard which ensures that every entity in the production chain has their quality assurance system in place and it is conform to the standards set in the AS9100 family. A third party inspection and auditing company will certificate the entire production chain according to this standard. For storage of aerospace parts and the maintenance of aerospace systems the AS9120 and AS9110 quality management standards apply, respectively. For the composites used in the fuselage separate certification standards apply. In AMC 20-29 acceptable means of conforming with the regulation provisions of CS25 are presented. [84]

26 | Life Cycle Analysis

A life cycle analysis is a tool used to determine the environmental influence of a project, taking into account every step from cradle to the end of life. Five stages have been determined in the life of the ARA project. In chapter 17 the optimal material for the skin and stringers is calculated to be a composite rather than an aluminium alloy. The composite type is a carbon fibre reinforced PEEK polymer. This was compared to the 7175 aluminium alloy. The environmental impact of this decision is studied in this section. The comparison of the two materials are conducted using information obtained from [49] on primary and secondary production emissions. These include data from cradle-to-manufacturing and the end-of-life processes. Areas of comparison include the inputs and outputs for each phase. Inputs are: energy, material and water. Outputs are emissions, waste and pollution. [85] An implementation of the ISO 14040 standard for Life Cycle Assessment is suggested in order to monitor the entire supply chain from raw materials manufacturing to the end-of-life process.

Raw Materials
The cradle of the ARA fuselage is the material from which its components will be made. All emissions produced in this process are to be taken into account, including extraction, transport and refining. Composite structures in the ARA, both the fibres and matrices, are commonly made from petrochemicals. This phase has large energy, material and water inputs in addition to large emissions and pollution. Since raw materials are supplied by external suppliers, an emission certification process is necessary to make a proper life cycle assessment. Table 26.1 shows the emissions and water usage during the production phase. As is evident from the data, per kg the production of the composite is more polluting and resource intensive than the production of aluminium.

Table 26.1: Energy use and emissions during primary production [49]

	HSCF-APC2	**Al-7175 T61511**	**Unit**
Embodied energy	556 - 615	189 - 209	MJ/kg
CO2	43 - 47.5	11.9 - 13.1	$\frac{kg_{CO2}}{kg_{mat}}$
Water usage	-	$1.07 \cdot 10^3$ - $1.19 \cdot 10^3$	dm^3/kg

Manufacturing
This may be done externally or in-house. The monitoring of in-house inputs and outputs is potentially more reliable than with external suppliers. Innovative areas of manufacturing such as Additive Metal Manufacturing may reduce wasted material to 5% [39]. Manufacturing has an impact on the operational phase. Saving component weight with innovative manufacturing methods can result in large fuel savings over the operational life of the ARA. Making a comparison between metal and composite manufacturing processes is difficult as the methods vary greatly. The data are estimates obtained from [49]. The CO2 and energy emissions are presented in tables: 26.2 and 26.3. Depending on how many process stages are used to manufacture a metal fuselage skin, the emissions may quickly rise over the per kg emissions of a composite skin. If only the initial production process is taken into account (autoclave molding for composites and rolling for the aluminium), which are the processes required to create comparable skin plates, it is evident that aluminium emits fewer emissions. This is still valid when a 22% weight saving is taken into account, see section 17.2.

Table 26.2: Energy use and emissions during composite manufacturing [49]

	HSCF-APC2	**Unit**
Autoclave molding energy	20.9 - 23	MJ/kg
Autoclave molding CO2	1.67 - 1.84	$\frac{kg_{CO2}}{kg_{mat}}$

Supply Chain
All components and sub-assemblies must be transported to a common assembly area for final assembly. Optimising the supply network with respect to travel distance and transport emissions can reduce the component specific environmental footprint. Trade-offs must be made to compare travel and cost savings during manufacturing and assembly compared to the operational benefits. This phase is not analysed for the two different materials as both most likely will be made close to the final assembly location. Otherwise, the mass would be the driving factor which would mean a positive result for the composite fuselage.

---

[39] url: http://www.airbusgroup.com/int/en/story-overview/factory-of-the-future.html [CITED: 05 June 2015]

Table 26.3: Energy use and emissions during aluminium manufacturing [49]

	Al-7175 T61511	Unit
Rough rolling, forging energy	12.80 - 14.10	MJ/kg
Rough rolling, forging CO2	0.96 - 1.06	$\frac{kg_{CO2}}{kg_{mat}}$
Extrusion, foil rolling energy	25.30 - 27.90	MJ/kg
Extrusion, foil rolling CO2	1.89 - 2.09	$\frac{kg_{CO2}}{kg_{mat}}$
Fine machining energy (per unit wt removed)	19.20 - 21.20	MJ/kg
Fine machining CO2 (per unit wt removed)	1.44 - 1.59	$\frac{kg_{CO2}}{kg_{mat}}$
Non-conventional machining energy (per unit wt removed)	155.00 - 171.00	MJ/kg
Non-conventional machining CO2 (per unit wt removed)	11.60 - 12.80	$\frac{kg_{CO2}}{kg_{mat}}$

Operation

This is the longest phase in the aircraft life, material inputs are limited to fuel and replacement parts. The most influential outputs are noise and exhaust emissions. Fuel burn is predominantly dictated by the weight of the aircraft and the engine choice, reducing weight during the design and manufacturing phases will accumulate rewards in terms of fuel savings over the lifespan of the aircraft. Noise emissions have the largest impacts on the environment (both settlements and ecosystems) during approach and take-off. The chosen engine is the most critical aspect in terms of noise emissions during take-off, on approach it may be the chosen high lift devices and landing gear which cause the most noise pollution. It is calculated in chapter 21 that during operations the composite fuselage saves a total of 5.2% of fuel per flight when compared to the aluminium fuselage. This must be weighed against higher emissions during all production phases and end-of-life emissions.

End of Life

Material choice and integration complexity dictate the extend to how an aircraft may be disposed of after it has reached its fatigue cycle limit. Metal components may be molten and recycled whereas composite structures are shredded and incinerated. Third party services may be used by the airline operator to scrap the main aircraft structure whereas certain parts like the avionics or engines could be recycled by their respective manufacturers. Documentation of all materials used (especially hazardous materials) must be available to avoid pollution and health concerns during the end-of-life phase. In table 26.4 the end-of-life processes are presented for Al-7175 and PEEK composites. Aluminium is easily recycled unlike composites which are often incinerated, as is indicated by the current percentage of recycled material. Downcycling however is possible for both aluminium and PEEK composites. The final option is to discard the material in a landfill. This option however is not recommended as neither aluminium nor PEEK are bio-degradable.

Table 26.4: End of Life and Recycling [49]

	HSCF-APC2	Al-7175 T61511	Unit
Recycle	False	True	-
Recycle fraction in current supply	0.1	32.2 - 35.6	%
Downcycle	True	True	-
Combust for energy recovery	True	False	-
Combustion CO2	3.32 - 3.48	-	$\frac{kg_{CO2}}{kg_{mat}}$
Landfill	True	True	-
Biodegrade	False	False	-
Embodied energy, recycling	-	32.2 - 35.6	MJ/kg
CO2 footprint, recycling	-	2.53 - 2.8	$\frac{kg_{CO2}}{kg_{mat}}$

CO2 Emission Differences - Composite vs Aluminium

The environmental impact of selecting a composite instead of an aluminium fuselage structure is calculated by summing all emission contributions over the entire life of the aircraft. Using a fuselage mass of 3800kg (see section 8.1) and data from tables 26.1, 26.2, 26.3 and 26.4 it is estimated that the composite fuselage produces $10^5 kg$ more CO2 during primary production and manufacturing. To estimate the CO2 savings during the operational phase of the ARA, emission data is obtained [40] on CO2 emitted per kg of fuel burned. Approximately 3.169kg CO2 is emitted per kg of fuel burned. To make up for the increased emission during the manufacturing phase (taking into account a reduction of burned fuel mass of 5.2% during operations) the ARA must fly 115 flights at the design range of 2000km with maximum payload. This proves that opting for a composite fuselage will save significant CO2 emissions over the life of the ARA.

---

[40]url: http://lipasto.vtt.fi/yksikkopaastot/henkiloliikennee/ilmaliikennee/ilmae.htm [CITED: 21 July 2015]

Part VI

Post Project Planning & Recommendations

27 | Post-Project Planning

In this chapter the post-project planning, the chain of activities taking place after the project is completed, will be discussed. Not only the continuation of the original ARA design and its support will be discussed, but also follow-up design opportunities will be explored. After the design process is completed and the project finished, development cannot stop: the competition will be eager to continue their development to try to retake the market share that the ARA will gain. Thus, the development of the ARA must continue to ensure a dominant market position.

27.1 Project Design and Development Logic

In order to have a clear overview of all the post-project activities, a project design and development logic (PD&DL) will be created. It explains all needed steps to ensure a successful continuation of the ARA program and shows all steps that logically flow into each other.

The PD&DL shows the steps to be taken after the ARA project is completed and is shown in figure 27.1.
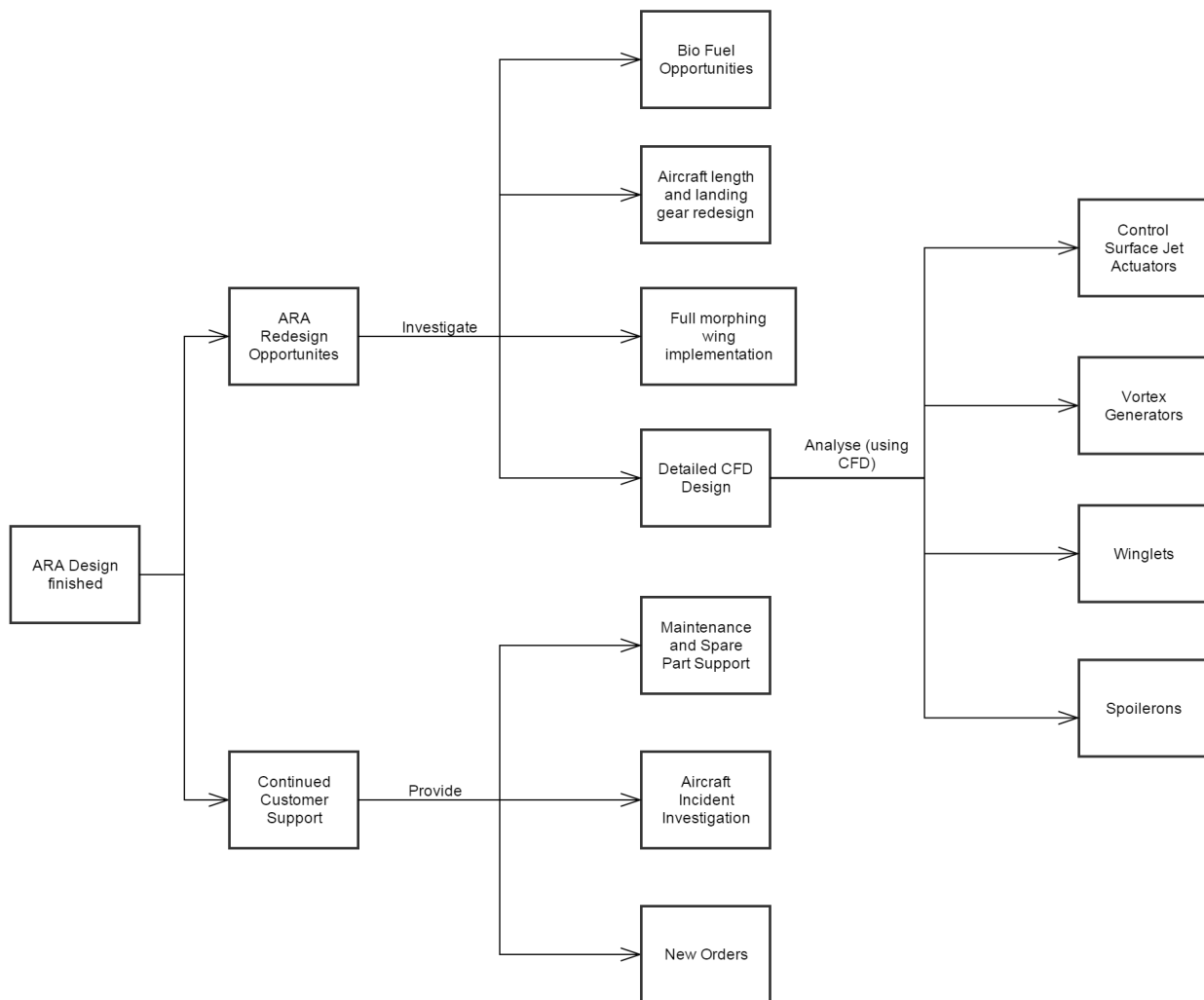

Figure 27.1: Project Design and Development Logic

It is primarily focused on technical improvement opportunities, for example using CFD analysis, to give a more accurate representation of values as drag coefficient improvement. These improvements will work towards a redesigned ARA.

27.2 Project Gantt Chart

The Gantt chart shown in figure 27.2 shows the post-DSE activities concerning improvement of the current design of the ARA and the time necessary for each subject. A shedule of approximately 7 weeks is needed to do further investigation in which the ARA will be redesigned and more detailed design on certain subsystems will be performed. Furthermore, the design needs to be verified and validated. Finally, all redesign opportunities will be implemented and assembled.
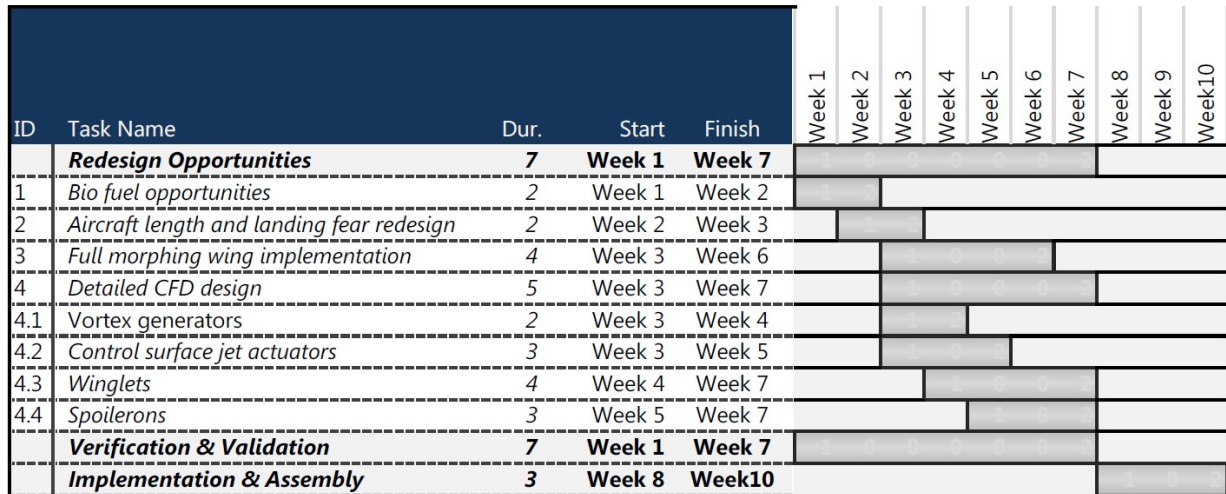

ID	Task Name	Dur.	Start	Finish
	Redesign Opportunities	**7**	**Week 1**	**Week 7**
1	Bio fuel opportunities	2	Week 1	Week 2
2	Aircraft length and landing fear redesign	2	Week 2	Week 3
3	Full morphing wing implementation	4	Week 3	Week 6
4	Detailed CFD design	5	Week 3	Week 7
4.1	Vortex generators	2	Week 3	Week 4
4.2	Control surface jet actuators	3	Week 3	Week 5
4.3	Winglets	4	Week 4	Week 7
4.4	Spoilerons	3	Week 5	Week 7
	Verification & Validation	**7**	**Week 1**	**Week 7**
	Implementation & Assembly	**3**	**Week 8**	**Week10**

Figure 27.2: Gantt chart of the post-DSE activities

27.3 Cost Breakdown Structure

The Cost Breakdown Structure (CBS) shows the costs that will occur after the initial design is finished. There will be several groups in which costs are made. This can be seen in figure 27.3.
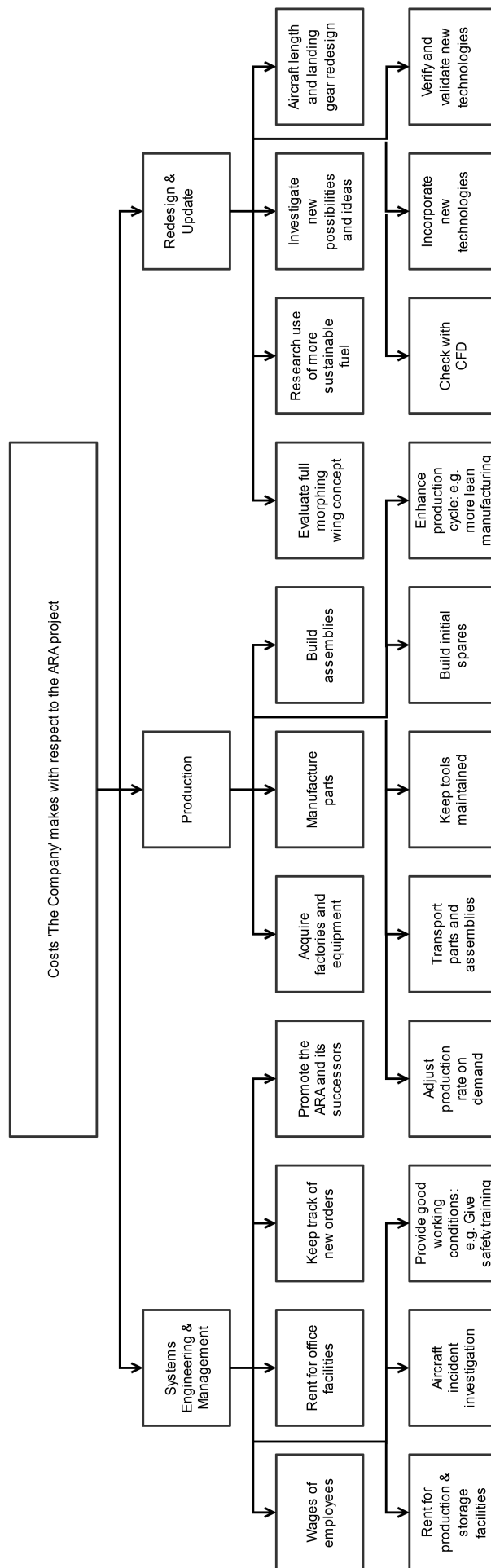
Figure 27.3: Cost Breakdown Structure of the ARA

28 | Conclusion

The conventional low wing with GTF engines underneath the wings configuration is found to be the optimal configuration for the ARA. After selecting the aircraft configuration, the preliminary subsystem design was initiated. Class I and II weight estimations were performed and an MTOW of 34500kg was determined. The selected wing planform is a two-piece complex sweptback planform with a wing area of $105m^2$, a wing span of 31m and a sweep angle of 27deg. The thrust is provided by two Pratt & Whitney 1217G GTFs with a maximum thrust of 76kN each. A trade-off was performed to select the fuselage configuration and the 2-2 configuration with cargo in the tail is found to be the best design choice. The required lift coefficient for take-off and landing are satisfied when using double slotted Fowler flaps. The tricycle configuration is chosen for the landing gear, for which the main gear consists of two struts with two tires each and the nose gear has a single strut with two tires.

After finishing the preliminary design of the ARA, the following subsystems were looked at in more detail: winglets, morphing control surfaces and the fuselage. The newly designed winglet is called the 'FLOTIN' winglet. The FLOTIN winglet consists of a large upward and a small downward winglet, both with raked tips. This winglet improves the efficiency by 6.1% when compared to an aircraft without winglets. For the morphing control surfaces, the fishbone concept was determined to be the optimal concept. A design for the ailerons of the ARA was made using requirements such as maximum deflection and several failure types. A detailed structural analysis design of the cargo section of the ARA has been performed. The optimised HSCF-APC2 cross-section, with 6 stringers and a skin thickness of 1.85mm, is found to be 21.9% lighter than the optimised Al-7175 T61511 fuselage cross-section.

The critical load factors have been determined with the maximum load factor being 2.61 and the minimum load factor being -1. All requirements are met, except for the requirement to produce 25 aircraft per month. It is decided to deviate from this value, since 100 aircraft per year fits the reflected order amount better. The ARA should obtain a leading market share due to technical advantages over the competition. The individual aircraft price is 42 million dollars (FY:2015), which accounts for 25% profit. The total profit for 'The Company' selling 1100 aircraft will be approximately 8.1 billion dollars.

29 | Recommendations

This final report presents the results of the 10 week design period of the ARA. In this time background research has been performed along with the preliminary sizing and detailed design of several subsystems of the ARA using knowledge and tools of an Aerospace Engineering Bachelor student. To further improve the design of the ARA a number of recommendations are made. Some are general recommendations and some with respect to specific subsystems which have already been preliminarily sized.

General
The ARA has been designed using limited software and analysis tools. For most subsystems it would be beneficial to perform a CFD or FEM analysis. A more detailed model should be made which includes effects such as dynamic loading and aeroelasticity. Furthermore, most information is currently obtained from textbooks, scientific articles and internet sources. These documents do not always give all the required or accurate data and the design could be improved if more accurate data is available. Finally, the improved design and subsystems should go through another series of sizing iterations until the design converges to an optimal configuration.

Fuselage
The analysis tool used to size the fuselage section currently considers a number of failure modes with the exception of buckling and stringer failure. These failure modes must be taken into account in future analysis tools. Additionally, non-linear behaviour such as impact damage and aeroelasticity effects must be taken into account. Currently the structural analysis is performed on a small section without cutouts or taper. To properly size the entire length of the fuselage, from nose to tail, these discontinuities must be adequately modelled. Validation and testing culminates in full scale prototypes being subjected to ultimate loads.

Winglet
For the design of the winglets XFLR5 is used, a program for the design of gliders. It is a very useful tool for initial sizing, however it does provide accurate results when applied to the design of a commercial aircraft. For example, XFLR5 does not account for viscosity. To validate the improvement of the winglets real-life wind-tunnel testing should be performed.

Control Surfaces
Currently an approximation for the mass moment of inertia of the aircraft is used. Increasing the accuracy on this value will result in a more accurate design of the horizontal/vertical tail and the ailerons. A thorough design of sweeping jet actuators and vortex generators can increase the efficiency of the ARA.

Morphing Control Surfaces
The design for the morphing control surfaces is currently applied to the ailerons. This could be further extended to the rudder and elevator. For the design itself a further investigation should be performed for more failure modes such as gusts and the Von Mises failure criterion.

Landing gear
An iteration in the fuselage length and location of the tail kink could reduce the required length of the landing gear.

Electrical System
The electrical system includes the fly-by-wire system, the use of green taxiing and the wiring located throughout the aircraft. Especially the use of the fly-by-wire and green taxiing systems could reduce the weight of the ARA whilst simultanously increasing its reliability. A thorough investigation of these subsystems should be performed to accurately determine the total weight savings.

Bibliography

[1] International Civil Aviation Society, "Aerodrome Design Manual Part 2," tech. rep., 2005.

[2] European Aviation Safety Agency, "Certification specifications for Large Aeroplanes CS-25," tech. rep., September 2007.

[3] European Aviation Safety Agency, "Certification Specifications for Aircraft Noise CS-36," tech. rep., 2007.

[4] European Aviation Safety Agency, "Certification Specifications and Acceptable Means of Compliance for Aircraft Engine Emissions and Fuel Venting CS-34," tech. rep., 2013.

[5] R. Vos and B.T.C.Zandbergen, "Lecture 3-4 Analysis of requirements." Lecture slides: AE1222-II Aerospace Design and System Engineering Elements I, 2015. Delft University of Technology.

[6] Embraer, "Market Outlook 2014-2033," tech. rep., July 2014.

[7] Bombardier, "Market Forecast 2014-2033," tech. rep., May 2014.

[8] Boeing, "Market Forecast 2014-2033," tech. rep., April 2014.

[9] Airbus, "Global Market Forecast," tech. rep., April 2014.

[10] A. von Schoenberg, "The case of investing in the regional airline industry," tech. rep., European Regions Airline Association, 2014.

[11] F. International, "World Airliners 2013 - Part 2." PDF from website: `https://d1fmezig7cekam.cloudfront.net/VPP/Global/Flight/FG%20Club/In%20Focus/france-special/World%20Airliners%202013%20-%20Part%202.pdf`, November 2013. Accessed: 11 May 2015.

[12] F. International, "World Airliner Census 2014." PDF from website: `https://d1fmezig7cekam.cloudfront.net/VPP/Global/WorldAirlinerCensus2014.pdf`, August 2014. Accessed: 11 May 2015.

[13] D. Group15, "Advanced Regional Aircraft," tech. rep., Delft University of Technology, May 2015. [Internal Use].

[14] R. Curran and W. Verhagen, "Concurrent Engineering & Design for Lifecycle." PDF from website: `https://blackboard.tudelft.nl/bbcswebdav/pid-2263326-dt-content-rid-7731006_2/courses/32577-141503/AE3211-I%20-%20L09%28b%29%20-%20Design%20for%20lifecycle.pdf`, 2014. Accessed: 28 April 2015.

[15] K. Willcox, "Cost Analyis." PDF from website: `http://ocw.mit.edu/courses/aeronautics-and-astronautics/16-885j-aircraft-systems-engineering-fall-2004/lecture-notes/pres_willcox.pdf`, 2004. Accessed: 28 April 2015.

[16] B. Sweetman, "The Short, Happy Life of the Prop-fan." Article from website: http://www.airspacemag.com/history-of-flight/the-short-happy-life-of-the-prop-fan-7856180/?no-ist.

[17] C. Conrad, E. Craig, and M. Eluk, "Three surface aircraft." Powerpoint presentation dowloaded from; url: `http://www.dept.aoe.vt.edu/~mason/.../ThreeSurfaceS04.ppt`, March 2004. Accessed: 23 June 2015.

[18] D. ir. G. La Rocca, "Lecture04 -Requirement Analysis and Design principles for A/C stability & control (Part 2)." Lecture slides: AE3221-I Systems Engineerign and Aerospace Design, 2015.

[19] J.A.Melkert, R.Vos, and B.T.C.Zandbergen, "A/C Preliminary Sizing(Class 1 weight estimation method)." Lecture slides AE1222-II Aerospace Design and System Engineering Elements I, 2015. Delft University of Technology.

[20] J.A.Melkert, R.Vos, and B.T.C.Zandbergen, "A/C Preliminary Sizing(T/W-W/S diagram part 1)." Lecture slides AE1222-II Aerospace Design and System Engineering Elements I, 2015. Delft University of Technology.

[21] J.A.Melkert, R.Vos, and B.T.C.Zandbergen, "A/C Preliminary Sizing(T/W-W/S diagram part 2)." Lecture slides AE1222-II Aerospace Design and System Engineering Elements I, 2015. Delft University of Technology.

[22] Dr. J. Roskam, *Part IV: Layout of Landing Gear and Systems*. Kansas, U.S.A.: DARcorporation, 6 ed., 2010. The University of Kansas.

[23] F. Margetan, "Modeling Cracks and Delaminations in Carbon Fiber Composites." `https://www.cnde.iastate.edu/ultrasonics-and-composites/modeling-cracks-and-delaminations-carbon-fiber-composites-frank-margetan`, 2015. Accessed: 21 May 2015.

[24] L. Nicolai and G. Carichner, *Fundamental of Aircraft and Airship Design Volume I*. Amer. Instit. of Aeronautics and Astronautics, 1 ed., 2010.

[25] Soutis, C., "Fibre reinforced composites in aircraft construction," *Progress in Aerospace Sciences*, pp. 143–151, 2005.

[26] Dr. J. Roskam, *Part III: Layout design of cockpit, fuselage, wing and empennage: cutaways and inboard profiles*. Kansas, U.S.A.: DARcorporation, 6 ed., 2010. The University of Kansas.

[27] D.Steenhuizen, "Wing Design Part 1-4." Lecture slides: AE2101 Aerospace Design and System Engineering Elements II, 2013. Delft University of Technology.

[28] R. Parker, "Future large civil aircraft propulsion: Evolution or revolution?." Rolls Royce presentation, March 2015. Accessed: 24 April 2015.

[29] R. O. W.H. Herkes and S. Uellenberg, "The Quiet Technology Demonstrator Program: Flight Validation of Airplane Noise-Reduction Concepts." Article from website: `http://arc.aiaa.org/doi/pdf/10.2514/6.2006-2720`. Accessed: 17 June 2015.

[30] *Synthesis of Subsonic Airplane Design*. Delft University Press, 1982.

[31] Roskam, Jan, Lan, and C.-T. Edward, "Airplane Aerodynamics and Performance," 1997.

[32] A. K. Kundu, *Aircraft design*. Cambridge university press, 2010.

[33] M. Sadraey, "Chapter 9: Landing Gear Design." PDF from website: `http://faculty.dwc.edu/sadraey/Chapter%209.%20Landing%20Gear%20Design.pdf`. Accessed: 3 June 2015.

[34] Dr. J. Roskam, *Part II: Preliminary Configuration Design and Integration of the Propulsion System*. Kansas, U.S.A.: DARcorporation, 6 ed., 2004. The University of Kansas.

[35] J.A.Melkert, R.Vos, and B.T.C.Zandbergen, "Analysis of aircraft configurations." Lecture slides AE1222-II Aerospace Design and System Engineering Elements I, 2015. Delft University of Technology.

[36] Safran and Honeywell, "Electric Taxiing System." PDF from website: `https://aerospace.honeywell.com/~/media/EGTS%20Brochure%20FINAL%20-%20June%202014(1).ashx`. Accessed: 23 June 2015.

[37] D. ir. G. La Rocca, "Lecture03 - Weight estimation and iteration in AC design." Lecture slides: AE3221-I Systems Engineerign and Aerospace Design, 2015.

[38] D. ir. G. La Rocca, "Lecture04 -Requirement Analysis and Design principles for A/C stability & control (Part 1)." Lecture slides: AE3221-I Systems Engineerign and Aerospace Design, 2015.

[39] M. Sadraey, *Aircraft Design: A Systems Engineering Approach*. Wiley Publications, September 2012.

[40] M. Sadraey, *Aircraft Design: A System Engineering Approach*. Wiley, 1 ed., 2012.

[41] Dr. J. Roskam, *Part VI: Preliminary Calculation of Aerodynamic, Thrust and Power Characteristics*. Kansas, U.S.A.: DARcorporation, 6 ed., 2010. The University of Kansas.

[42] L.L.M. Veldhuis, "Aircraft Aerodynamics." Lecture slides: AE4130 Aircraft Aerodynamics Winglet Design, 2014. Delft University of Technology.

[43] A. Mann, "The Modelling and Design of Advanced Wing Tip Devices." PDF From Website: `http://www.aerodays2006.org/sessions/D_Sessions/D6/D62.pdf`, 2006. Aeronautics days Vienna.

[44] I. Sen, "Aircraft Fuselage Design Study," Master's thesis, Delft University of Technology, Faculty of Aerospace Engineering, December 2010.

[45] J.Roskam and C.-T. E. Lan, *Airplane Aerodynamics and Performance*. Design Analysis and Research Corporation, 1 ed., 1997.

[46] T. H. G. Megson, *Aircraft Structures for Engineering Students*. Butterworth-Heinemann, 5 ed., 2012.

[47] M. Tuttle, "Effects of Moisture Diffusion in Sandiwch Composites." Powerpoint presentation downloaded from; url: `https://depts.washington.edu/amtas/events/amtas_09spring/Tuttle_Moist.pdf`, 2009. Accessed: 29 June 2015.

[48] A. S. Herrmann, P. C. Zahlen, and I. Zuardy, "Sandwich Structures Technology in Commercial Aviation," *International Conference on Sandwich Structures (ICSS)*, pp. 13–26, 2005.

[49] Granta Design Limited, "CES EduPack v14.3.5." Software downloaded from: http://www.grantadesign.com/education/edupack/, 2014.

[50] Z. Hashin, "Analysis of composite materials - a survey," *ASME J. Appl. Mech*, vol. 50, no. 3, pp. 481–505, 1983.

[51] A. K. Kaw, *Mechanics of Composite Materials*. Taylor & Francis Group, LLC, second edition ed., 2006.

[52] R. Younes, A. Hallal, F. Fardoun, F. H. Chehade, *Comparative Review Study on Elastic Properties Modeling for Unidirectional Composite Materials*. INTECH Open Access Publisher, 1 ed., 2012.

[53] C. C. Chamis, "Mechanics of Composite Materials: Past, Present and Future," tech. rep., NASA, 1984.

[54] Cytec, *CYCOM 5250-4 Prepreg System*, March 2012.

[55] Cytec, *APC-2 PEEK Thermoplastic Polymer*, March 2012.

[56] Cytec, *CYCOM 381 Epoxy Prepreg*, March 2012.

[57] T. Cate, *Ten Cate Cetex TC1200*, May 2014.

[58] W. F. Smith, *Principles of Materials Science And Engineering*. McGraw Hill, 3 ed., 1995.

[59] T. Cate, *Ten Cate Cetex TC1120*, May 2014.

[60] S. Kota, R. Osborn, G. Ervind, D. Maric, "Mission Adaptive Compliant Wing - Design, Fabrication and Flight Test," *NATO Research and Technology Organisation*, 2006.

[61] B. Trease, S. Kota, "Design of Adaptive and Controllable Compliant Systems With Embedded Actuators and Sensors," *Journal of Mechanical Design*, vol. 131, 2009.

[62] Benjamin King Sutton Woods, Michael I. Friswell, "Preliminary Investigation of a Fishbone Active Camber Concept." PDF from website: `michael.friswell.com/PDF_Files/C327.pdf`, July 2012. Accessed: 3 June 2015.

[63] A.V. Srinivasan, *Smart Structures*. Cambridge University Press, 2001. Accessed: 3 June 2015.

[64] Prof. Dr. Jan G. Korvink, "Chapter 9: Extension of Structure Topology Optimization - Synthesis of Compliant Mechanisms." PDF from website: `https://portal.uni-freiburg.de/imteksimulation/Teaching/Teaching_Dr_Tamara_Bechtold/files/structuraltopologyoptimization_chapter09.pdf`, February 2012. Accessed: 3 June 2015.

[65] R. C. Hibbeler, *Mechanics of Materials*. Prentice Hall, 8 ed., 2011.

[66] V.P. Brügemann, J.M.A.M. Hol, R.M. Groves, F.D. Moriniere, C. Fuchs, "AE1222-I Project Manual, Design and Construction," tech. rep., Delft Univeristy of Technology, 2013.

[67] L. Howell, S. Magleby, B. Olsen, *Handbook of Compliant Mechanisms*. John Wiley & Sons Ltd., 1 ed., 2013.

[68] H. Mahfuz, M.R. Khan, T. Leventouri, E. Liaropkapis, "Investigation of MWCNT Reinforcement on the Srain Hardening Behavior of Ultrahigh Molecular Weight Polyethylene," *Journal of Nanotechnology*, vol. 2011, 2011.

[69] Andre Ludovic, "Vortex Generators." PDF from website: `http://www.smartcockpit.com/aircraft-ressources/Vortex_Generators.html`, 2001. Accessed: 2 June 2015.

[70] N. Technology, "Fly-by-Wire Systems Enable Safer, More Efficient Flight." PDF from website: `http://ntrs.nasa.gov/archive/nasa/casi.ntrs.nasa.gov/20120001875.pdf`, 2011. Accessed: 23 April 2015.

[71] T. C. Atul Garg, Rezawana Islam Linda, "Evolution of Aircraft Flight Control System and Fly-By-Light Flight Control System," *International Journal of Emerging Technology and Advanced Engineering*, pp. 60–64, Dec 2013.

[72] V. Hampl, "Avionics in the view of reliability: Fly-By-Wire." PDF from website: `http://lrss.fri.uni-lj.si/sl/teaching/rzd/tutorials/hampl2010_avionics.pdf`, 2010. Accessed: 23 April 2015.

[73] W. Timmer, R. D. Breuker, and C. Kassapoglou, "AE2111-I Systems Design Project Reader-Aircraft," August 2014. Faculty of Aerospace Engineering, Delft University of Technology.

[74] M. Voskuijl, "Altitude effects on aircraft performance." Lecture slides: AE1110-I Introduction to Aerospace Engineering I, 2014. Delft University of Technology.

[75] S. C. James and C. Savaglio, "The Expanded Reach of Simulation Based Aircraft System Verification and its Software Capability Requirements." PDF from website: `http://www.adi.com/wp-content/uploads/2014/10/simulationBasedAircraftSystemVerification.pdf`, October 2014. Accessed: 8 May 2015.

[76] S. Arthasartsri and H. Ren, "Validation and Verification Methodologies in A380 Aircraft Reliability Program." PDF from website: `http://ieeexplore.ieee.org/stamp/stamp.jsp?tp=&arnumber=5270030`, 2009. Accessed: 07 May 2015.

[77] P. Curran and dr.W.Verhagen, "Lecture 8- Risk management & reliability, Part1-Risk management & technical performance management." Lecture slides: AE3221-I Systems Engineerign and Aerospace Design, 2015.

[78] FAA, *Risk Management Handbook*, 2009. Accessed: 13 May 2015.

[79] Gloria Kulesa, "Weather and Aviation." PDF from website: `http://climate.dot.gov/documents/workshop1002/kulesa.pdf`, 2009. Accessed: 04 June 2015.

[80] J. Rosetta, "fs aircraft maintenance procedures." PDF from website: `https://www.aa.com/content/images/aboutUs/newsroom/fs_aircraft_maintenance_procedures.pdf`, November 2012. Accessed: 18 May 2015.

[81] J. Fraga, "AERO - Boeing 787 from the Ground Up." PDF from website: `www.boeing.com/commercial/aeromagazine/articles/qtr_4_06`, September 2006. Accessed: 18 May 2015.

[82] R. Resto, "Non Routine, Unscheduled Maintenance." Article from website: `http://www.messier-bugatti-tracer.com/news/blog/blog_16.htm`, 2005. Accessed: 18 May 2015.

[83] FAA, "System Software Safety." PDF from website: `https://www.faa.gov/regulations_policies/handbooks_manuals/aviation/risk_management/ss_handbook/media/Chap10_1200.pdf`, 2000. Accessed: 28 May 2015.

[84] European Aviation Safety Agency, "AMC 20-29," tech. rep., July 2010.

[85] Airbus, "Streamlined Life Cycle Assessment," 2008.

[86] Bombardier, "CRJ700 NextGen." PDF from website: `www.commercialaircraft.bombardier.com`, November 2014. Accessed: 25 May 2015.

[87] Bombardier, "CS-100 NextGen." PDF from website: `www.commercialaircraft.bombardier.com`, November 2014. Accessed: 25 May 2015.

[88] Embraer, "Embraer 175, cabin." PDF from website: `www.embraercommercialaviation.com`, June 2013. Accessed: 25 May 2015.
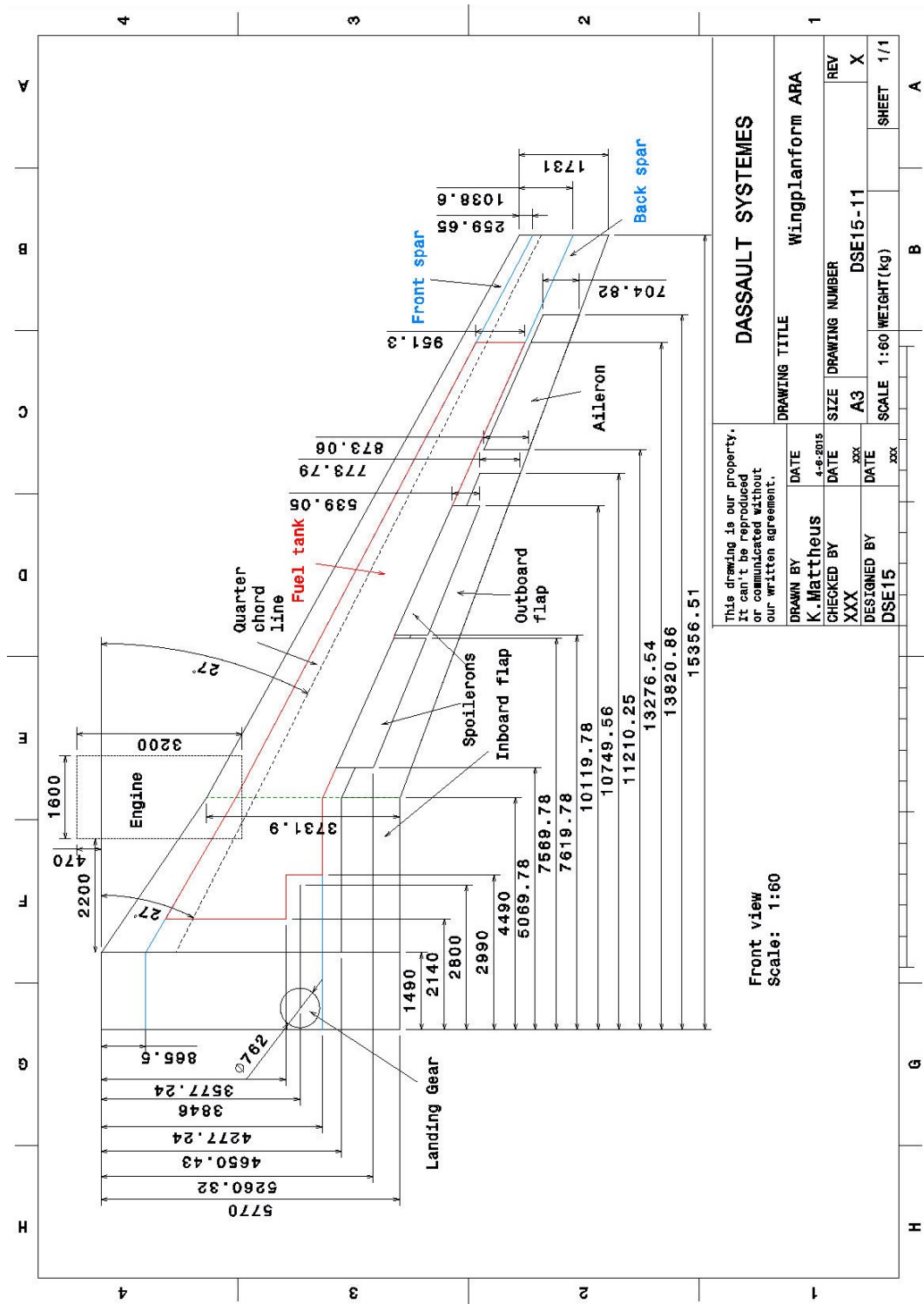
A | Wing Planform

Figure A.1: The wing planform of the ARA

B | Data Reference Aircraft

Most of the data obtained in this appendix are obtained from Janes [41], otherwise the source is given in the tables.

Table B.1: MTOW and OEW for different reference aircraft

Aircraft	MTOW [kg]	OEW [kg]
MRJ-90 STD single class	39600	25100
CRJ-700 1-class dense	32999	20069
CRJ-900 1-class dense	36514	21845
Fokker 70	39915	22784
Fokker 100	43090	24593
Fokker F28	33112	16780
Comac ARJ21-700 STD 1-class dense	40500	24955
Antonov An-148-100B 1-class dense	38550	22490
Avro RJ-100	46040	25600
Avro RJ-85	43998	24600
Avro RJ-70	43091	23900
Dornier 728	35200	21950
E170-200 STD 1-class dense	37500	21670
E175 STD 1-class dense	37500	21810
E190	47790	27720
CS-100 Base 1-class dense	58515	33300
ATR 42	18600	11250
CRJ-1000 NExt gen	40823	23188
Tu-334 100	47900	28950
XAC MA600	21800	13700

Table B.2: Typical fuselage seating dimensions in millimeters [32]

	4-Abreast (2-2)	5-Abreast (3-2)
Aisle width	482.6	508
Cabin height	1905	2082.8
Fuselage height	2895.6	3454.4
Gap between wall and seat	2 x 25.4	2 x 12.7
Seat width (LHS)	2 x 457.2	2 x 457.2
Seat width (RHS)	2 x 457.2	3 x 457.2
Total cabin width	2590.8	3200.4
Total elbowroom	6 x 12.7	7 x 50.8
Total fuselage width	2819.4	3454.4
Total wall thickness	2 x 114.3	2 x 127

---

[41] url: https://janes.ihs.com/CustomPages/Janes/ReferenceHome.aspx [CITED: 23 May 2015]

Table B.3: Overview of important fuselage mid-section dimensions and parameters

Aircraft	R [km]	n_{pax} [−]	x_{sp} [mm]	n_a [−]	n_r [−]	l_{cab} [m]	w_{cab} [m]	$d_{in,avg}$ [m]	V_{car} [m³]
Bombardier CRJ-700 [86]	2022	74	787.4	4	19	17.25	2.55	2.55	68.8
Bombardier CS-100STD [87]	2778	125	762	5	25	23.72	3.28	2.71	23.7
Dornier 728-200	2944	80	-	-	-	18.02	3.25	2.70	14.5
Embraer 175 [88]	3241	88	736.6	4	22	23.7	2.74	2.74	-
MRJ-90	1670	92	736.6	4	23	-	2.76	-	18.24
Sukhoi SJ 100-75	2900	83	762	5	17	17.15	3.24	-	16.1

Table B.4: Overview of important fuselage mid-section dimensions and parameters.

Aircraft	l_{ac} [m]	d_{out} [m]	l_f [m]	l_a [m]	l/d	l_f/d	l_a/d	l_w [m]	TA [deg]
Avro RJ-100 [32]	30.00	3.56	5.92	10.37	8.43	1.66	2.91	3.59	13.6
Bombardier CRJ-700	32.3	2.69	3.78	8.21	12.01	1.41	3.05	2.27	13.5
Bombardier CS-100STD	34.98	3.71	5.88	11.38	9.43	1.58	3.07	4.70	12.2
Comac ARJ21-700	33.46	3.26	5.52	8.58	10.3	1.69	2.63	3.44	16.44
Dornier 728-200	27.04	2.56	4.74	8.17	10.56	1.85	3.19	3.93	10.3
Embraer 175	31.68	2.86	5.14	11.12	11.08	1.80	3.89	3.34	11.3
Fokker 100	32.50	3.30	3.90	9.39	9.85	1.20	2.85	2.67	10.2
MRJ-90	35.8	2.96	4.18	7.17	12.09	1.41	2.42	1.78	13.8
Sukhoi Superjet 100-75	26.44	3.35	4.91	7.51	7.89	1.47	2.24	3.66	15.4

C | Load Cases Fuselage
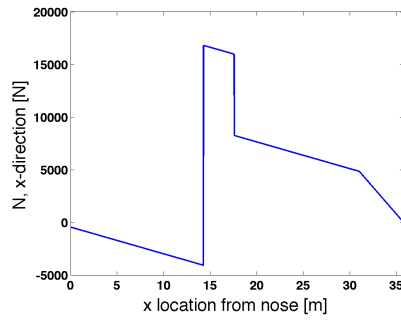
Figure C.1: Cruise, normal force
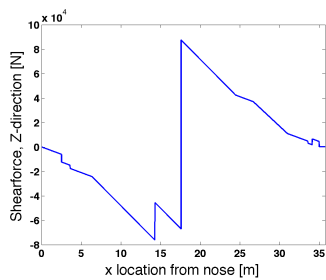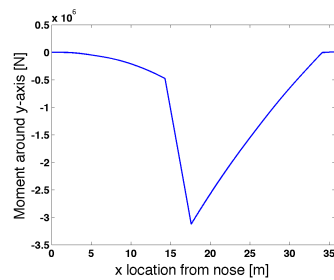

Figure C.2: Cruise 1g, shear force
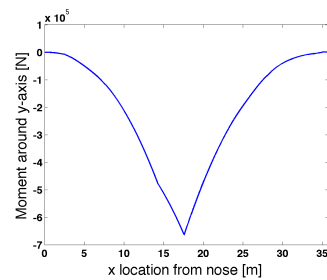
Figure C.3: Cruise 1g, moment
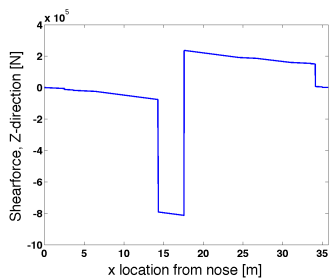
Figure C.4: Horizontal tail force downwards, shear force

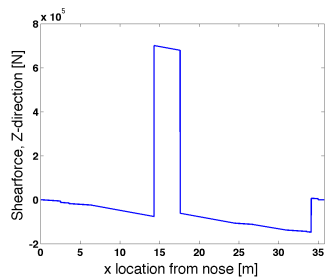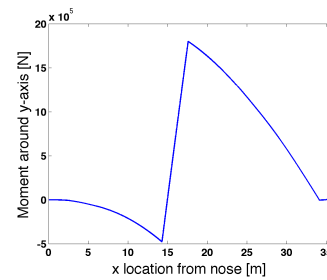Figure C.5: Horizontal tail force downwards, moment

Figure C.6: Horizontal tail force upward, shear force

Figure C.7: Horizontal tail force, upward, moment
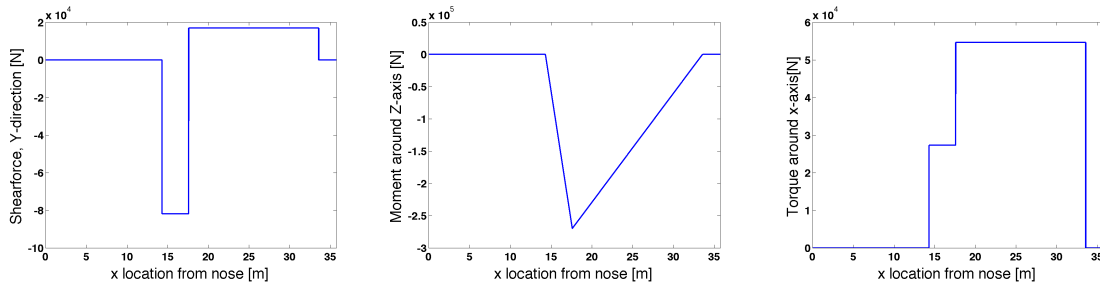
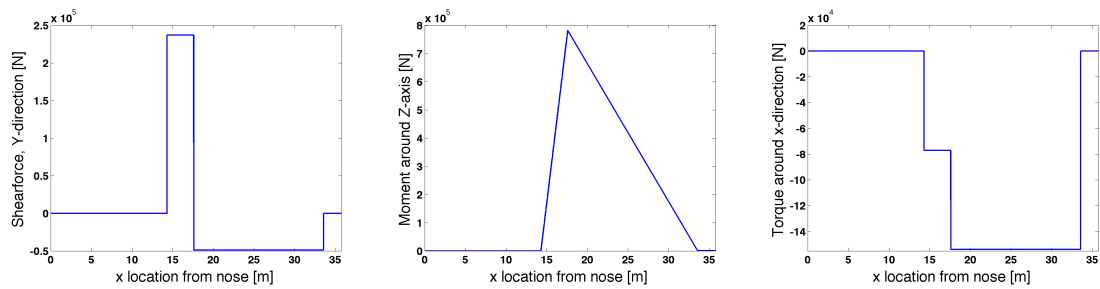Figure C.8: Side slipping flight, Figure C.9: Side slipping flight, Figure C.10: Side slipping flight, shear force   moment   torque

Figure C.11: Lateral gust, shear Figure C.12: Lateral gust, mo- Figure C.13: Lateral gust, force   ment   torque
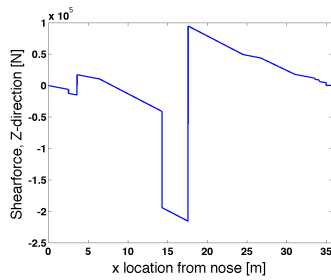
Figure C.14: Ground 1g, shear force
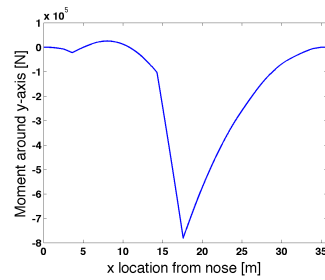
Figure C.15: Ground 1g, moment
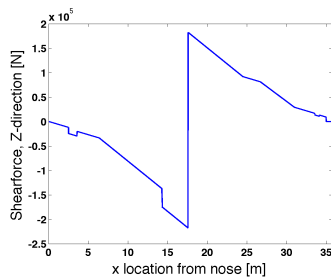
Figure C.16: Three point landing, shear force
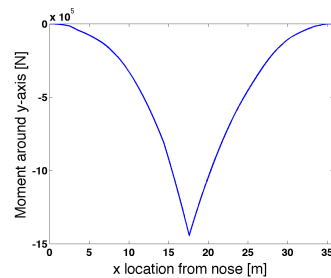
Figure C.17: Three point landing, moment
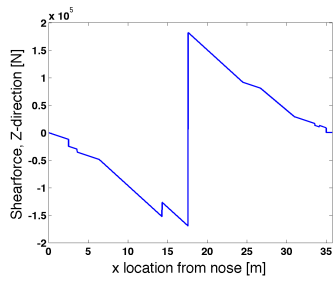
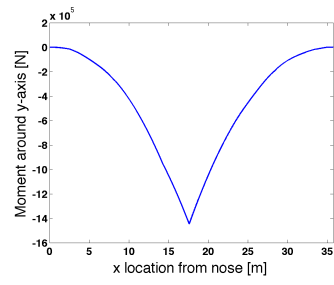Figure C.18: Two point landing, shear force

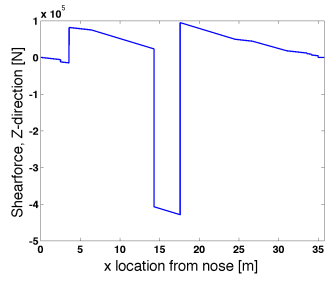Figure C.19: Two point landing, moment

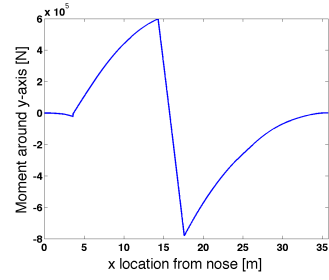Figure C.20: Abrupt ground breaking, shear force

Figure C.21: Abrupt ground breaking, moment
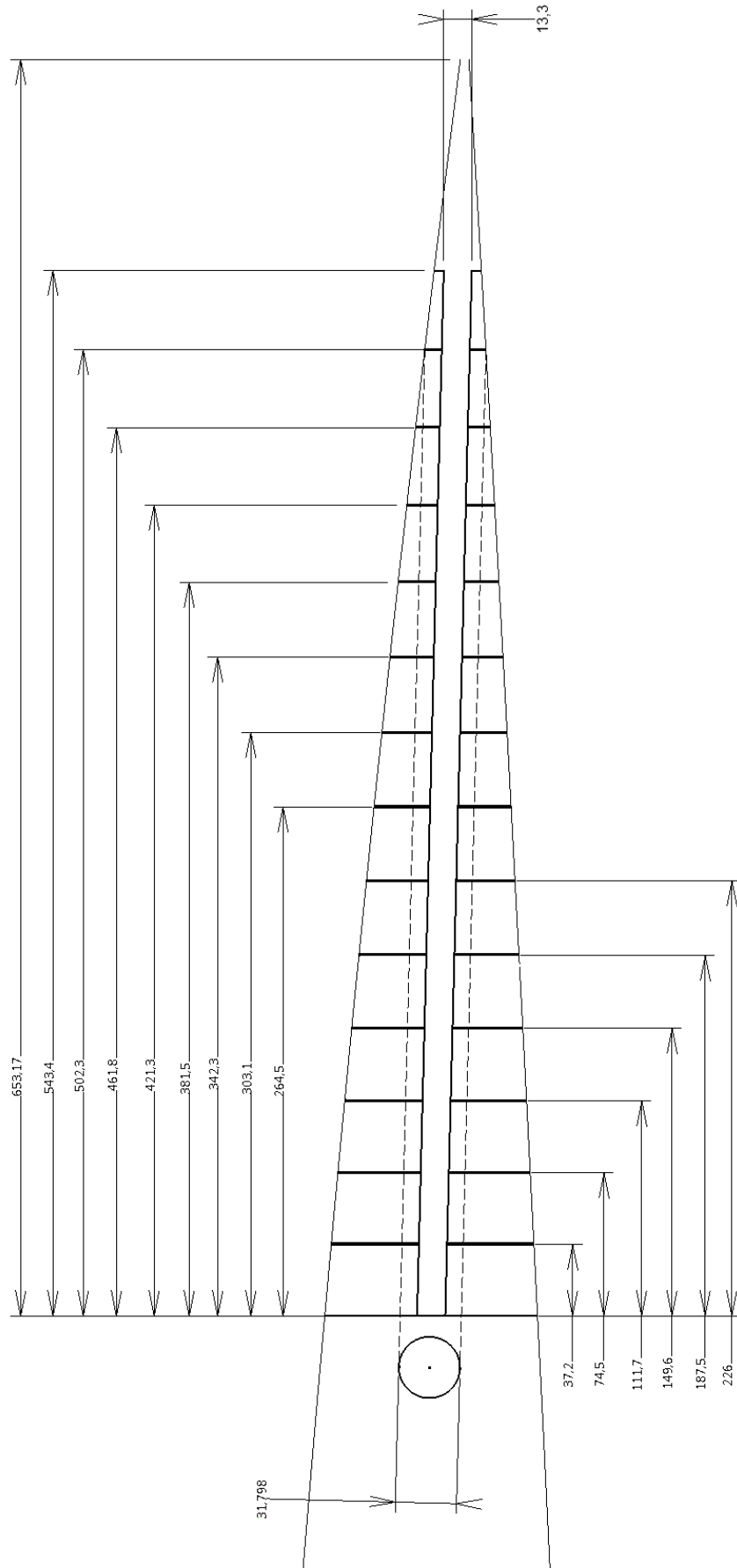
D | Aileron Mechanism Dimensions

Figure D.1: Final layout of the aileron mechanism with stringer placement dimensions
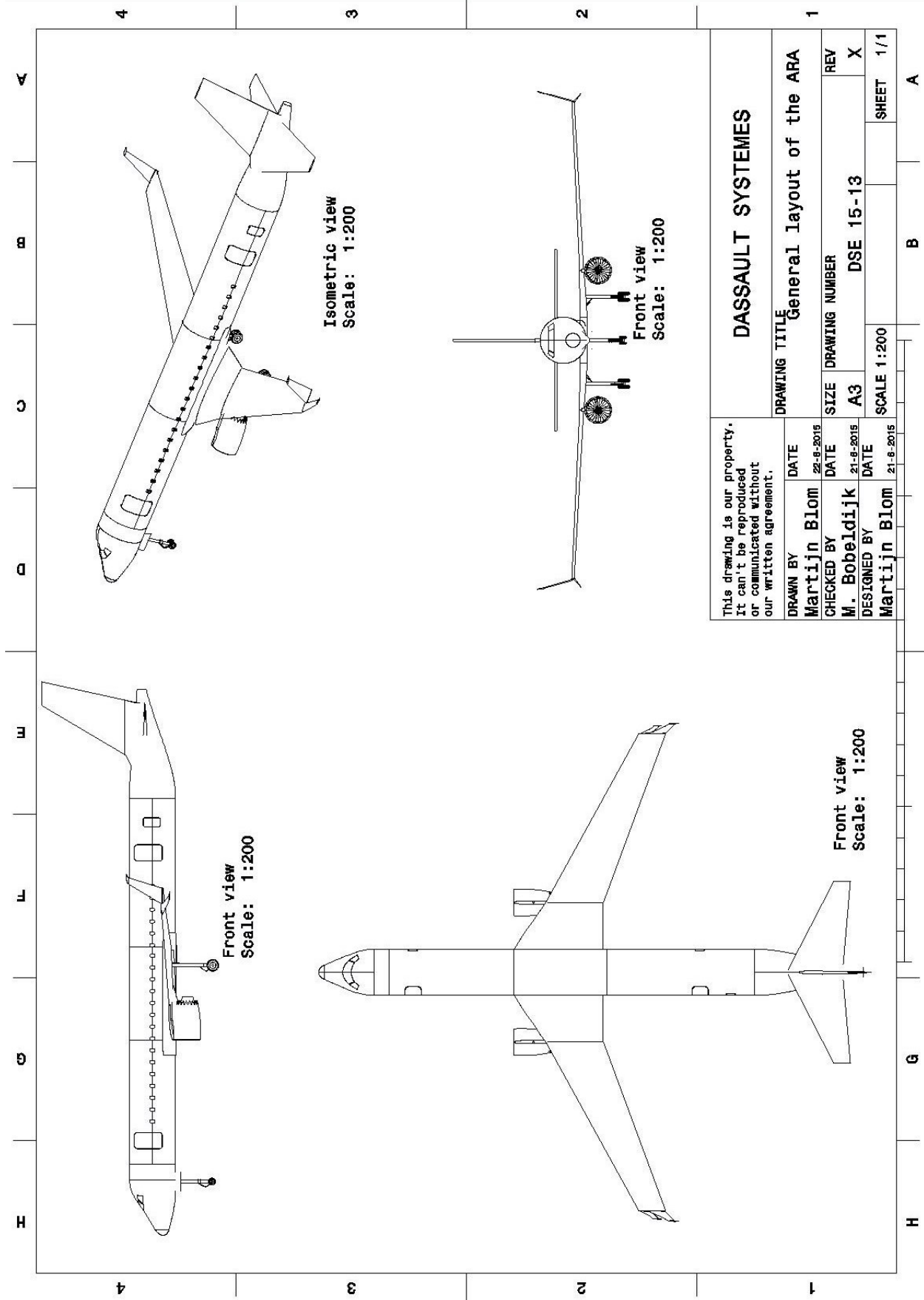
E | CAD Drawings
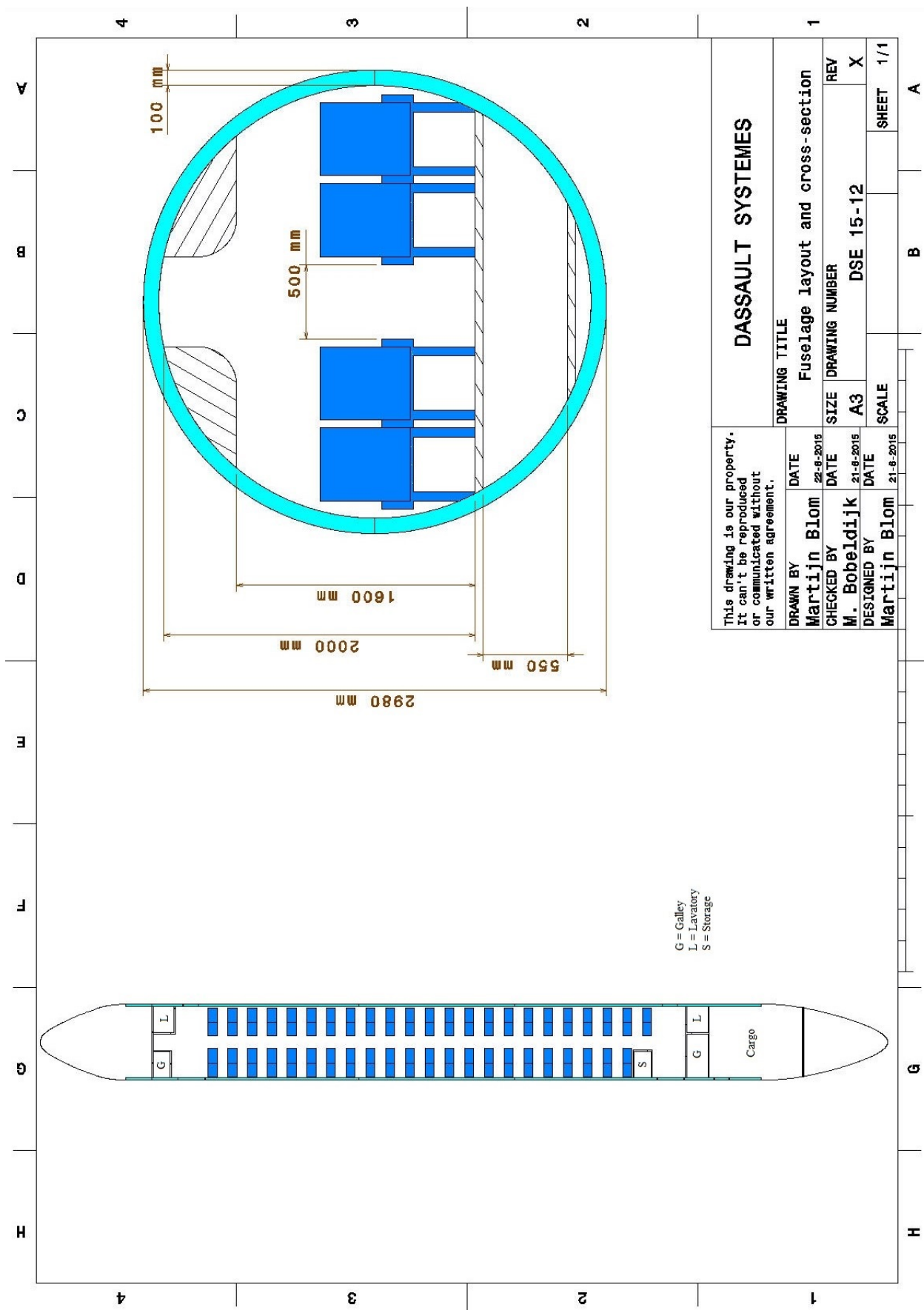

Figure E.1: Four different general views of the ARA

Figure E.2: The cabin layout and the fuselage cross-section of the ARA

F | Work Division

Table F.1: Workdivision(MBl = Martijn Blom, MBo = Mark Bobeldijk, A-L = Anne-Liza Bruggeman, D = Daan Cederløf, MH= Mohammed Haddaoui, F = Floris Heeres, K = Katleen Mattheus, U = Umair Mehmood, P = Pascal Mestrom, MM = Mark Miedema)

Section in report or task	Responsible person	Rewriten by:	Proofreader
Preface	F	F	K, U, MH
Summary	U	U	MH, K
List of Symbols	MBl	MBl	K
List of Abbreviations	MBl	MBl	K
1 Introduction	F	F	K, MBl
I Project Management			
2 Requirements	F, D	F	U, MH
3 Market Analysis and Return on Investment	MBl, MBo, MM, P	P	U, MH
4 Design Philosophy	U	MH, U	F, MBl
5 Project Process	A-L, MH	A-L	U, P
II Preliminary Subsystem Sizing			
6 Configuration Design	MBo, U	U	MH, A-L
7 Iteration Process	A-L, K, MBo	K, MBo	U, MH
8 Class I & Class II Weight Estimations	A-L, K, MBl, MBo, MH	MBo, K	F, MBl
9 Initial Wing Sizing	A-L, F, K, MH	F	MBo, U, D
10 Propulsion Systems	A-L, MH, U	U, A-L	MM, MBl
11 Fuselage	D, MBo	D	U, K
12 High Lift Devices	MBo, MH	MBo	MM, U
13 Landing Gear	A-L, K, MH, U	A-L, U	MM, P
14 Empennage	MBl, MBo	MBo	MM, U
15 Control Surfaces	MH, U, MM	MH, U, MM	P, D
III Detailed Design			
16 Winglets	F, MBl	F, MBl	MM, MBo, A-L, D
17.2 Cargo Bay Structural Design	D, MBo	D, MBo	F, P, D
17.1 Load Cases	K, MH	K, MH	F, P, D
18 Control Surfaces	A-L, MM, P	A-L, MM, P	K, MH, D
IV Aircraft Performance			
19 V-n Diagrams and Flight Envelope	A-L, K	K	U, MH, D
20 Configuration and Innovation	MBl	MBl	U, D, MH
21 Sensitivity Analysis	MBl, MM, P	MM, MBl	MH, A-L, D
V Production, Life and Investment			
22 Verification & Validation	MBl, MM, P	MM	U, F, D
23 Risk Analysis	MBl, MM	MM	MBl, A-L, D
24 Operations and Logistics	MM, P	MM	MH, MBl
25 Production Plan	D, MBo	D, MBo	A-L, MBl, D
26 Life Cycle Analysis	D	D	K, F
VI Post Project Planning & Recommendations			
27 Post-Project Planning	MBl, MM, P	MBl, MM, P	MBl, A-L
28 Conclusion	U	U, MBl	MH, A-L, MBl
29 Recommendations	F	D	K, A-L
Appendices			
A Wing Planform	K	K	MBl, MM
B Data Reference Aircraft	K	K	MBl, MM
C Load Cases Fuselage	MH	K	MBl, MM
D Aileron Mechanism Dimensions	A-L	A-L	MM, MBl
E Catia	MBl	MBl	MBo, K
F Work Division	MBl	MBl	K, MM